Lipid droplets are required for lipid mediator production and cancer cell proliferation

Eva Jarc Jovičić[1,2], Anja Pucer Janež[1,2], Thomas O. Eichmann[3,4], Vesna Brglez[1,2], Paul M. Jordan[5], Jana Gerstmeier[5], Gérard Lambeau[6], Oliver Werz[5], Robert Zimmermann[3,7], and Toni Petan[1,*]

[1]Department of Molecular and Biomedical Sciences, Jožef Stefan Institute, Ljubljana, Slovenia
[2]Jožef Stefan International Postgraduate School, Ljubljana, Slovenia
[3]Institute of Molecular Biosciences, University of Graz, Graz, Austria
[4]Center for Explorative Lipidomics, BioTechMed-Graz, Graz, Austria
[5]Department of Pharmaceutical/Medicinal Chemistry, Institute of Pharmacy, Friedrich Schiller University Jena, Jena, Germany
[6]Université Côte d'Azur (UCA), Centre National de la Recherche Scientifique (CNRS), Institut de Pharmacologie Moléculaire et Cellulaire (IPMC), UMR7275, Valbonne Sophia Antipolis, France
[7]BioTechMed-Graz, University of Graz, Graz, Austria

Running title: Lipid droplets and lipid mediators

*To whom correspondence should be addressed:
Toni Petan
Department of Molecular and Biomedical Sciences
Jožef Stefan Institute
Jamova cesta 39
SI-1000 Ljubljana
Slovenia
Tel: +386-1-4773713
Fax: +386-1-4773984
E-mail: toni.petan@ijs.si

Abstract

Lipid droplets are dynamic organelles with a central role in fatty acid metabolism. They protect cells from lipotoxicity by sequestering excess fatty acids but also provide fatty acids for metabolic reactions and signalling events. Here we show that lipid droplet turnover in cancer cells is required for production of ω-3 and ω-6 polyunsaturated fatty acid (PUFA)-derived inflammatory lipid mediators, including eicosanoids and specialised pro-resolving mediators. We show that incorporation of PUFAs into triglycerides mediated by diacylglycerol acyltransferase 1 (DGAT1), and their release by adipose triglyceride lipase (ATGL), are required for cyclooxygenase- and lipoxygenase-dependent lipid mediator production and cancer cell proliferation. The human group X secreted phospholipase A_2 (hGX $sPLA_2$) drives the delivery of membrane-derived PUFAs into lipid droplets, while ATGL promotes the incorporation of lipid droplet-derived PUFAs into phospholipids. The group IVA cytosolic PLA_2 ($cPLA_2\alpha$) acts on membrane phospholipids and complements ATGL in the regulation of PUFA trafficking between phospholipids and triglycerides. This study identifies lipid droplets as essential cellular hubs that control PUFA availability for production of lipid mediators involved in inflammation and tumorigenesis.

Keywords: lipid droplets, diacylglycerol acyltransferase, adipose triglyceride lipase, phospholipase A_2, eicosanoids, cancer

61 **Synopsis**

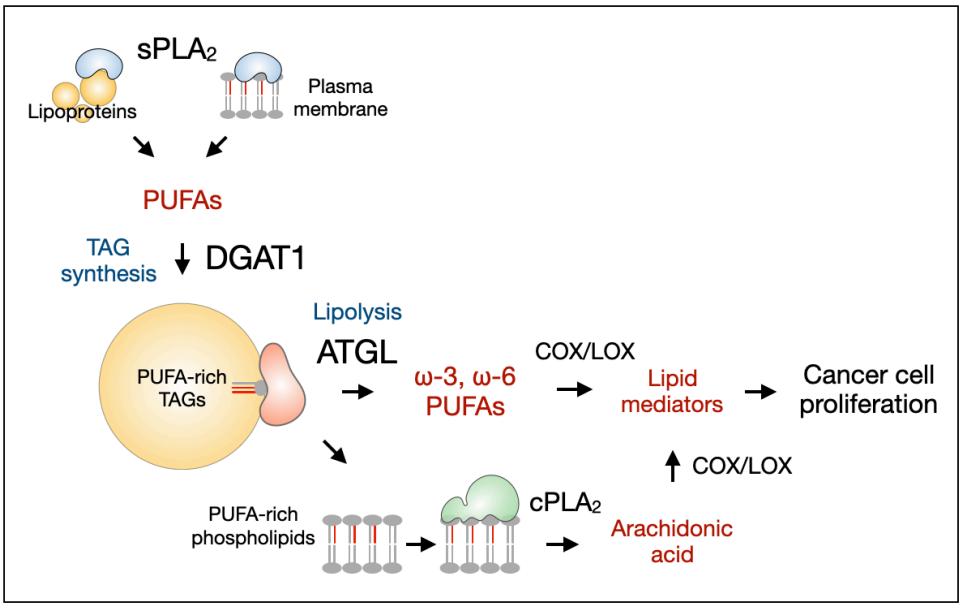

62

63 This study shows that lipid droplets in cancer cells control the supply of ω-3 and ω-6
64 polyunsaturated fatty acids (PUFAs) for the production of lipid mediators, which in turn drive
65 cancer cell proliferation. The esterification of PUFAs into triacylglycerols (TAGs) and their
66 release from lipid droplets are necessary for PUFA entry into lipid mediator production
67 pathways.

68 - Lipid mediator production induced by the human group X secreted phospholipase A_2
69 (hGX sPLA2), which releases PUFAs from the plasma membrane and serum
70 lipoproteins, depends on diacylglycerol acyltransferase 1 (DGAT1)-mediated TAG
71 synthesis.
72 - Adipose triglyceride lipase (ATGL) liberates ω-3 and ω-6 PUFAs from TAGs and
73 drives lipid mediator production via cyclooxygenase (COX) and lipoxygenase (LOX)
74 pathways.
75 - ATGL promotes the incorporation of lipid droplet-derived PUFAs into phospholipids,
76 which are targeted by the group IVA cytosolic PLA_2 ($cPLA_2\alpha$), thereby selectively
77 supplying arachidonic acid for lipid mediator production.
78 - Lipid droplets are required for $cPLA_2\alpha$-induced lipid mediator production also in cells
79 that do not depend on ATGL for the supply PUFAs into lipid mediator pathways.

80

81

Introduction

Fatty acids (FAs) are universal energy sources and membrane building blocks that are essential for cell growth and proliferation. FAs also stimulate signalling pathways involved in tumour initiation and progression (Röhrig & Schulze, 2016). Cancer cells use various strategies to satisfy their increased needs for FAs, which include reprogramming of FA metabolism (Pavlova & Thompson, 2016; Röhrig & Schulze, 2016) and elevated lipid storage within cytosolic lipid droplets (Olzmann & Carvalho, 2019; Petan, 2020). Lipid droplets are dynamic organelles that transiently store FAs and other lipids in their inert, esterified forms (Krahmer *et al*, 2013; Welte & Gould, 2017; Henne *et al*, 2018). Cancer cells use lipid droplets to maintain their energy and redox homeostasis, and to support membrane synthesis and preserve organelle integrity (Koizume & Miyagi, 2016; Cruz *et al*, 2020; Petan, 2020). Recent studies have also suggested the involvement of lipid droplets in various aspects of inflammation and immunity (Brok *et al*, 2018; Pereira-Dutra *et al*, 2019; Jarc & Petan, 2020; Bosch *et al*, 2021).

Lipid droplets consist of a neutral lipid core that primarily contains triglycerides (TAGs) and sterol esters, and is surrounded by a single layer of phospholipids, wherein numerous proteins are embedded (Olzmann & Carvalho, 2019). Lipid droplets are assembled at the endoplasmic reticulum (ER), where *de novo* synthesized neutral lipids are packaged into nascent lipid droplets that bud from the ER membrane (Walther *et al*, 2017; Thiam & Ikonen, 2020). TAG biosynthesis, catalysed by diacylglycerol acyltransferases 1 and 2 (DGAT1, 2), protects cells and tissues against lipotoxicity by sequestering excess FAs (Listenberger *et al*, 2003; Bailey *et al*, 2015; Nguyen *et al*, 2017; Jarc *et al*, 2018), and reduces diet-induced insulin resistance and inflammation (Koliwad *et al*, 2010; Greenberg *et al*, 2011). However, recent studies have suggested that DGAT1-dependent lipid droplet formation is exploited by cancer cells for the prevention of oxidative damage and organelle dysfunction, thereby supporting cancer cell survival and tumour growth (Ackerman *et al*, 2018; Jarc *et al*, 2018; Cheng *et al*, 2020; preprint: Wilcock *et al*, 2020; Dierge *et al*, 2021).

Lipid droplet breakdown occurs via either lipolysis, which is initiated by adipose TAG lipase (ATGL), or lipophagy, which is a selective form of autophagy (Zechner *et al*, 2017). ATGL is the major cytosolic neutral TAG hydrolase in mammalian cells. Its activity is crucial for mobilisation of TAG reserves from adipose tissue, and for energy production during fasting and exercise (Zimmermann *et al*, 2004; Zechner *et al*, 2012). At the cellular level, ATGL promotes FA transfer from lipid droplets to mitochondria and fuels oxidative metabolism (Smirnova *et al*, 2005; Haemmerle *et al*, 2011; Rambold *et al*, 2015). Furthermore, ATGL regulates signalling pathways that coordinate metabolism, stress responses and inflammation (Schweiger *et al*, 2017; Zechner *et al*, 2017; Jarc & Petan, 2020). Several reports have shown

118 that ATGL can support tumour growth (Nieman *et al*, 2010; Zagani *et al*, 2015; Wang *et al*,
119 2017; Yin *et al*, 2021), but a tumour-suppressor role for ATGL has also been suggested (Al-
120 Zoughbi *et al*, 2016).

121 The oxygenation of ω-6 and ω-3 polyunsaturated FAs (PUFAs) by cyclooxygenases
122 (COXs), lipoxygenases (LOXs) and CYP450 epoxygenases leads to the production of several
123 families of bioactive lipid mediators that collectively modulate inflammatory and immune
124 responses (Serhan, 2014; Dennis & Norris, 2015). Eicosanoids, derived from the ω-6 PUFA
125 arachidonic acid (C20:4n-6; AA), have been shown to promote tumour growth (Wang &
126 DuBois, 2010; Greene *et al*, 2011), whereas the ω-3 PUFA-derived resolvins suppress tumour-
127 associated inflammation and reduce tumour growth (Sulciner *et al*, 2018; Fishbein *et al*, 2020).
128 The compositions of the lipid mediator mixtures released from cells are dictated by the
129 availability of particular PUFAs for lipid mediator-producing enzymes (Wang & DuBois, 2010;
130 Greene *et al*, 2011; Jarc & Petan, 2020). However, our current understanding of the control of
131 PUFA supply for lipid mediator production is poor, particularly as this is intrinsically dependent
132 on the complex control of cellular (PU)FA metabolism, which includes their uptake, synthesis,
133 storage, breakdown, remodelling and trafficking between different lipid pools (Pérez-Chacón
134 *et al*, 2009; Serhan, 2014; Astudillo *et al*, 2019; Jarc & Petan, 2020).

135 The canonical pathway that supplies AA for eicosanoid production depends on group
136 IVA cytosolic phospholipase A_2 (cPLA$_2$α). cPLA$_2$α has long been known to be the major PLA$_2$
137 involved in stimulus-induced eicosanoid production and promotion of inflammation in various
138 pathophysiological settings (Bonventre *et al*, 2004; Shimizu, 2009; Murakami *et al*, 2011;
139 Leslie, 2015). Upon cell activation, cPLA$_2$α binds to perinuclear membranes of the ER and
140 Golgi complex and selectively hydrolyses phospholipids containing AA at the *sn*-2 position
141 (Hayashi *et al*, 2021). Numerous other members of the PLA$_2$ superfamily also promote lipid
142 mediator production, either through activation of cPLA$_2$α or by acting independently on their
143 respective phospholipid pools, thereby also releasing PUFAs other than AA (Saiga *et al*, 2005;
144 Duchez *et al*, 2019; Astudillo *et al*, 2019). In particular, several secreted PLA$_2$s (sPLA$_2$s) have
145 been implicated in the production of eicosanoids and ω-3 PUFA-derived specialised pro-
146 resolving mediators (Mounier *et al*, 2004; Surrel *et al*, 2009; Murakami, 2017; Sato *et al*, 2020).

147 Among mammalian sPLA$_2$s, the group X sPLA$_2$ is the most potent enzyme at
148 hydrolysing phosphatidylcholine-rich membranes, including the plasma membrane of
149 mammalian cells and lipoproteins (Lambeau & Gelb, 2008). Group X sPLA$_2$ can release
150 various unsaturated FAs, including ω-3 and ω-6 PUFAs, and it is involved in inflammation,
151 immunity, adipogenesis and tumorigenesis (Li *et al*, 2010; Ait-Oufella *et al*, 2013; Murase *et*
152 *al*, 2016; Murakami, 2017; Ogden *et al*, 2020). It can induce colon cancer cell proliferation
153 through production of eicosanoids and other lipid mediators (Surrel *et al*, 2009; Schewe *et al*,
154 2016). Our previous studies have shown that human group X (hGX) sPLA$_2$ stimulates lipid

155 droplet biogenesis in breast cancer cells, which is associated with increased cell proliferation
156 and resistance to starvation-induced stress (Pucer *et al*, 2013). In breast cancer cells exposed
157 to excess PUFAs, hGX sPLA$_2$ modulates unsaturated FA trafficking and lipid droplet turnover,
158 thus protecting from oxidative stress and cell death (Jarc *et al*, 2018). Other PLA$_2$s, including
159 cPLA$_2$α, also influence lipid droplet metabolism, although the potential links between various
160 PLA$_2$s, lipid droplets and lipid mediator production have been poorly explored to date (Guijas
161 *et al*, 2014; Jarc & Petan, 2020).

162 Recent evidence has suggested that besides membrane phospholipids, other lipid
163 pools can also provide PUFAs for lipid mediator production (Jarc & Petan, 2020). This includes
164 neutral lipids that are stored within lipoproteins and lipid droplets (Dichlberger *et al*, 2014;
165 Schlager *et al*, 2015, 2017). Lipid droplets in immune cells have been implicated in AA
166 trafficking and inflammatory responses (Dvorak *et al*, 1983; Triggiani *et al*, 1994; Bozza *et al*,
167 2011). Furthermore, several eicosanoid biosynthetic enzymes localise to lipid droplets, which
168 suggests that lipid droplet-derived fatty acids can participate in eicosanoid production (Accioly
169 *et al*, 2008). In agreement with this, ATGL- and hormone-sensitive lipase (HSL)-mediated
170 lipolysis have been shown to participate in eicosanoid production in mast cells, neutrophils and
171 adipocytes (Dichlberger *et al*, 2014; Schlager *et al*, 2015; Gartung *et al*, 2016; Sohn *et al*,
172 2018). In addition, monoacylglycerol lipase, which acts on monoglycerides derived from TAG
173 lipolysis or phospholipid hydrolysis, has been shown to promote tumorigenesis through the
174 dual control of endocannabinoid removal and eicosanoid production (Nomura *et al*, 2010,
175 2011). Most notably, ATGL deficiency has been shown to reduce PUFA availability for lipid
176 mediator production and enhance neutrophil immune responses *in vivo* (Schlager *et al*, 2015).
177 Whether ATGL has a similar role in cancer cells is not known. It is also not clear whether lipid
178 droplets merely act as optional and transient storage sites for PUFAs, or whether they are *de-*
179 *facto* required for lipid mediator production.

180 Lipid droplets are emerging as modulators of the subcellular distribution of mono-
181 unsaturated FAs (MUFAs) and PUFAs, which is important for various cellular responses to
182 stress and for determination of cell fate (Bailey *et al*, 2015; Ackerman *et al*, 2018; Jarc *et al*,
183 2018; Dierge *et al*, 2021). Here, we investigated whether lipid droplets can influence the
184 delivery of PUFAs into the oxygenation pathways that are responsible for regulated production
185 of lipid mediators. We examined how DGAT and ATGL affect lipid mediator production in
186 cancer cells, and how they cooperate with different PLA$_2$ enzymes in the control of PUFA
187 trafficking between membrane phospholipids and TAGs. We show that incorporation of PUFAs
188 into TAGs and their subsequent release via lipolysis are essential for the production of various
189 lipid mediators, and that this process is linked to cancer cell proliferation.
190
191

192

193 # Results

194

195 ***Membrane phospholipid hydrolysis by hGX sPLA$_2$ leads to enrichment of lipid droplets***
196 ***with long-chain PUFA-TAGs***

197 We have shown previously that hGX sPLA$_2$ stimulates TAG synthesis and induces lipid droplet
198 accumulation in several breast cancer cell lines, including the highly invasive and metastatic
199 triple-negative MDA-MB-231 cells (Pucer *et al*, 2013; Jarc *et al*, 2018). To determine whether
200 this extends to other cancer cell types, a panel of cancer cell lines was treated with 10 nM
201 recombinant hGX sPLA$_2$ and changes in lipid droplet levels were quantified using flow
202 cytometry, and visualised using confocal microscopy. hGX sPLA$_2$ stimulated lipid droplet
203 accumulation in the majority of these cancer cell lines, including neuroblastoma, prostate,
204 colorectal, ovarian and lung cancer cell lines (Fig. 1A, B). An increase in neutral lipid
205 accumulation was also seen for several immortalised non-tumorigenic cell lines (Fig. 1A). Of
206 note, there was a reduction in lipid droplet content and TAG levels upon hGX sPLA$_2$ treatment
207 only in the HeLa cervical cancer cells (Appendix Fig. S1A). Therefore, hGX sPLA$_2$ is a potent
208 stimulator of lipid droplet turnover, the activity of which in most cell types, but not all, leads to
209 a net increase in lipid droplet accumulation.

210 We have previously reported that hGX sPLA$_2$ hydrolyses membrane phospholipids in
211 intact MDA-MB-231 breast cancer cells to release various unsaturated FAs, including primarily
212 oleic acid (C18:1n–9; OA), plus significant amounts of ω-3 and ω-6 PUFAs (Jarc *et al*, 2018).
213 Furthermore, hGX sPLA$_2$ induces significant TAG acyl-chain remodelling in MDA-MB-231 cells
214 exposed to excess exogenous docosahexaenoic acid (C22:6n–3; DHA), thereby increasing
215 the levels of MUFAs esterified in lipid droplet-stored TAGs (Jarc *et al*, 2018). To support the
216 idea that FAs released from MDA-MB-231 cell membrane phospholipids by hGX sPLA$_2$ are
217 incorporated into growing lipid droplets (Fig. 1C), we examined the effects of hGX sPLA$_2$ on
218 the incorporation of radiolabelled [^{14}C]-OA into cellular lipids (Appendix Fig. S1B). Thin-layer
219 chromatography (TLC) analysis revealed that the hGX sPLA$_2$ treatments increased the
220 amounts of [^{14}C]-OA that were esterified in TAG species in MDA-MB-231 cells grown under
221 serum-rich conditions (Fig. 1D; Appendix Fig. S1C). This enrichment of TAGs with OA
222 persisted after removal of hGX sPLA$_2$ and during prolonged periods of serum starvation. As
223 hGX sPLA$_2$ acts on both serum lipoproteins and intact adherent cells (Guillaume *et al*, 2015;
224 Jarc *et al*, 2018), it is possible that the FA flux from either or both of these lipid pools supported
225 the lipid droplet biogenesis. As the hGX PLA$_2$ induction of OA incorporation into TAGs was not
226 abolished during treatments in the absence of serum (Fig. 1D; Appendix Fig. S1C), this
227 confirmed a direct action of hGX sPLA$_2$ on the cancer cells to drive the incorporation of cell-

228 membrane-derived OA into TAGs, and thus to induce long-lasting changes in the TAG acyl-
229 chain composition.
230 To determine the full extent of TAG remodelling induced by hGX $sPLA_2$, we performed
231 lipidomic analysis of untreated and hGX-$sPLA_2$-treated MDA-MB-231 cells grown in the
232 presence and absence of serum (Fig. 1E–K; Appendix Fig. S1D, E). As expected, a significant
233 increase in the total amount of TAGs was observed in the hGX-$sPLA_2$-treated cells grown
234 under both conditions (Fig. 1F). Both serum-fed (Fig. 1G, H) and serum-starved (Fig. 1I) cells
235 treated with hGX $sPLA_2$ had elevated levels of long-chain and highly unsaturated TAG species.
236 Significant changes were observed in TAG species of at least 60 C-atoms (Fig. 1J) and more
237 than seven double bonds (Fig. 1K), such as 58:8, 58:9, 60:8, 60:9, 62:10, 62:12 and 64:12
238 (Appendix Fig. S1D, E). On the other hand, there was a significant reduction in the abundance
239 of shorter-chain saturated and weakly unsaturated TAG species; i.e., those with 52 or less C-
240 atoms (Fig. 1J) and containing exclusively saturated or only one mono-unsaturated acyl chain
241 (Fig. 1K). Therefore, the lipid droplets in breast cancer cells treated with hGX $sPLA_2$ are
242 significantly enriched with PUFA-containing TAG species.
243
244 ***ATGL-mediated lipid droplet breakdown is required for PGE_2 production in serum-***
245 ***starved cancer cells***
246 Serum withdrawal induces lipid droplet breakdown in most cell types (Bosch *et al*, 2020). Given
247 the hGX-$sPLA_2$-induced enrichment of lipid droplets with PUFAs, we hypothesised that
248 starvation-induced lipid droplet breakdown provides PUFAs for lipid mediator production. To
249 find out if the breakdown of PUFA-rich lipid droplets facilitates eicosanoid production in cancer
250 cells, lipid droplet biogenesis was first stimulated with hGX $sPLA_2$ or with exogenous AA in
251 serum-rich medium (Fig. 2A). Then the cells were serum-starved in the absence of these
252 stimuli to induce lipid droplet breakdown (Fig. EV1A, B) and quantify the release of glycerol,
253 an indicator of TAG lipolysis, and the production of prostaglandin (PG)E_2, a major
254 inflammation- and cancer-related eicosanoid. Serum-starved MDA-MB-231, HeLa and A549
255 cancer cells pre-treated with hGX $sPLA_2$ released more glycerol (Fig. EV1C) and produced
256 more PGE_2 than control untreated cells (Fig. 2B). Accordingly, hGX-$sPLA_2$-treated MDA-MB-
257 231 and A549 cells had more lipid droplets at the beginning of the starvation and a greater
258 proportion of these lipid droplets were broken down during the starvation (Fig. EV1A, B).
259 Although HeLa cells treated with hGX $sPLA_2$ showed a net reduction in neutral lipid levels (Fig.
260 EV1A), during serum starvation they still released more glycerol (Fig. EV1F) and produced
261 more PGE_2 (Fig. 2B) than the untreated cells. MDA-MB-231 and HeLa cells pre-treated with
262 exogenous AA also increased their production of PGE_2 during starvation (Fig. EV1D). Together
263 with the observed hGX-$sPLA_2$-induced PUFA-TAG enrichment of lipid droplets, the elevated

264 lipid droplet turnover, lipolytic activity and PGE_2 production in hGX-sPLA$_2$-treated cells suggest
265 that lipid droplet breakdown drives PGE_2 synthesis in serum-starved cancer cells.
266 Recent evidence has suggested that TAG lipolysis mediated by ATGL contributes to
267 the production of lipid mediators in endothelial and immune cells (Dichlberger *et al*, 2014;
268 Schlager *et al*, 2015; Riederer *et al*, 2017). Here we asked whether lipid droplet breakdown via
269 ATGL is required for lipid mediator production in serum-starved cancer cells, and whether it
270 mediates hGX-sPLA$_2$-stimulated PGE_2 synthesis. ATGL-specific siRNAs were used to
271 suppress ATGL expression in cancer cells exposed to nutrient-rich conditions, followed by
272 serum starvation (Fig. 2C; Fig. EV1E). The deficiency of ATGL augmented lipid droplet levels
273 under both serum-rich and serum-starvation conditions (Fig. 2D, F; Fig. EV1F, H, I, K).
274 Importantly, ATGL depletion reduced basal PGE_2 production in serum-starved untreated MDA-
275 MB-231 and HeLa cells, and fully blocked hGX-sPLA$_2$-induced PGE_2 production in these two
276 cell lines (Fig. 2E; Fig. EV1G). ATGL silencing also attenuated lipid droplet breakdown and
277 suppressed the production of PGE_2 in MDA-MB-231 cells pre-treated with exogenous AA (Fig.
278 EV1L, M). However, ATGL deficiency did not suppress the basal or hGX-sPLA$_2$-induced PGE_2
279 production in the A549 cells, and even resulted in a slight increase in PGE_2 levels (Fig. EV1J).
280 Furthermore, in contrast to MDA-MB-231 and HeLa cells, where ATGL deficiency suppressed
281 glycerol release, ATGL depletion in A549 cells augmented hGX-sPLA$_2$-induced glycerol
282 release (Fig. EV1N, O).
283 To support these findings, we next asked whether ATGL overexpression leads to
284 increased lipolysis and PGE_2 production in the breast and cervical cancer cells (Fig. 2G). Here,
285 ectopic ATGL expression stimulated glycerol release (Fig. 2H; Fig. EV1P) without having any
286 significant effects on the total neutral lipid levels (Fig. EV1R). Both untreated and sPLA$_2$-
287 treated ATGL-overexpressing cells produced significantly more PGE_2 during starvation (Fig.
288 2I). The increase in lipolytic glycerol release and PGE_2 production induced by ATGL
289 overexpression was fully reversed in the presence of ATGL-specific siRNA in both of these
290 cell lines (Fig. 2H, I), which confirmed the specificity of the effect of ATGL overexpression.
291 Collectively, these data suggested that lipid droplet breakdown via ATGL is required for basal,
292 AA-induced and hGX-sPLA$_2$-stimulated PGE_2 production in serum-starved MDA-MB-231
293 breast and HeLa cervical cancer cells, but not in A549 lung cancer cells (Fig. 2J).
294
295 ***ATGL-mediated lipid droplet breakdown drives production of eicosanoids and***
296 ***specialised pro-resolving mediators***
297 The data presented above demonstrate that transient storage of AA within lipid droplet TAGs
298 followed by AA release from TAGs by ATGL are intermediate steps in basal and hGX-sPLA$_2$-
299 stimulated production of PGE_2, a major pro-inflammatory and pro-tumorigenic AA-derived
300 eicosanoid. To find out if ATGL-mediated TAG lipolysis promotes the production of a wider

301 range of eicosanoids and related lipid mediators (which might also derive from other PUFAs),
302 we performed targeted liquid chromatography-tandem mass spectrometry-based
303 metabololipidomics to examine the effects of ATGL silencing on the lipid mediator profiles of
304 untreated and hGX-sPLA$_2$-treated breast cancer cells. Here, pre-treatment of breast cancer
305 cells with hGX sPLA$_2$, which enriches PUFA-TAGs in lipid droplets, stimulated the starvation-
306 induced production of various lipid mediators, biosynthesised from different PUFAs by various
307 enzymatic pathways, including prostaglandins, specialized pro-resolving mediators and
308 numerous hydroxylated PUFAs (Fig. 3A–C). We quantified 34 different lipid mediators with 18
309 lipid mediator species that were elevated in cells pre-treated with hGX sPLA$_2$ (Fig. 3A–C;
310 Appendix Fig. S2). hGX sPLA$_2$ promoted the synthesis of eicosapentaenoic acid (EPA)-derived
311 lipid mediators (6/6 species), as well as the production of AA-derived (5/13 species) and DHA-
312 derived (7/15 species) products (Fig. 3B, C; Appendix Fig. S2). Importantly, ATGL depletion
313 suppressed the release of all of the hGX-sPLA$_2$-induced lipid mediators. Furthermore, ATGL
314 silencing strongly inhibited the basal, hGX-sPLA$_2$-independent production of numerous lipid
315 mediators, including PGE$_2$ (Fig. 3B, C; Appendix Fig. S2). Cells pre-treated with hGX sPLA$_2$
316 under serum-fed conditions also released significantly more unesterified PUFAs, including AA,
317 EPA and DHA, during the following serum starvation, which was prevented by ATGL silencing
318 (Fig. 3D). This suggested that a significant portion of hGX sPLA$_2$-released PUFAs is not used
319 for lipid mediator production and that these “excess” membrane-derived PUFAs still undergo
320 a cycle of esterification into TAGs and release from TAGs by ATGL. Therefore, lipid droplets
321 drive starvation-induced production by cancer cells of a wide spectrum of lipid mediators that
322 are derived from PUFAs stored within TAGs and are released by ATGL-mediated lipolysis (Fig.
323 3E).
324
325 ***Cancer cells depleted of lipid droplets have impaired PGE$_2$ production***
326 The data presented above demonstrate that lipid droplets and ATGL-mediated lipolysis
327 promote the entry of exogenously added and hGX-sPLA$_2$-derived PUFAs into lipid mediator
328 production pathways in serum-starved cancer cells. To determine whether the incorporation of
329 PUFAs into TAGs is indeed a prerequisite for PUFA use as substrates for lipid mediator
330 biosynthesis, DGAT-mediated TAG synthesis was inhibited using a combination of specific
331 inhibitors of DGAT1 and DGAT2 (DGATi), T863 and PF-06424439, and changes in lipid droplet
332 turnover and PGE$_2$ release were examined. DGAT inhibition during serum feeding strongly
333 suppressed basal, hGX-sPLA$_2$-induced and exogenous AA-induced lipid droplet accumulation
334 (Fig. 4A, B, D). There was an almost complete depletion of lipid droplets in serum-fed DGATi-
335 treated cells (Fig. 4B), which allowed only a minimal residual lipid droplet breakdown during
336 the subsequent serum starvation (Fig. 4A). Importantly, cancer cells depleted of lipid droplets
337 did not produce eicosanoids during serum starvation, showing low basal PGE$_2$ release and no

338 increase in PGE_2 production upon stimulation with either hGX $sPLA_2$ or AA (Fig. 4C, E). DGAT
339 inhibition also abolished PGE_2 production in A549 lung cancer cells (Fig. 4C), whereas ATGL
340 depletion failed to do so (Fig. EV1J), suggesting a role of lipid droplets in eicosanoid production
341 in A549 lung cancer cells as well. Therefore, DGAT-mediated TAG biosynthesis under serum-
342 rich conditions is a prerequisite for lipid mediator production in serum-starved cancer cells.
343 Serum removal induces strong activation of *de-novo* lipogenesis in MDA-MB-231 cells
344 (Pucer *et al*, 2013), and treatment of serum-starved cells with hGX $sPLA_2$ resulted in a net
345 increase in TAG levels (Fig. 1F). To examine whether TAG synthesis during serum starvation
346 has a role in eicosanoid production, control and ATGL-depleted cells were treated with DGATi
347 during serum feeding or during serum starvation. As expected, DGAT inhibition during serum
348 feeding abolished both hGX-$sPLA_2$-stimulated and ATGL-depletion-induced changes in lipid
349 droplet accumulation in MDA-MB-231 and HeLa cells (Fig. EV2A). In contrast, DGAT inhibition
350 during serum starvation did not significantly affect lipid droplet levels in these two cell lines
351 (Fig. 4F; Fig. EV2B), nor did it affect PGE_2 release in MDA-MB-231 cells (Fig. 4F). However,
352 DGAT inhibition in serum-starved A549 cells reduced lipid droplet abundance and suppressed
353 PGE_2 production, both in control and in ATGL-deficient cells (Fig. 4G). This suggested that
354 during serum starvation significant TAG biosynthesis occurred in A549 cells and contributed
355 to eicosanoid production, via ATGL-independent mechanisms. Accordingly, in A549 cells,
356 DGAT inhibition during both serum feeding and starvation was necessary for full suppression
357 of PGE_2 production (Fig. EV2C). These data demonstrate that serum-starvation-induced TAG
358 synthesis contributes to eicosanoid production in A549 cells, but not in the breast and cervical
359 cancer cells.
360 In summary, while the breakdown of pre-existing DGAT-induced lipid droplets is the
361 predominant mechanism of lipid droplet-driven eicosanoid production in the serum-starved
362 breast and cervical cancer cells, A549 lung cancer cells also employ starvation-induced TAG
363 synthesis to support eicosanoid production.
364
365 ***$cPLA_2\alpha$ cooperates with ATGL and depends on lipid droplet turnover to drive***
366 ***eicosanoid production***
367 Given the well-accepted role of $cPLA_2\alpha$ in providing AA for eicosanoid biosynthesis, we next
368 asked whether $cPLA_2\alpha$ participates in lipid droplet-driven lipid mediator production in serum-
369 starved cancer cells. We speculated that, in principle, $cPLA_2\alpha$ might cooperate with ATGL to
370 provide AA for eicosanoid release via at least three possible mechanisms (Fig. 5A): (a) ATGL-
371 mediated transfer of TAG-derived AA into phospholipid pools that are then targeted by $cPLA_2\alpha$;
372 (b) $cPLA_2\alpha$-induced incorporation of phospholipid-derived AA into TAGs, followed by AA
373 release by ATGL; or (c) independent actions of $cPLA_2\alpha$ and ATGL on their respective lipid
374 pools.

375 To examine these hypotheses, we first used siRNAs to deplete cancer cells of $cPLA_2\alpha$
376 alone or in combination with ATGL (Fig. 5B; Fig. EV3A, B), and measured lipid droplet levels
377 and PGE_2 release. $cPLA_2\alpha$-depleted cells showed slightly higher levels of neutral lipids during
378 serum feeding (Fig. EV3C) and this effect persisted during the subsequent serum starvation
379 (Fig. 5B), being particularly evident in starving MDA-MB-231 and A549 cells pre-treated with
380 hGX $sPLA_2$. Moreover, in all three cell lines, silencing of both $cPLA_2\alpha$ and ATGL potentiated
381 the enhancing effects of individual depletion on neutral lipid accumulation (Fig. 5B). Notably,
382 $cPLA_2\alpha$ depletion abolished basal and hGX-$sPLA_2$-elicited eicosanoid release in A549 cells
383 (Fig. 5B), while ATGL silencing increased PGE_2 production (Figs. 5B, EV1J). On the other
384 hand, $cPLA_2\alpha$ knockdown had no effects on eicosanoid production in MDA-MB-231 cells, while
385 ATGL knockdown decreased PGE_2 production. Surprisingly, the silencing of $cPLA_2\alpha$ in HeLa
386 cells resulted in a marked increase in PGE_2 production, which was partially reduced in HeLa
387 cells depleted of both ATGL and $cPLA_2\alpha$ (Fig. 5B). These data suggested that $cPLA_2\alpha$
388 modulates lipid droplet turnover in all three cancer cell lines. However, its contribution to PGE_2
389 production is serum-starved cancer cells is cell-type-specific. It appears to be of either a minor
390 importance in MDA-MB-231 breast cancer cells or to have a modulatory role in HeLa cervical
391 cancer cells, whereby both cell types rely on ATGL for PGE_2 production. In contrast, in serum-
392 starved A549 cells $cPLA_2\alpha$ has a predominant role in PGE_2 production.
393 To find out more about the possible interplay between $cPLA_2\alpha$ and ATGL, we asked
394 how reciprocal overexpression of one and silencing of the other might affect lipid droplet
395 turnover and PGE_2 production (Fig. 5C). In all three cell lines, the individual overexpression of
396 ATGL or $cPLA_2\alpha$ had minimal effects on neutral lipid levels (Fig. EV3D, E). Nevertheless, the
397 overexpression of either ATGL or $cPLA_2\alpha$ induced significant increases in PGE_2 production,
398 which reached comparable levels in the three cell lines (Fig. 5C). Importantly, ATGL silencing
399 blocked PGE_2 production induced by overexpression of $cPLA_2\alpha$ in MDA-MB-231 and HeLa
400 cells, whereas $cPLA_2\alpha$ silencing only partially reduced eicosanoid production induced by ATGL
401 overexpression in MDA-MB-231 cells, and even increased that in HeLa cells. On the contrary,
402 in A549 cells, ATGL knockdown did not affect $cPLA_2\alpha$-induced PGE_2 production, but silencing
403 of $cPLA_2\alpha$ reduced PGE_2 release from ATGL-overexpressing cells (Fig. 5C). Taken together,
404 these data suggested that ATGL is the main enzyme in the provision of PUFAs for eicosanoid
405 production in MDA-MB-231 and HeLa cells, whereby $cPLA_2\alpha$ stimulation of eicosanoid
406 production depends on ATGL. In contrast, in A549 cells, $cPLA_2\alpha$ has a dominant role in PGE_2
407 production, which is independent of ATGL, but is still associated with changes in lipid droplet
408 turnover.
409 To determine whether lipid droplets are required for $cPLA_2\alpha$-driven lipid mediator
410 production, $cPLA_2\alpha$ and ATGL were overexpressed in cells depleted of lipid droplets using
411 DGAT inhibitors (Fig. 5D; Fig. EV3F). As expected, TAG synthesis was necessary for ATGL

412 stimulation of both basal and $sPLA_2$-induced eicosanoid production (Fig. 5D). In all three cell
413 lines, $cPLA_2\alpha$-overexpression-induced eicosanoid production was completely abolished upon
414 depletion of lipid droplets (Fig. 5D). Therefore, lipid droplets are required for both $cPLA_2\alpha$-
415 driven and ATGL-driven lipid mediator production. $cPLA_2\alpha$ and ATGL appear to have cell-type-
416 specific roles that are either cooperative or complementary for both lipid droplet turnover and
417 eicosanoid production. In the breast and cervical cancer cells, deficiency of ATGL impairs
418 $cPLA_2\alpha$-induced PGE_2 production, which suggests the possibility that the transfer of AA from
419 TAGs to phospholipids is a prerequisite for the action of $cPLA_2\alpha$.
420
421 ***ATGL and $cPLA_2\alpha$ have complementary roles in TAG and phospholipid acyl-chain***
422 ***remodelling***
423 To support the finding that $cPLA_2\alpha$ affects lipid droplet turnover (Fig. 5B), the changes in lipid
424 droplet morphology in $cPLA_2\alpha$ and ATGL single and double knockdown cells were visualised
425 and quantified under the microscope. For ATGL-depleted MDA-MB-231 and HeLa cells, the
426 diameters of the lipid droplets were significantly increased relative to control cells, under both
427 serum-fed and serum-starved conditions (Fig. 6A, B; Fig. EV4A, B). However, ATGL depletion
428 had only a modest effect on the number of lipid droplets per cell (Fig. 6C, D). In serum-starved
429 A549 cells, ATGL silencing reduced the number of lipid droplets per cell, but did not
430 significantly affect the diameter (Fig. 6E; Fig. EV4C, D). Of note, among the three cell lines,
431 A549 cells had the highest number of lipid droplets, which had the greatest diameters and the
432 widest size heterogeneity. Surprisingly, depletion of $cPLA_2\alpha$ in all three of these cancer cell
433 lines resulted in more lipid droplets per cell, which was particularly evident in hGX-$sPLA_2$-
434 treated cells (Fig. 6C–E). In most cases, depletion of $cPLA_2\alpha$ had no effects on lipid droplet
435 size. In comparison with ATGL-deficient cells, the silencing of both $cPLA_2\alpha$ and ATGL led to
436 increased lipid droplet numbers in all of these cell lines, and particularly under serum-starved
437 conditions, which suggested that $cPLA_2\alpha$ affects lipid droplet numbers independently of ATGL.
438 Thus, while ATGL predominantly affects lipid droplet size, which is in line with its role in TAG
439 lipolysis, $cPLA_2\alpha$ appears to have a modulatory role in lipid droplet turnover, whereby its
440 deficiency leads to a minimal increase in total cellular neutral lipid content and a significant
441 increase in lipid droplet numbers. These effects might be a consequence of the direct or
442 indirect involvement of $cPLA_2\alpha$ in the lipid droplet biogenesis and/or breakdown processes.
443 On the basis that the above data suggested that ATGL is required for $cPLA_2\alpha$-induced
444 eicosanoid production in serum-starved MDA-MB-231 and HeLa cells (Fig. 5C), we speculated
445 that this occurs by ATGL-induced transfer of TAG-derived AA into phospholipid pools that are
446 then targeted by $cPLA_2\alpha$ (Fig. EV5A). Additionally, given that $cPLA_2\alpha$ has been reported to
447 modulate lipid droplet biogenesis, possibly by inducing changes in the composition of the ER
448 membrane and thereby affecting nascent lipid droplet formation (Guijas *et al*, 2014), we

449 hypothesised that $cPLA_2\alpha$ affects lipid droplet turnover (and thus indirectly impacts upon
450 ATGL-mediated lipolysis) by inducing global changes in the composition of the phospholipid
451 and/or TAG lipid pools. To examine these hypotheses and determine how hGX $sPLA_2$, ATGL
452 and $cPLA_2\alpha$ affect PUFA trafficking between the phospholipid and TAG pools during serum
453 starvation in MDA-MB-231 cells, we performed single and double knockdowns followed by
454 lipidomic analyses comparing the lipid compositions of cells first pre-treated with hGX $sPLA_2$
455 during nutrient sufficiency and subsequently serum-starved for 0 h, 3 h or 24 h (Fig. EV5B).
456 First, treatment of breast cancer cells with hGX $sPLA_2$ led to PUFA enrichment of both
457 TAGs and phospholipids (Figs. 7A, EV5C; Appendix Fig. S3A). hGX-$sPLA_2$-induced PUFA-
458 TAG enrichment was seen for serum-fed cells (i.e., 0 h serum starvation), and it persisted upon
459 hGX $sPLA_2$ and serum removal. Importantly, the enrichment of phospholipids with PUFA acyl
460 chains progressively increased during the course of serum starvation (Fig. EV5C). By the end
461 of the 24 h of serum starvation, the levels of numerous long-chain PUFA-phosphatidylcholine
462 and several PUFA-phosphatidylinositol and PUFA-phosphatidylethanolamine species were
463 increased. These data suggested that a significant portion of $sPLA_2$-released PUFAs that are
464 incorporated into TAGs in serum-fed cells are gradually released via lipolysis during serum
465 starvation and are re-esterified into phospholipids.
466 Second, depletion of ATGL increased TAG content across all of the lipid species, and
467 also altered the cellular phospholipid composition (Figs. 7A, EV5C; Appendix Fig. S3A). The
468 effect of ATGL depletion on TAG levels gradually increased during the serum starvation, and
469 was greatest after 24 h without serum (Fig. 7B). Here, numerous PUFA-TAG species were
470 elevated, which confirmed that ATGL hydrolyses PUFA-TAGs during serum starvation. ATGL
471 silencing did not significantly affect the already high PUFA-TAG contents in hGX-$sPLA_2$-treated
472 cells (Fig. 7A), although it increased the levels of some saturated FA (SFA)/MUFA-TAG
473 species (Fig. 7C). The retention of various TAG species within lipid droplets due to ATGL
474 deficiency is in agreement with the general lack of TAG acyl-chain specificity of ATGL
475 (Eichmann *et al*, 2012). Importantly, ATGL deficiency reverted the elevation of PUFA
476 phospholipids induced by hGX $sPLA_2$ and observed in serum-starved cells (Fig. EV5C;
477 Appendix Fig. S3A). This is consistent with a reduced flux of PUFAs from TAGs into
478 phospholipids due to ATGL depletion. A similar, but less apparent, trend towards a decrease
479 in PUFA-phospholipid levels was observed for ATGL-deficient cells that were not treated with
480 hGX $sPLA_2$ (Fig. EV5C). Thus, in serum-starved cancer cells, ATGL hydrolyses various TAG
481 species, including numerous PUFA-TAGs, and provides PUFAs for esterification into
482 phospholipids.
483 Third, depletion of $cPLA_2\alpha$ had a predominant effect on the phospholipids (Fig. 7A;
484 Figs. EV5C; Appendix Fig. S3A), and also affected TAG composition (Fig. 7C). Numerous
485 PUFA-containing phosphatidylcholine and phosphatidylethanolamine species were

486 progressively elevated in $cPLA_2\alpha$-deficient cells over the course of the serum starvation, in
487 both control and hGX-$sPLA_2$-treated cells (Fig. EV5C), which suggested that these lipids are
488 targeted by $cPLA_2\alpha$ during serum starvation. The enrichment of phospholipids with PUFAs as
489 a result of $cPLA_2\alpha$ deficiency was more pronounced than that induced by hGX $sPLA_2$ treatment
490 alone (Fig. EV5C; Appendix Fig. S3A). A LION/web lipid ontology analysis suggested that the
491 enrichment of phospholipids with PUFAs in $cPLA_2\alpha$-deficient cells is indicative of significant
492 changes in membrane biophysical properties, including increased lateral diffusion, reduced
493 bilayer thickness and a lower transition temperature (Appendix Figs. S3B, C). Furthermore, in
494 $cPLA_2\alpha$ and ATGL double-knockdown cells, the decreased abundance of PUFA-phospholipid
495 species observed in ATGL-deficient cells was reversed (Figs. 7A, EV5D; Appendix Fig. S3A),
496 which suggested the possibility that ATGL-derived PUFAs are incorporated into a phospholipid
497 pool that is targeted by $cPLA_2\alpha$. On the other hand, $cPLA_2\alpha$ silencing did not affect hGX-$sPLA_2$-
498 induced PUFA-TAG enrichment (Fig. 7A), which indicated that $cPLA_2\alpha$ is not required for
499 incorporation of hGX-$sPLA_2$-released PUFAs into TAGs. However, $cPLA_2\alpha$ depletion reduced
500 the content of SFA/MUFA-TAGs in lipid droplets of hGX-$sPLA_2$-treated cells (Fig. 7C). This
501 was fully reversed in the $cPLA_2\alpha$ and ATGL double-knockdown cells, which suggested that the
502 effect of $cPLA_2\alpha$ depletion on TAG composition depends on ATGL-mediated lipolysis (Fig. 7A,
503 C). Therefore, during cancer cell starvation, ATGL promotes the transfer of PUFAs from TAGs
504 into a phospholipid pool that might be targeted by $cPLA_2\alpha$, but $cPLA_2\alpha$ also alters TAG
505 composition in an ATGL-dependent manner.

506 Collectively, these data suggested that hGX-$sPLA_2$-liberated PUFAs are used for the
507 synthesis of both phospholipids and TAGs, whereby the phospholipids are targeted by $cPLA_2\alpha$
508 and the TAGs are targeted by ATGL, while both $cPLA_2\alpha$ and ATGL may also reciprocally
509 modulate these two major lipid pools. At least in MDA-MB-231 cells, hGX-$sPLA_2$-liberated
510 PUFAs are first and predominantly incorporated into TAGs of growing lipid droplets, and are
511 then redistributed into phospholipids upon TAG lipolysis by ATGL, particularly during serum
512 starvation (Fig. 7D). Some of the ATGL-released PUFAs are directly used for eicosanoid
513 production (i.e., independent of $cPLA_2\alpha$), while some are re-esterified into phospholipids and
514 become targets for $cPLA_2\alpha$ activity. In agreement with this, TAG synthesis and lipolysis
515 determine phospholipid composition and consequently affect $cPLA_2\alpha$ mobilisation of PUFAs
516 for the production of eicosanoids.
517

518 ***Lipid droplets drive cancer cell proliferation by promoting eicosanoid production***

519 Prostaglandin E_2 and other eicosanoids are mitogenic factors that promote cancer cell
520 proliferation (Wang & DuBois, 2010). Based on our findings showing that lipid droplets are
521 required for lipid mediator production, we next examined whether lipid droplets and their
522 breakdown via ATGL-mediated lipolysis promote the proliferation of cancer cells. As hGX

523 $sPLA_2$ stimulates the proliferation of MDA-MB-231 and other cancer cells (Surrel *et al*, 2009;
524 Pucer *et al*, 2013), we first investigated whether lipid droplet depletion by inhibition of DGAT-
525 mediated TAG synthesis blocks this proliferative effect. Here, the induction of cell proliferation
526 by hGX $sPLA_2$ was fully blocked by DGAT1 inhibition and by concurrent inhibition of both
527 DGAT1 and DGAT2; however, DGAT2 inhibition alone had no effects (Fig. 8A). Importantly,
528 inhibition of DGAT1, but not DGAT2, also reduced the basal, hGX-$sPLA_2$-independent rate of
529 breast cancer cell proliferation. As ATGL overexpression promotes PGE_2 production, we
530 hypothesized that ATGL overexpression should induce cell proliferation in a COX/LOX-
531 dependent manner. Indeed, alone or in combination with $sPLA_2$ treatments, ATGL
532 overexpression stimulated the proliferation of breast cancer cells (Fig. 8B, C). Importantly, both
533 hGX-$sPLA_2$-mediated and ATGL-mediated cell proliferation were suppressed by indomethacin
534 and nordihydroguaiaretic acid, which are non-selective COX and LOX inhibitors, respectively
535 (Fig. 8B, C). This suggested that the conversion of hGX-$sPLA_2$-released and ATGL-released
536 PUFAs into lipid mediators is responsible for the mitogenic effects. After being secreted into
537 the extracellular space, eicosanoids can act on neighbouring cells by binding to their cognate
538 G-protein-coupled receptors that activate various signalling pathways (Wang & DuBois, 2010;
539 Jarc & Petan, 2020). To confirm the mitogenic potency of PGE_2 under the present conditions,
540 cell proliferation was measured in MDA-MB-231 cells treated with exogenous PGE_2. As
541 expected, PGE_2 stimulated cell proliferation, although, interestingly, this effect was suppressed
542 by inhibition of DGAT1-dependent TAG synthesis (Fig. 8D), but not by DGAT2 inhibition. This
543 suggested a positive-feedback loop between eicosanoids and DGAT1-mediated lipid droplet
544 turnover.

545 $cPLA_2\alpha$-induced eicosanoid production has already been shown to promote cancer cell
546 proliferation and tumour growth (Leslie, 2015; Koundouros *et al*, 2020), although this activity
547 has not been associated with lipid droplets. As $cPLA_2\alpha$ has a major role in lipid droplet-
548 dependent eicosanoid production in A549 cells (Fig. 5B), we asked whether $cPLA_2\alpha$
549 overexpression stimulates A549 cell proliferation in a DGAT-dependent manner. Indeed,
550 DGAT inhibition fully blocked $cPLA_2\alpha$-overexpression-induced cell proliferation (Fig. 8E), which
551 confirmed that DGAT-mediated lipid droplet biogenesis is required for $cPLA_2\alpha$-stimulated A549
552 lung cancer cell proliferation. This A549 cell proliferation was suppressed by the COX inhibitor
553 indomethacin (Fig. 8E), which suggested that it depends on COX-mediated conversion of
554 $cPLA_2\alpha$-released AA into mitogenic lipid mediators, such as PGE_2. Importantly, exogenous
555 hGX $sPLA_2$ also stimulated A549 cell proliferation, which was suppressed by inhibition of
556 DGAT and COX (Fig. 8E). Finally, in MDA-MB-231 cells, where we found that DGAT-mediated
557 TAG synthesis is required for $cPLA_2\alpha$-stimulated PGE_2 production (Fig. 5D), $cPLA_2\alpha$
558 overexpression resulted in higher proliferation rates, which were reduced by DGAT inhibition
559 (Fig. 8F).

560 Together, these data demonstrate that DGAT1-dependent TAG synthesis and lipid
561 droplet formation are involved in hGX-sPLA$_2$-, cPLA$_2$α- and ATGL-mediated, COX- and LOX-
562 dependent eicosanoid production and for cancer cell proliferation.
563
564
565 ## Discussion
566
567 In this study, we provide evidence that lipid droplet turnover is required for the production of a
568 wide range of pro-inflammatory and anti-inflammatory PUFA-derived lipid mediators in cancer
569 cells. We show that the esterification of PUFAs into TAGs and their release from lipid droplets
570 is necessary for their entry into lipid mediator production pathways. Namely, impeding the
571 incorporation of PUFAs, either added exogenously or derived from hGX sPLA$_2$ membrane
572 hydrolysis, into lipid droplets by inhibition of DGAT-mediated TAG synthesis, or blocking PUFA
573 release from TAGs by silencing ATGL, compromises lipid mediator production under starvation
574 conditions. Lipid droplet turnover is also required for stimulation of eicosanoid production by
575 cPLA$_2$α, the canonical PLA$_2$ responsible for AA release from membrane phospholipids. The
576 data from the aggressive breast cancer cells suggest that ATGL-mediated TAG lipolysis
577 promotes the incorporation of PUFAs into phospholipids. cPLA$_2$α acts downstream of lipid
578 droplet breakdown and targets PUFA-rich phospholipids. Furthermore, although ATGL was
579 dispensable for lipid mediator production in the A549 lung cancer cells, uninterrupted TAG
580 synthesis was still necessary for basal and cPLA$_2$α-induced eicosanoid production in these
581 cells. In summary, this study identifies the lipid droplet organelle as a central hub of lipid
582 mediator synthesis pathways underlying cancer cell proliferation.
583
584 ***DGAT-mediated TAG synthesis is required for eicosanoid production in cancer cells***
585 The trafficking of PUFAs between membranes and lipid droplets is emerging as a major
586 mechanism in the control of PUFA oxygenation and in the protection of various cells against
587 oxidative damage (Bailey *et al*, 2015; Jarc *et al*, 2018; Dierge *et al*, 2021). In immune and
588 cancer cells, lipid droplets have been implicated in AA storage and trafficking, and they have
589 also been suggested to act as platforms for eicosanoid production (Dvorak *et al*, 1983;
590 Triggiani *et al*, 1994; Bozza *et al*, 2011). Accordingly, the release of PUFAs from TAGs via
591 ATGL/HSL-mediated lipolysis has been shown to promote eicosanoid production in immune
592 cells and adipocytes (Dichlberger *et al*, 2014; Schlager *et al*, 2015; Gartung *et al*, 2016).
593 Here, we show that DGAT-mediated incorporation of PUFAs into TAGs stored within
594 lipid droplets, and their subsequent release via lipolysis, are indeed required for eicosanoid
595 production, which, in turn, drives cancer cell proliferation. In agreement with this, it was shown

596 recently that DGAT1-mediated TAG synthesis is required for PGE_2 production and activation
597 of inflammatory macrophages (Castoldi *et al*, 2020). Moreover, a recent study showed that
598 lipid droplet biogenesis by DGAT1 is necessary for prostaglandin synthesis during *Drosophila*
599 oogenesis (preprint: Giedt *et al*, 2021). One of the most striking findings of the present study
600 is that DGAT controls eicosanoid production and cancer cell proliferation suggesting that the
601 build-up of PUFA-rich TAG stores drives eicosanoid production pathways. A similar
602 mechanism has been described in cardiomyocytes, whereby exogenous FAs have to be
603 esterified into TAGs and then released by ATGL to activate peroxisome-proliferator-activated
604 receptor (PPAR) signalling pathways (Haemmerle *et al*, 2011; Zechner *et al*, 2012).
605 Furthermore, as DGAT activity is a prerequisite for both ATGL-induced and $cPLA_2\alpha$-induced
606 eicosanoid production in serum-starved cancer cells, it can be assumed that lipid droplets
607 control PUFA availability for eicosanoid production through regulation of both the TAG and
608 membrane phospholipid pools.

609 Based on our results that suggest that lipid droplets drive lipid mediator production and
610 cancer cell proliferation via the control of PUFA trafficking through the TAG and phospholipid
611 pools, we propose that targeting the DGAT enzymes might improve cancer treatments,
612 particularly under conditions of elevated lipid influx (e.g., abundance of dietary fats, oncogene-
613 driven elevated endogenous FA synthesis, high autophagic flux). Indeed, DGAT1 was
614 identified recently as a potent oncoprotein that increases the resilience of cancer cells against
615 the stress of increased FA acquisition, which is a hallmark of transformed cells (preprint:
616 Wilcock *et al*, 2020). Furthermore, our previous data showed that breast cancer cells
617 challenged with exogenous PUFAs depend on the balance between DGAT1-mediated
618 sequestration of PUFAs into lipid droplets and their release via ATGL-mediated lipolysis to
619 survive lethal oxidative damage (Jarc *et al*, 2018). In support of this, inhibition of DGAT activity
620 diverts dietary PUFAs towards esterification into membrane phospholipids, thereby increasing
621 their peroxidation and leading to ferroptosis in acidic tumours (Dierge *et al*, 2021). Interestingly,
622 high levels of dietary AA in mice compromise $cPLA_2\alpha$ inhibitor-mediated suppression of
623 eicosanoid production and *PIK3CA* mutant-driven tumour growth (Koundouros *et al*, 2020).
624 Although the involvement of lipid droplet metabolism was not assessed in this study, it will be
625 important to examine whether lipid droplets control the supply of AA for eicosanoid production
626 under this and similar scenarios.

627 Our results suggest that DGAT activity controls cancer cell proliferation by generating
628 PUFA stores in lipid droplets, which can be used for the production of potent, albeit short-lived,
629 pro-inflammatory and anti-inflammatory lipid signalling molecules. As these signalling
630 molecules are released from cells to act in autocrine and paracrine manners, they can
631 modulate tumour growth by altering the function of cancer cells, immune cells and other cells
632 in the tumour microenvironment (Wang & DuBois, 2010; Greene *et al*, 2011). Thus, in addition

633 to their protective role against nutrient deficiency, lipotoxicity and oxidative stress in cancer
634 cells (Petan, 2020), lipid droplets modulate tumour growth through the control of lipid mediator-
635 dependent cell-autonomous and non-cell-autonomous mitogenic and inflammatory signalling
636 pathways, and are thus a promising target for therapeutic intervention.
637
638 ***Lipid droplets control hGX-sPLA$_2$-induced and cPLA$_2$α-induced eicosanoid production***
639 Several members of the sPLA$_2$ family are involved in lipid mediator production under various
640 inflammatory conditions, including cancers (Brglez *et al*, 2014a). Group X sPLA$_2$ is the most
641 potent enzyme among mammalian sPLA$_2$s in terms of its binding to and hydrolysis of the
642 phosphatidylcholine-rich extracellular leaflet of mammalian cells, thereby releasing various
643 unsaturated FAs and PUFAs, and stimulating lipid mediator production (Hanasaki *et al*, 1999;
644 Bezzine *et al*, 2002; Surrel *et al*, 2009; Murase *et al*, 2016; Jarc *et al*, 2018). Some other sPLA$_2$
645 isoforms, such as group IIA sPLA$_2$s, bind very poorly to phosphatidylcholine-rich membranes,
646 and thus do not hydrolyse the plasma membranes of resting cells, but instead depend on their
647 internalisation and interaction with intracellular cPLA$_2$α to promote eicosanoid production
648 (Lambeau & Gelb, 2008). Here, we show that both hGX sPLA$_2$ and cPLA$_2$α depend on lipid
649 droplet turnover to drive lipid mediator production in cancer cells.
650 Our finding that PUFAs released by hGX sPLA$_2$ from cancer cell membranes and
651 serum lipoproteins are incorporated into growing lipid droplets, thereby enriching TAGs with
652 various ω-3 and ω-6 PUFAs, is important because it identifies a mechanism of enzymatically
653 induced enrichment of lipid droplets with phospholipid-derived PUFAs. Its relevance is not
654 likely to be limited to *in vitro* conditions, because group X sPLA$_2$ has been shown to modulate
655 lipid metabolism and adipogenesis *in vivo* (Li *et al*, 2010; Shridas *et al*, 2010; Sato *et al*, 2011),
656 to promote release of ω-3 and ω-6 PUFAs and their conversion into lipid mediators in several
657 tissues (Murase *et al*, 2016; Murakami *et al*, 2020), and to control intestinal lipid mediator
658 production, inflammation and tumorigenesis *in vivo* (Schewe *et al*, 2016). Furthermore, PUFA-
659 enriched TAGs have been observed in visceral adipose tissue of patients with colorectal
660 cancer, along with elevated expression of hGX sPLA$_2$ and prostaglandin-biosynthetic enzymes
661 (Liesenfeld *et al*, 2015).
662 Although the sPLA$_2$-treated MDA-MB-231 breast cancer cells showed an enrichment
663 of both TAGs and phospholipids with PUFAs, their release from TAGs by ATGL was essential
664 for their conversion into lipid mediators. On the contrary, in the A549 lung cancer cells, ATGL
665 was not necessary for lipid mediator production and the silencing of cPLA$_2$α suppressed hGX-
666 sPLA$_2$-induced PGE$_2$ production. Even in these cells, however, we showed that intact TAG
667 synthesis is a prerequisite for both hGX-sPLA$_2$-induced and cPLA$_2$α-induced eicosanoid
668 synthesis and cancer cell proliferation. These results are important because the provision of
669 PUFAs for conversion into lipid mediators by two of the most potent mammalian PLA$_2$s has

670 been shown here to depend on lipid droplet turnover. Our results thus provide a novel view of
671 PLA_2-mediated inflammatory signalling, which tightly integrates PLA_2-mediated regulation of
672 PUFA availability with cellular lipid droplet metabolism. Lipid droplets could be the missing link
673 that will help explain the elusive cross-talk between $sPLA_2$s and $cPLA_2\alpha$ in lipid mediator
674 biosynthesis (Mounier *et al*, 2004; Saiga *et al*, 2005; Lambeau and Gelb, 2008). We speculate
675 that the relevance of these findings extends beyond cancer cells to various pathophysiological
676 settings, whereby context-specific characteristics of FA and lipid droplet metabolism will
677 modulate, or even govern, PLA_2-induced inflammatory lipid mediator production.

678 Our results indicate that different cell-type-specific mechanisms might explain the
679 dependence of $cPLA_2\alpha$-induced eicosanoid production on lipid droplets. In the MDA-MB-231
680 and HeLa cells, $cPLA_2\alpha$ depended on TAG synthesis and ATGL-mediated TAG lipolysis to
681 drive the incorporation of AA (and other PUFAs) into phospholipids, which were then targeted
682 by $cPLA_2\alpha$. In A549 cells, $cPLA_2\alpha$ controls basal and $sPLA_2$-induced PGE_2 production
683 independently of ATGL, although its activity still depends on TAG synthesis. In both cases, our
684 data suggest that $cPLA_2\alpha$-mediated AA release for eicosanoid production occurs downstream
685 of, and is controlled by, lipid droplet turnover. Interestingly, $cPLA_2\alpha$ has also been shown to
686 drive mitochondrial β-oxidation of both FAs and eicosanoids for energy production (Slatter *et*
687 *al*, 2016), which is another indication that ATGL and $cPLA_2\alpha$ share common metabolic and
688 signalling pathways. Altogether, our findings suggest that lipid droplet turnover regulates the
689 supply of PUFAs for the lipid mediator production machinery via at least two pathways: direct
690 $cPLA_2\alpha$-independent delivery of TAG lipolysis-derived PUFAs via ATGL; and an indirect
691 $cPLA_2\alpha$-dependent route that involves lipolysis-induced phospholipid acyl-chain remodelling
692 that controls the availability of PUFAs for (c)PLA_2-induced lipid mediator production. Notably,
693 our data indicate that other lipases and lipid droplet breakdown mechanisms (e.g., lipophagy)
694 besides (or instead of) ATGL might contribute to lipid droplet-dependent lipid mediator
695 biosynthesis.

696 One of the intriguing questions that remains to be addressed in future studies is
697 whether PUFA trafficking between the TAG core and the lipid droplet phospholipid monolayer
698 is relevant for lipid mediator production. In principle, TAG lipolysis-derived PUFAs can be re-
699 esterified in monolayer phospholipids and targeted by $cPLA_2\alpha$ or other PLA_2s. In agreement
700 with this, $cPLA_2\alpha$, COXs, several prostaglandin synthetases and *de-novo* produced
701 eicosanoids have been localised to lipid droplets (Wooten *et al*, 2008; Moreira *et al*, 2009;
702 Bozza *et al*, 2011; Cruz *et al*, 2020; Ward *et al*, 2020). The molecular basis and functional
703 relevance of these findings is currently unclear, but we speculate that eicosanoid production
704 does not necessarily occur on lipid droplets as isolated cytosolic platforms, but at specific lipid
705 droplet–ER contact sites that provide rapid lipid and protein transfer between the lipid
706 structures involved (i.e., the ER membrane bilayer, the lipid droplet phospholipid monolayer

707 and TAG core) (Schuldiner & Bohnert, 2017). Such compartmentalisation would support the
708 interplay among $cPLA_2\alpha$, ATGL and other enzymes in the control of lipid droplet turnover,
709 membrane remodelling and the eicosanoid synthesis machinery.
710
711 ***$cPLA_2\alpha$ modulates membrane PUFA-phospholipid content and lipid droplet metabolism***
712 Our results also indicate that $cPLA_2\alpha$-induced membrane remodelling affects lipid droplet
713 dynamics. We showed that $cPLA_2\alpha$ silencing induces significant changes in lipid droplet
714 numbers, neutral lipid content, and phospholipid and TAG acyl-chain compositions. Previous
715 studies have shown that $cPLA_2\alpha$ is involved in remodelling of membrane shape, and that it
716 might facilitate lipid droplet biogenesis in severely-starved cells (Gubern *et al*, 2008; Guijas *et*
717 *al*, 2014; Astudillo *et al*, 2019; Jarc & Petan, 2020). Intriguingly, the N-terminal membrane-
718 binding C2 domain of $cPLA_2\alpha$ is sufficient to induce changes in membrane shape, and it
719 selectively localises to lipid droplets (Ward *et al*, 2012, 2020). However, our findings that
720 $cPLA_2\alpha$ depletion leads to elevated TAG accumulation and increases lipid droplet numbers
721 during serum starvation argue against a mechanism in which $cPLA_2\alpha$ promotes lipid droplet
722 biogenesis. On the contrary, the increased numbers of lipid droplets upon $cPLA_2\alpha$ silencing
723 (particularly in serum-starved cells when TAG lipolysis is activated) might instead reflect
724 secondary activation of lipid droplet biogenesis, which can occur under lipolytic conditions to
725 sequester excess free FAs and to reduce lipotoxicity (Paar *et al*, 2012; Chitraju *et al*, 2017;
726 Schott *et al*, 2019).
727 In line with this idea, our lipidomic data suggest that the changes in TAG acyl-chain
728 composition as a result of $cPLA_2\alpha$ depletion are dependent on ATGL. Furthermore, our lipid
729 ontology enrichment analysis suggests that the elevated PUFA content in membrane
730 phospholipids of $cPLA_2\alpha$-depleted cells is indicative of changes in membrane biophysical
731 properties, including fluidity, thickness and bending properties (Antonny *et al*, 2015), which
732 might facilitate lipid droplet biogenesis. Indeed, PUFA-containing phospholipids have recently
733 been shown to induce seipin enrichment at specific ER–lipid droplet contact sites, to thereby
734 promote the expansion of nascent lipid droplets (Cao *et al*, 2019). Furthermore, elevated acyl-
735 chain unsaturation and phosphatidylethanolamine content in ER membranes, along with a
736 reduction in overall TAG saturation, have been shown to strongly promote lipid droplet
737 nucleation (Zoni *et al*, 2021). We thus propose that $cPLA_2\alpha$ modulates membrane PUFA
738 composition in serum-starved cancer cells, to thereby fine-tune its biophysical properties,
739 which indirectly affects lipid droplet biogenesis (and possibly also lipolysis at the lipid droplet
740 phospholipid monolayer). Depletion of $cPLA_2\alpha$ in serum-starved cancer cells induces a gradual
741 enrichment of PUFAs in phospholipids that might in turn alter the membrane properties in a
742 way that favours lipid droplet biogenesis. It remains to be established in future studies whether

743 these hypotheses can explain the relationships between $cPLA_2\alpha$, lipid droplet turnover and
744 lipid droplet-dependent lipid mediator production.
745 In conclusion, our study reveals that lipid droplets are essential for lipid mediator
746 production and cancer cell proliferation. Esterification of PUFAs into TAGs by the DGAT
747 enzymes and PUFA release from lipid droplets (which depends on TAG lipolysis by ATGL,
748 and/or other lipases in some cancer cells) drives lipid mediator production either directly, by
749 feeding PUFAs into the COX/LOX machinery, or by redirecting some of the PUFAs into
750 membrane phospholipids first, whereby they are then targeted by $cPLA_2\alpha$. Notably, both
751 exogenous and $sPLA_2$-membrane-hydrolysis-derived PUFAs have to cycle through lipid
752 droplets to be converted into lipid mediators, which reveals that lipid droplets are not optional
753 storage reservoirs for excess PUFAs, but instead consolidate different PUFA sources and
754 actively control PUFA release. Lipid droplets thus have an important regulatory role in lipid
755 mediator production, thereby potentially affecting numerous downstream signalling pathways
756 that are involved in inflammation, immunity and cancer.
757
758

759 ## Materials and methods

760

761 ***Materials***

762 MDA-MB-231 human breast adenocarcinoma cells, A549 human lung carcinoma cells, HeLa
763 human cervical adenocarcinoma cells, C2C12 mouse myoblasts cells, and Caco-2 human
764 colorectal adenocarcinoma cells were obtained from American Type Culture Collection (ATCC,
765 USA). J774A.1 mouse reticulum cell sarcoma macrophages were from the European
766 Collection of Authenticated Cell Cultures (ECACC, UK), and MDA-MB-231 human breast
767 adenocarcinoma cells with stable luciferase 2A and RFP expression (MDA-MB-
768 231/Luciferase-2A-RFP) were from GeneTarget (USA). PC-3 human prostate
769 adenocarcinoma cells were a kind gift from Dr. Mojca Pavlin (University of Ljubljana, Slovenia).
770 OV-90 human ovarian papillary serous adenocarcinoma cells, TOV-112D human ovarian
771 endometrioid carcinoma cells, TOV-21G human ovarian clear cell carcinoma cells and
772 Ishikawa human endometrial adenocarcinoma cells were a kind gift from Dr. Brett McKinnon
773 (Berne University Hospital, Switzerland). SGBS human Simpson-Golabi-Behmel syndrome
774 preadipocytes were a kind gift from Dr. Merce Miranda (Joan XXIII University Hospital
775 Tarragona, Spain), and SH-SY5Y human neuroblastoma cells were a kind gift from Dr. Boris
776 Rogelj (Jožef Stefan Institute, Slovenia). RPMI-1640 culture medium was from ATCC (USA),
777 and Dulbecco's modified Eagle's medium nutrient mixture F-12 (DMEM/F12), DMEM with high
778 glucose and GlutaMAX supplement (DMEM-GlutaMax), foetal bovine serum, Dulbecco's

779 phosphate-buffered saline (DPBS), TrypLE Select and Opti-MEM were from Life Technologies
780 (USA). AA and PGE_2 standards were from Cayman Chemical (USA), and BODIPY 493/503,
781 Lipofectamine RNAiMAX, Lipofectamine 3000, High-capacity cDNA reverse transformation
782 kits were from Thermo Fisher Scientific (USA). Hoechst 33342 nuclear stain was from Enzo
783 Life Sciences (USA). Human ATGL-targeting and $cPLA_2\alpha$-targeting siRNAs and the AllStars
784 Negative Control siRNA were from Qiagen (Germany). T863 (DGAT1 inhibitor), PF-06424439
785 (DGAT2 inhibitor), indomethacin (COX inhibitor), nordihydroguaiaretic acid (LOX inhibitor),
786 essentially fatty acid-free (EFAF) bovine serum albumin (BSA) (cat. no. A7511), FAF-BSA (cat.
787 no. A8806) and Nile red were from Sigma-Aldrich (USA). High Pure RNA isolation kits were
788 from Roche (Germany), horseradish-peroxidase-labelled secondary antibodies were from
789 Jackson ImmunoResearch Laboratories (USA), ATGL antibodies (cat. no. #2138) were from
790 Cell Signaling Technology (USA), $cPLA_2\alpha$ antibodies (cat. no. sc-454) were from Santa Cruz
791 (USA) and β-actin antibodies (cat. no. NB600-532) were from Novus Biologicals (UK).
792 Recombinant wild-type hGX $sPLA_2$ was prepared as described previously (Pucer *et al*, 2013).
793 The full-length cDNAs coding for human $cPLA_2\alpha$ (NCBI RefSeq NM.024420.3) and ATGL
794 (NCBI RefSeq NM.020376.4) were cloned into the pcDNA 4/HisMaxC vector (Thermo Fisher
795 Scientific, USA) using Gibson assembly cloning kits (New England Biolabs, USA), after
796 removal of the N-terminal His-tag region. All of the other chemicals were of at least analytical
797 grade, and were purchased from Sigma-Aldrich (USA) or Serva (Germany).
798
799 ***Cell culture and treatments***
800 MDA-MB-231 cells were cultured in RPMI-1640 medium, A549 cells in DMEM/F12 medium
801 containing 2 mM L-glutamine (Gibco, USA), and HeLa cells in DMEM-Glutamax medium, all
802 supplemented with 10% foetal bovine serum. Adherent cells were detached using TrypLE
803 Select. Unless otherwise indicated, the cells were seeded in 24-well plates at a density of 3
804 $\times 10^4$ (MDA-MB-231), 2.5 $\times 10^4$ (A549) or 1.5 $\times 10^4$ (HeLa) cells/well and grown for 48 h in
805 complete medium, followed by 24 h of serum deprivation in their respective media containing
806 0.02% EFAF-BSA. Aliquots of stock solutions of AA and PGE_2 in absolute ethanol were stored
807 under argon at –80 ºC. Prior to addition to cell cultures, AA was resuspended in the relevant
808 complete medium and incubated for 1 h at room temperature. Unless otherwise indicated,
809 T863 and PF-06424439 were added to cells 2 h before treatments with recombinant hGX
810 $sPLA_2$ (1–10 nM) or AA (10 μM), and were present in the medium for the duration of the
811 treatments. Prior to addition to cell culture, radiolabelled [^{14}C]-OA was saponified by removing
812 ethanol from the stock aliquot of [^{14}C]-OA and resuspending in 50 μL 0.1 mM NaOH. Saponified
813 [^{14}C]-OA was incubated in the relevant complete medium for 30 min at room temperature and
814 stored at –20 ºC.
815

816 ***Silencing of ATGL and cPLA$_2$α expression using small-interfering RNAs***

817 Reverse transfection was performed in 24-well plates at cell densities of 6 ×10^4 (MDA-MB-
818 231), 5 ×10^4 (A549) or 3 ×10^4 (HeLa) cells/well, or in 6-well plates at 3 ×10^5 (MDA-MB-231),
819 2.5 ×10^5 (A549) or 1.5 ×10^5 (HeLa) cells/well. Gene expression silencing was performed with
820 a 20 nM mixture of two ATGL-specific siRNAs (10 nM each) or a 40 nM mixture of four siRNAs
821 specific for cPLA$_2$α. Non-targeting siRNA controls contained 20 nM (for ATGL) or 40 nM (for
822 cPLA$_2$α) AllStars Negative Control siRNA (Qiagen). Transfection complexes were generated
823 using 1 µL/well Lipofectamine RNAiMAX in 24-well plates, or 7.5 µL/well in 6-well plates, with
824 Opti-MEM medium, according to manufacturer instructions.

825

826 ***Transient overexpression of ATGL and cPLA$_2$α***

827 For transient overexpression experiments, the cells were seeded in complete medium in 24-
828 well plates at a density of 9 ×10^4 (MDA-MB-231), 6 ×10^4 (A549) and 4.5 ×10^4 (HeLa) cells/well,
829 or in 6-well plates at 4.5 ×10^5 (MDA-MB-231), 3 ×10^5 (A549) and 2.5 ×10^5 (HeLa) cells/well.
830 Cells were then incubated for 24 h in complete medium, washed, and transfected with 0.5
831 µg/well plasmid DNA in 24-well plates, or 2.5 µg/well in 6-well plates, using Lipofectamine 3000
832 and Opti-MEM medium, according to manufacturer instructions; they were then left for 6 h in
833 serum-depleted medium containing 0.02% EFAF-BSA (serum starvation). After 6 h, the cells
834 were washed and treated according to the experimental set-up.

835

836 ***Real-time quantitative PCR***

837 Real-time quantitative (q)PCR analysis was performed as described previously (Pucer *et al*,
838 2013; Brglez *et al*, 2014b). Briefly, the cells were seeded in complete medium in 6-well plates
839 at 3 ×10^5 (MDA-MB-231), 2.5 ×10^5 (A549) and 1.5 ×10^5 (HeLa cells) cells/well, grown 48 h in
840 complete medium, followed by 24 h under serum deprivation in medium containing 0.02%
841 EFAF-BSA. Total RNA was isolated from cell lysates and first-strand cDNA was generated
842 using High-Capacity cDNA Reverse Transcription kits (Applied Biosystems, USA), according
843 to the manufacturer instructions. qPCR analysis was performed on a StepOnePlus real-time
844 PCR system (Thermo Scientific, USA) using FastStart Universal SYBR Green Master (Rox;
845 Roche, Switzerland). Calibrator cDNA was transcribed from Quantitative PCR Human
846 Reference Total RNA (Agilent Technologies, USA). Relative gene expression was calculated
847 upon normalisation to two reference genes, considering primer-specific PCR efficiency and
848 error propagation.

849

850 ***Western blotting***

851 The cells were seeded in complete medium in 6-well plates and reverse transfected with
852 siRNAs and/or transiently transfected with pDNA, as described above. Cell lysates were
853 prepared by scrapping adherent cells in Tris-glycine sodium dodecyl sulphate (SDS) sample
854 buffer (2×) (Novex, Life Technologies, USA) that contained 800 mM dithiothreitol (Sigma-
855 Aldrich, USA), with the addition of Halt protease inhibitor cocktail (Thermo Scientific, USA).
856 Lysates were incubated at 95 °C for 10 min and stored on ice. Total protein concentrations
857 were determined using Pierce 660 nm protein assays (Thermo Scientific, USA). Proteins (10–
858 40 μg) were separated on 10% SDS-PAGE gels and then transferred to nitrocellulose
859 membranes (Serva, Germany). The membranes were blocked for 1 h (for ATGL) or 2 h (for
860 $cPLA_2\alpha$) in 5% non-fat dry milk in TBS/0.1% Tween-20 (TBST) or in 1% Western blocking
861 reagent (WBR) (Roche Applied Science, Germany) in TBS (for β-actin), and incubated
862 overnight at 4 °C in the presence of rabbit anti-human primary antibodies for ATGL (1:1000
863 dilution) or mouse anti-human primary antibodies for $cPLA_2\alpha$ (1:250 dilution), both in 5% non-
864 fat dry milk in TBST, or in rabbit anti-human primary antibodies for β-actin (1:5000 dilution) in
865 0.5% WBR in TBS. After washing with TBST, the membranes were incubated for 1 h with
866 horseradish-peroxidase-conjugated secondary antibodies (1:10,000 dilution) in 5% non-fat dry
867 milk in TBST for ATGL, in 0.5% WBR in TBST for $cPLA_2\alpha$, and in 0.5% WBR in TBS for β-
868 actin. The signals were visualised using Lumi-Light Western Blotting Substrate (Roche Applied
869 Science, Germany) on a Gel Doc XR system (Bio-Rad, USA).

870

871 ***Neutral lipid quantification by flow cytometry***

872 Cellular neutral lipid levels were quantified by flow cytometry as described previously (Pucer
873 *et al*, 2013). Floating and adherent cells were harvested and centrifuged at 300× *g* for 10 min,
874 and the pellets were resuspended in 500 μL 1 μg/mL Nile Red solution in DPBS. After a 10-
875 min incubation in the dark, cell analysis was performed by flow cytometry on a FACSCalibur
876 system, equipped with a 488-nm Ar-ion laser, and using the CellQuest software (Becton
877 Dickinson, USA) and an FL-1 (530/30) filter, for at least 2×10^4 events per sample.

878

879 ***Triglyceride assays***

880 Cellular TAG contents were determined using TAG assay kits - quantification (Abcam, USA).
881 MDA-MB-231 and HeLa cells were seeded in 6-well plates at 1.5×10^5 and 7×10^4 cells/well,
882 respectively. After 24 h, MDA-MB-231 cells were treated with 10 nM hGX $sPLA_2$ and HeLa
883 cells with 1 nM hGX $sPLA_2$ in complete medium for 48 h. Cell lysates were prepared and used
884 for TAG quantification according to the manufacturer instructions.

885

886 ***Glycerol release assays***

887 Cellular lipolytic activity was assessed by measuring glycerol release in cell supernatants.
888 Briefly, the cells were reverse transfected and seeded in 48-well plates at a density of 3 $\times 10^4$
889 (MDA-MB-231 cells) or 1.5 $\times 10^4$ cells/well (HeLa cells). For reverse transfection, 0.5 µL
890 Lipofectamine RNAiMAX, 20 nM siRNA and 40 µL OPTI-MEM medium were used per well.
891 After 24 h, the cells were washed, placed in serum-starvation medium containing 0.02% EFAF-
892 BSA, and transfected with 0.250 µg plasmid DNA for protein overexpression using
893 Lipofectamine 3000, according to the manufacturer instructions. After 6 h, the cells were
894 washed and treated with 10 nM hGX $sPLA_2$ for 48 h in complete medium. Cell supernatants
895 were collected in low-binding microcentrifuge tubes and centrifuged for 10 min (4 °C, 16,000×
896 *g*), and the glycerol concentrations were determined using the Glycerol Cell-Based assay kits
897 (Cayman Chemicals, USA), according to the manufacturer instructions.

898

899 ***Untargeted lipidomic analysis of phospholipids and triglycerides***

900 For untargeted lipidomic analysis of hGX-$sPLA_2$-induced changes in TAG acyl-chain
901 composition, MDA-MB-231 cells were seeded in complete medium on 10-cm plates at 1 $\times 10^6$
902 cells/plate. After 24 h, the cells were treated with 1 nM hGX $sPLA_2$ in complete medium for 48
903 h. Cell lysates were prepared by washing the cells twice with DPBS and scraping in 1 mL lysis
904 buffer (20 mM Tris-HCl, pH 7.4, 2 mM EDTA, 2 µL Halt protease inhibitor cocktail), followed
905 by centrifugation for 10 min (1000× *g*, 4 °C). Cell pellets were resuspended in 150 µL lysis
906 buffer and sonicated on ice. Total lipids were extracted in chloroform/methanol (2/1, v/v)
907 containing 1% acetic acid, 500 nM butylated hydroxytoluene (BHT) and internal standards (IS;
908 100 pmol 17:0/17:0/17:0 triacylglycerol, Larodan, Solna, Sweden) under constant shaking for
909 1 h (30 rpm/min, 4 °C). After centrifugation at 3300 rpm for 20 min at room temperature, the
910 upper aqueous layer was removed, and the organic solvents were evaporated using a sample
911 concentrator (Techne, UK) equipped with the Dri-Block DB-3 heater (Techne, UK). Lipids were
912 resolved in 200 µL chloroform and stored at –20 ºC. Prior to mass spectrometry, the samples
913 were placed at room temperature and dried and resuspended in 1 mL chloroform/methanol
914 (2/1, v/v). An aliquot of each sample (20 µL) was mixed with 180 µL isopropanol, and 5 µL was
915 used for chromatographic separation on an Acquity-UPLC system (Waters Corporation,
916 Milford, MA, USA), equipped with an ACQUITY BEH C18 column (2.1 × 50 mm, 1.7 µm;
917 Waters Corporation, Milford, MA, USA). A SYNAPT^{TM}G1 qTOF HD mass spectrometer
918 (Waters Corporation, Milford, MA, USA) equipped with an ESI source was used for detection.
919 Data acquisition was carried out using the MassLynx 4.1 software (Waters), and the lipid
920 classes were analysed with the Lipid Data Analyser 1.6.2 software. The data were normalised
921 for recovery, extraction and ionisation efficacy by calculating analyte/internal standard ratios
922 (AU) and expressed as percentage composition.

923 To determine the changes in the phospholipid and TAG profiles in ATGL-depleted and
924 $cPLA_2\alpha$-depleted cells, MDA-MB-231 cells were seeded in complete medium on 6-well plates
925 at 3×10^5 cells/well and reverse transfected with ATGL-specific and/or $cPLA_2\alpha$-specific siRNAs,
926 as described above. After 24 h, the cells were washed and grown for 48 h in complete medium
927 in the presence or absence of 10 nM $sPLA_2$. The cells were then washed twice with DPBS and
928 serum starved for the following 24 h in RPMI-1640 medium containing 0.02% EFAF-BSA.
929 Samples were collected (at 0, 3, 24 h of serum starvation) by placing the plates on ice, washing
930 the cells twice with ice-cold DPBS, and scraping the cells in 300 µL lysis buffer, followed by
931 centrifugation for 10 min (1000× *g*, 4 °C). The cell pellets were resuspended in 150 µL lysis
932 buffer and sonicated on ice. Then, 10 µL of each sample was used for protein determination
933 (Pierce 660). Total lipids were extracted by transferring the pellets into 2 ml tubes followed by
934 homogenisation in 700 µL of a 3:1 (v/v) mixture of methyl tert-butyl ether and methanol,
935 containing 1% acetic acid, 500 nM BHT and IS (8 pmol 18:3/18:3/18:3 triacylglycerol, 14:0/14:0
936 phosphatidylcholine, Larodan, Solna, Sweden; 50 pmol 17:0/17:0 phosphatidylethanolamine,
937 12 pmol 17:0/17:0 phosphatidylserine, Avanti Polar Lipids, Alabaster, AL, USA), with two steel
938 beads on a mixer mill (30 Hz, Retsch, Germany) at 4 °C. After homogenisation, the samples
939 were mixed at room temperature under constant shaking for 30 min. Then 140 µL distilled H_2O
940 was added, and the samples were thoroughly mixed and centrifugated (14,000 rpm, 10 min),
941 to establish phase separation. The organic phase (500 µL) was transferred into new tubes and
942 the organic solvent was evaporated off under a stream of nitrogen. The residual protein slurry
943 was dried and used for protein determination after lysis in 400 µL NaOH/SDS (0.3 M/0.1%).
944 Prior to mass spectrometry analysis, the lipids were resolved in 200 µL isopropanol
945 /methanol/H_2O (70/25/10, v/v/v). Chromatographic separation was performed on a 1290
946 Infinity II LC system (Agilent, Santa Clara, CA, USA) equipped with a C18 column (Zorbax
947 RRHD Extend; 2.1 × 50 mm, 1.8 µm; Agilent, Santa Clara, CA, USA), using a 16 min linear
948 gradient from 60% solvent A (H_2O; 10 mM ammonium acetate, 0.1% formic acid, 8 µM
949 phosphoric acid) to 100% solvent B (2-propanol; 10 mM ammonium acetate, 0.1% formic acid,
950 8 µM phosphoric acid). The column compartment was kept at 50 °C. A Q-TOF mass
951 spectrometer (6560 Ion Mobility; Agilent, Santa Clara, CA, USA) equipped with electrospray
952 ionisation source (Dual AJS) was used for detection of the lipids in positive and negative Q-
953 TOF mode. Data acquisition was carried out using the MassHunter Data Acquisition software
954 (B.09; Agilent, Santa Clara, CA, USA). Lipid species were manually identified and lipid data
955 were processed using MassHunter Quantitative Analysis (B.09.00; Agilent, Santa Clara, CA,
956 USA). Data were normalised for recovery, extraction and ionisation efficiency by calculation of
957 the analyte/ internal standard ratios, and are expressed as fmol/µg protein. Lipidomic data
958 were analysed by multiple t-test analysis of log-transformed data to compare two conditions at
959 a time, using GraphPad Prism 9.0.2 (GraphPad Software, USA). Lipid ontology enrichment

960 analysis was performed using the LION/web enrichment and principal component analysis
961 modules (Molenaar *et al*, 2019).
962
963 ***Thin layer chromatography of radiolabelled cellular lipids***
964 MDA-MB-231 cells were seeded in complete medium on T-25 flasks at a density of 5 ×10^5
965 cells/flask. After 24 h, the cells were treated with 1 µCi/sample [^{14}C]-OA for 18 h, washed twice
966 with DPBS, and treated with 10 nM hGX $sPLA_2$ under three different conditions: (a) 24 h in
967 complete medium; (b) 24 h in complete medium followed by 96 h serum deprivation in 0.02%
968 EFAF-BSA in RPMI-1640; and (c) 24 h in 0.02% FAF-BSA in RPMI-1640 followed by 96 h in
969 0.02% EFAF-BSA in RPMI-1640. Lipid extraction was performed with 1 mL hexane/
970 isopropanol (3:2, v/v) under constant shaking for 10 min at room temperature, and repeated
971 twice. The samples were stored in microcentrifuge tubes at –20 ºC. Total proteins were isolated
972 from cell remnants in 2 mL lysis buffer (0.3 M NaOH, 0.1% SDS) under constant shaking for 2
973 h at room temperature. Protein concentrations were determined using BSA standard solutions
974 (Thermo Scientific, USA) and the BCA protein assay reagent (Thermo Scientific, USA).
975 Samples of cellular lipids were dried, resuspended in 20 µL chloroform (repeated three times),
976 and loaded onto the stationary phase of silica TLC plates immobilised on a polymeric binder
977 (Merck, Germany). Dry TLC plates were developed using chloroform/ methanol/ acetone/
978 acetic acid/ H_2O (50/10/20/12/5, v/v/v/v/v) for phospholipid separation, and hexane/ diethyl
979 ether/ acetic acid (70:29:1, v/v/v) for neutral lipid separation. Radiolabelled lipids were detected
980 with autoradiography using an imager (PhosphorImager SI; Amersham Biosciences, UK). To
981 quantify the TAG content, the TLC plates were incubated in an iodine steam, the TAG patches
982 were cut out and placed in vials with scintillation cocktail, and the radioactivity was measured
983 using a liquid scintillation counter (Tri-Carb 1600CA; PerkinElmer, USA).
984
985 ***Lipid mediator analysis using UPLC-MS-MS***
986 MDA-MB-231 cells were seeded in complete medium in 6-well plates at 3 × 10^5 cells/well and
987 reverse transfected with ATGL-specific siRNAs as described above. After 24 h, the cells were
988 treated with 10 nM hGX $sPLA_2$ for 48 h, washed with DPBS and left for 24 h in RPMI-1640
989 medium containing 0.02% EFAF-BSA. The cells were lysed and total protein concentrations
990 were determined as described above. Supernatants were collected in low-binding
991 microcentrifuge tubes, centrifuged at 4 °C (16,000× *g*, 10 min) and stored at –80 °C before
992 shipping on dry ice. Lipid mediator analysis using UPLC-MS-MS was performed as described
993 previously (Werz *et al*, 2018) with some minor modifications (Werner *et al*, 2019). Briefly,
994 aliquots of the supernatants were first mixed with the same volume of ice-cold methanol
995 containing deuterium-labelled internal standards (200 nM d8-5S-HETE, d4-LTB_4, d5-LXA_4, d5-
996 RvD2, d4-PGE_2 and 10 µM d8-AA; Cayman Chemical/Biomol GmbH, Hamburg, Germany) to

997 facilitate quantification and sample recovery. Samples were kept at −20 °C for 60 min to allow
998 protein precipitation. After centrifugation (1200× *g*, 4 °C, 10 min) 8 mL of acidified H_2O was
999 added (final pH = 3.5) and the samples were subjected to solid phase extraction. The solid
1000 phase cartridges (Sep-Pak® Vac 6cc 500 mg/ 6 mL C18; Waters, Milford, MA) were
1001 equilibrated with 6 mL methanol and then with 2 mL H_2O prior sample loading onto the
1002 columns. After washing with 6 mL H_2O and additional 6 mL *n*-hexane, lipid mediators were
1003 eluted with 6 mL methyl formate. The eluates were brought to dryness using a TurboVap LV
1004 evaporation system (Biotage, Uppsala, Sweden) and resuspended in 100 µL methanol/water
1005 (50/50, v/v) for UPLC-MS-MS analysis. Lipid mediator profiling was analyzed with an Acquity™
1006 UPLC system (Waters, Milford, MA, USA) and a QTRAP 5500 Mass Spectrometer (ABSciex,
1007 Darmstadt, Germany), equipped with a Turbo V™ Source and electrospray ionization. Lipid
1008 mediators were separated using an ACQUITY UPLC® BEH C18 column (1.7 µm, 2.1 × 100
1009 mm; Waters, Eschborn, Germany) at 50 °C with a flow rate of 0.3 ml/min and a mobile phase
1010 consisting of methanol/water/acetic acid of 42/58/0.01 (v/v/v) that was ramped to 86/14/0.01
1011 (v/v/v) over 12.5 min and then to 98/2/0.01 (v/v/v) for 3 min (Werner *et al*, 2019). The QTrap
1012 5500 was operated in negative ionization mode using scheduled multiple reaction monitoring
1013 (MRM) coupled with information-dependent acquisition. The scheduled MRM window was 60
1014 sec, optimized lipid mediator parameters were adopted (Werner *et al*, 2019), and the curtain
1015 gas pressure was set to 35 psi. The retention time and at least six diagnostic ions for each lipid
1016 mediator were confirmed by means of external standards (Cayman Chemical/Biomol GmbH,
1017 Hamburg, Germany). Quantification was achieved by calibration curves for each lipid mediator.
1018 Linear calibration curves were obtained for each lipid mediator and gave r^2 values of 0.998 or
1019 higher (for fatty acids 0.95 or higher). Additionally, the limit of detection for each targeted lipid
1020 mediator was determined (Werner *et al*, 2019).
1021

1022 ***ELISA-based quantification of PGE_2 in cell supernatants***

1023 The amounts of PGE_2 released into culture medium were determined using a commercial
1024 enzyme immunoassay (Prostaglandin E_2 Express ELISA kits; Cayman Chemicals, USA). The
1025 cells were seeded in 24-well plates and reverse transfected with siRNAs as described above.
1026 After 24 h, the cells were transfected with plasmid DNA as described above and treated with
1027 10 nM hGX $sPLA_2$ and/or 10 µM AA and/or a mixture of 20 µM T863 and 20 µM PF-06424439
1028 (DGAT inhibitors) for 48 h in complete medium. The cells were then washed and serum starved
1029 for 24 h in the appropriate culture medium containing 0.02% EFAF-BSA. In some experiments,
1030 DGAT inhibitors were included in the serum-starvation phase. Cell supernatants were collected
1031 in low-binding microcentrifuge tubes, centrifuged at 4 °C (16,000× *g*, 10 min) and immediately
1032 used for analysis or stored at –80 °C for up to 7 days. For analysis, 50 µL undiluted samples
1033 were used, and standard curves prepared by diluting the PGE_2 standard in culture medium.

1034

1035 ***Confocal microscopy***

1036 Cytosolic lipid droplets were visualised using BODIPY 493/503 neutral lipid staining. Cells were
1037 reverse transfected and seeded on glass-bottomed culture plates at 6 ×10^4 (MDA-MB-231
1038 cells), 3 ×10^4 (HeLa cells) and 5 ×10^4 (A549 cells) cells/well. Twenty-four hours later, the media
1039 were replaced and the cells were treated with 10 nM hGX $sPLA_2$ and the DGAT inhibitors in
1040 complete medium for 48 h, followed by 24-h starvation in serum-free medium containing 0.02%
1041 EFAF-BSA. For confocal microscopy, the cells were washed twice with DPBS, stained with 1
1042 µg/mL BODIPY 493/503 and 1 µg/mL Hoechst stain solution in RPMI-1640 medium for 15 min
1043 in a CO_2 incubator, washed twice with DPBS, and left in fresh RPMI-1640 medium. Live
1044 imaging was carried out at the beginning of and after the 24-h serum starvation using a
1045 confocal laser scanning microscope (LSM 710; Carl Zeiss, Germany) and a stage-top
1046 microscope CO_2 incubation system (Tokai Hit, Japan). Images were processed using the Zen
1047 software (Carl Zeiss, Germany).

1048

1049 ***Lipid droplet counting and diameter analysis***

1050 Confocal microscopy images of BODIPY 493/503 stained lipid droplets were used for computer
1051 image analysis with the ImageJ software (National Institutes of Health, USA) and the Lipid
1052 Droplet Counter Plugin (https://doi.org/10.5281/zenodo.2581434). Analysis was performed on
1053 32-bit two-dimensional images, whereby the numbers and sizes of the lipid droplets were
1054 determined according to the plugin instructions. Lipid droplet diameters were calculated from
1055 the lipid droplet surface areas. Analyses were performed on at least 40 cells/sample. Data
1056 were loaded into the Prism 9.0.2 software (GraphPad Software, USA), with the geometric
1057 means of the lipid droplet diameters and numbers calculated per individual cell in the samples,
1058 followed by the statistical analysis.

1059

1060 ***Cell proliferation***

1061 MDA-MB-231/Luciferase-2A-RFP cells were seeded in complete medium in 96-well plates at
1062 5 ×10^3 cells/well in at least triplicates. After 24 h, the cells were treated with 20 µM DGAT1 and
1063 20 µM DGAT2 inhibitors and/or 1 µM PGE_2 and/or 10 nM hGX $sPLA_2$ as described above, and
1064 left in complete medium for 72 h. PGE_2 was replenished every 24 h by direct addition to the
1065 culture medium. In transient transfection experiments, the cells were seeded in complete
1066 medium on 48-well plates at 3 ×10^4 (MDA-MB-231/Luciferase-2A-RFP cells) or 1.5 ×10^4 (A549
1067 cells) cells/well. After 24 h, the cells were washed and transfected with 0.250 µg plasmid
1068 DNA/well using 0.5 µL P3000 reagent and 1 µL Lipofectamine 3000 in OptiMEM medium, and
1069 incubated in RPMI-1640 (MDA-MB-231) or DMEM/F12 with 2 mM L-glutamine (A549)

containing 0.02% EFAF-BSA. After 6 h, the cells were treated with 10 nM recombinant hGX $sPLA_2$ in complete medium, with 25 μM (A549) or 50 μM (MDA-MB-231) indomethacin, 25 μM nordihydroguaiaretic acid, and/or 20 μM each of the T863 and PF-06424439 DGAT1 and DGAT2 inhibitors, respectively. A549 cell proliferation was determined after 48 h using the direct cell proliferation assay kits (CyQUANT; Invitrogen, USA). MDA-MB-231/Luciferase-2A-RFP cell proliferation was determined by measuring RFP fluorescence emission (excitation, 558 nm; emission, 583 nm) on a microplate reader (Infinite M1000; Tecan, Austria). The final data were obtained after subtracting the background signal of the blank samples that contained culture medium without cells.

Statistical analysis

Statistical analyses were performed using Prism 9.0.2 (GraphPad Software, USA). Unless otherwise indicated, the data are presented as means ±SEM of at least three independent experiments. Statistical significance was determined using t-tests, one-way or two-way ANOVA, followed by Bonferroni, Sidak or Tukey's multiple comparison tests. P values <0.05 were considered as statistically significant.

Acknowledgements

We are grateful to Ana Temprano Lopez, Petra Hruševar, Ana Kump, Ema Guštin, Belen Vilanova Baeza and Špela Koren for their technical help, Dr. Mojca Pavlin (University of Ljubljana, Slovenia), Dr. Brett McKinnon (Berne University Hospital, Switzerland), Dr. Merce Miranda (Joan XXIII University Hospital Tarragona, Spain) and Dr. Boris Rogelj (Jožef Stefan Institute, Slovenia) for kindly providing cell lines. We thank Dr. Chris Berrie for critical reading of the manuscript. This work was supported by a Young Researcher grant (1000-15-106) and a postdoctoral grant (Z3-2650) to E.J.J., a Research Programme grant (P1-0207) and a Research Project grant (J7-1818) to T.P., from the Slovenian Research Agency; by the Deutsche Forschungsgemeinschaft (DFG, German Research Foundation), Project-ID 239748522 - SFB 1127 ChemBioSys, and the EU COST Action CA19105 EpiLipidNet.

Author contributions

EJJ performed most of the experiments, analysed the data, and prepared the figures and initial manuscript drafts; APJ and VB performed initial lipidomic experiments; TOE and RZ performed mass spectrometry analyses, designed experiments, contributed ideas and revised the paper; GL contributed materials, ideas and revised the paper; PMJ, JG and OW performed lipid

mediator mass spectrometry analyses and revised the paper; TP conceptualised the study, analysed the data, prepared the figures and illustrations, and wrote the manuscript.

Conflicts of interest

The authors declare that they have no conflicts of interest.

1113 ## References

1114

1115 Accioly MT, Pacheco P, Maya-Monteiro CM, Carrossini N, Robbs BK, Oliveira SS, Kaufmann
1116 C, Morgado-Diaz JA, Bozza PT & Viola JPB (2008) Lipid bodies are reservoirs of
1117 cyclooxygenase-2 and sites of prostaglandin E_2 synthesis in colon cancer cells. *Cancer*
1118 *Res* 68: 1732–1740

1119 Ackerman D, Tumanov S, Qiu B, Michalopoulou E, Spata M, Azzam A, Xie H, Simon MC &
1120 Kamphorst JJ (2018) Triglycerides promote lipid homeostasis during hypoxic stress by
1121 balancing fatty acid saturation. *Cell Reports* 24: 2596–2605.e5

1122 Ait-Oufella H, Herbin O, Lahoute C, Coatrieux C, Loyer X, Joffre J, Laurans L, Ramkhelawon
1123 B, Blanc-Brude O, Karabina S, *et al* (2013) Group X secreted phospholipase A_2 limits the
1124 development of atherosclerosis in LDL-receptor-null mice. *Arteriosclerosis Thrombosis*
1125 *Vasc Biology* 33: 466–473

1126 Al-Zoughbi W, Pichler M, Gorkiewicz G, Guertl-Lackner B, Haybaeck J, Jahn SW, Lackner C,
1127 Liegl-Atzwanger B, Popper H, Schauer S, *et al* (2016) Loss of adipose triglyceride lipase
1128 is associated with human cancer and induces mouse pulmonary neoplasia. *Oncotarget* 7:
1129 33832–33840.

1130 Antonny B, Vanni S, Shindou H & Ferreira T (2015) From zero to six double bonds:
1131 phospholipid unsaturation and organelle function. *Trends Cell Biol* 25: 427–436

1132 Astudillo AM, Balboa MA & Balsinde J (2019) Selectivity of phospholipid hydrolysis by
1133 phospholipase A_2 enzymes in activated cells leading to polyunsaturated fatty acid
1134 mobilization. *Biochim Biophys Acta - Mol Cell Biol Lipids* 1864: 772–783.

1135 Bailey AP, Koster G, Guillermier C, Hirst EMA, MacRae JI, Lechene CP, Postle AD & Gould
1136 AP (2015) Antioxidant role for lipid droplets in a stem cell niche of *Drosophila*. *Cell* 163:
1137 340–353

1138 Bezzine S, Bollinger JG, Singer AG, Veatch SL, Keller SL & Gelb MH (2002) On the binding
1139 preference of human groups IIA and X phospholipases A_2 for membranes with anionic
1140 phospholipids. *J Biol Chem* 277: 48523–48534

1141 Bonventre J (2004) Cytosolic phospholipase A_2alpha reigns supreme in arthritis and bone
1142 resorption. *Trends Immunol* 25, 116–119

1143 Bosch M, Parton RG & Pol A (2020) Lipid droplets, bioenergetic fluxes, and metabolic flexibility.
1144 *Semin Cell Dev Biol* 108: 33–46

1145 Bosch M, Sweet MJ, Parton RG & Pol A (2021) Lipid droplets and the host–pathogen dynamic:
1146 FATal attraction? *J Cell Biol* 220: e202104005

1147 Bozza PT, Bakker-Abreu I, Navarro-Xavier RA & Bandeira-Melo C (2011) Lipid body function
1148 in eicosanoid synthesis: an update. *Prostaglandins Leukot Essent Fatty Acids* 85: 205–
1149 213
1150 Brglez V, Lambeau G & Petan T (2014a) Secreted phospholipases A_2 in cancer: diverse
1151 mechanisms of action. *Biochimie* 107 Pt A: 114–23
1152 Brglez V, Pucer A, Pungerčar J, Lambeau G & Petan T (2014b) Secreted phospholipases A_2
1153 are differentially expressed and epigenetically silenced in human breast cancer cells.
1154 *Biochem Biophys Res Commun* 445: 230–235
1155 Brok MH den, Raaijmakers TK, Collado-Camps E & Adema GJ (2018) Lipid droplets as
1156 immune modulators in myeloid cells. *Trends Immunol* 39: 380–392
1157 Cao J, Zhou Y, Peng H, Huang X, Stahler S, Suri V, Qadri A, Gareski T, Jones J, Hahm S, *et*
1158 *al* (2011) Targeting acyl-CoA:diacylglycerol acyltransferase 1 (DGAT1) with small
1159 molecule inhibitors for the treatment of metabolic diseases. *J Biol Chem* 286: 41838–
1160 41851
1161 Cao Z, Hao Y, Fung CW, Lee YY, Wang P, Li X, Xie K, Lam WJ, Qiu Y, Tang BZ, *et al* (2019)
1162 Dietary fatty acids promote lipid droplet diversity through seipin enrichment in an ER
1163 subdomain. *Nat Commun* 10: 2902
1164 Castoldi A, Monteiro LB, Bakker N van T, Sanin DE, Rana N, Corrado M, Cameron AM,
1165 Hässler F, Matsushita M, Caputa G, *et al* (2020) Triacylglycerol synthesis enhances
1166 macrophage inflammatory function. *Nat Commun* 11: 4107
1167 Cheng X, Geng F, Pan M, Wu X, Zhong Y, Wang C, Tian Z, Cheng C, Zhang R, Puduvalli V,
1168 *et al* (2020) Targeting DGAT1 ameliorates glioblastoma by increasing fat catabolism and
1169 oxidative stress. *Cell Metab* 32: 229–242.e8
1170 Chitraju C, Mejhert N, Haas JT, Diaz-Ramirez LG, Grueter CA, Imbriglio JE, Pinto S, Koliwad
1171 SK, Walther TC & Farese RV (2017) Triglyceride synthesis by DGAT1 protects adipocytes
1172 from lipid-induced ER stress during lipolysis. *Cell Metab* 26: 407–418.e3
1173 Coleman RA & Mashek DG (2011) Mammalian triacylglycerol metabolism: synthesis, lipolysis,
1174 and signaling. *Chem Rev* 111: 6359–6386
1175 Cruz ALS, Barreto E de A, Fazolini NPB, Viola JPB & Bozza PT (2020) Lipid droplets: platforms
1176 with multiple functions in cancer hallmarks. *Cell Death Dis* 11: 105
1177 Dalli J & Serhan CN (2012) Specific lipid mediator signatures of human phagocytes:
1178 microparticles stimulate macrophage efferocytosis and pro-resolving mediators. *Blood*
1179 120: e60–e72
1180 Dennis EA & Norris PC (2015) Eicosanoid storm in infection and inflammation. *Nat Rev*
1181 *Immunol* 15: 511–523

1182 Dichlberger A, Schlager S, Maaninka K, Schneider WJ & Kovanen PT (2014) Adipose
1183 triglyceride lipase regulates eicosanoid production in activated human mast cells. *J Lipid*
1184 *Res* 55: 2471–2478
1185 Dierge E, Debock E, Guilbaud C, Corbet C, Mignolet E, Mignard L, Bastien E, Dessy C,
1186 Larondelle Y & Feron O (2021) Peroxidation of n-3 and n-6 polyunsaturated fatty acids in
1187 the acidic tumor environment leads to ferroptosis-mediated anticancer effects. *Cell Metab*
1188 33: 1701–1715.e5
1189 Dvorak AM, Dvorak HF, Peters SP, Shulman ES, MacGlashan DW, Pyne K, Harvey VS, Galli
1190 SJ & Lichtenstein LM (1983) Lipid bodies: cytoplasmic organelles important to
1191 arachidonate metabolism in macrophages and mast cells. *J Immunol* 131: 2965–2976
1192 Duchez A-C, Boudreau LH, Naika GS, Rousseau M, Cloutier N, Levesque T, Gelb MH &
1193 Boilard E (2019) Respective contribution of cytosolic phospholipase A2α and secreted
1194 phospholipase A_2 IIA to inflammation and eicosanoid production in arthritis. *Prostaglandins*
1195 *Other Lipid Mediat* 143: 106340
1196 Eichmann TO, Kumari M, Haas JT, Farese RV, Zimmermann R, Lass A & Zechner R (2012)
1197 Studies on the substrate and stereo/ regioselectivity of adipose triglyceride lipase,
1198 hormone-sensitive lipase, and diacylglycerol-O-acyltransferases. *J Biol Chem* 287:
1199 41446–41457
1200 Fishbein A, Hammock BD, Serhan CN & Panigrahy D (2020) Carcinogenesis: failure of
1201 resolution of inflammation? *Pharmacol Ther* 218: 107670
1202 Futatsugi K, Kung DW, Orr STM, Cabral S, Hepworth D, Aspnes G, Bader S, Bian J, Boehm
1203 M, Carpino PA, *et al* (2015) Discovery and optimization of imidazopyridine-based inhibitors
1204 of diacylglycerol acyltransferase 2 (DGAT2). *J Med Chem* 58: 7173–7185
1205 Gartung A, Zhao J, Chen S, Mottillo E, VanHecke GC, Ahn Y-H, Maddipati KR, Sorokin A,
1206 Granneman J & Lee M-J (2016) Characterization of eicosanoids produced by adipocyte
1207 lipolysis: implication of cyclooxygenase-2 in adipose inflammation. *J Biol Chem* 291:
1208 16001–16010
1209 Giedt MS, Thomalla JM, Johnson MR, Lai ZW, Tootle TL & Welte MA (2021) Lipid droplets
1210 regulate actin remodeling via prostaglandin signaling during *Drosophila* oogenesis.
1211 *bioRxiv* 2021.08.02.454724; doi: https://doi.org/10.1101/2021.08.02.454724 [PREPRINT]
1212 Greenberg AS, Coleman RA, Kraemer FB, McManaman JL, Obin MS, Puri V, Yan Q-W,
1213 Miyoshi H & Mashek DG (2011) The role of lipid droplets in metabolic disease in rodents
1214 and humans. *J Clin Invest* 121: 2102–2110
1215 Greene ER, Huang S, Serhan CN & Panigrahy D (2011) Regulation of inflammation in cancer
1216 by eicosanoids. *Prostag Other Lipid Mediat* 96: 27–36

1217 Gubern A, Casas J, Barceló-Torns M, Barneda D, Rosa X de la, Masgrau R, Picatoste F,
1218 Balsinde J, Balboa MA & Claro E (2008) Group IVA phospholipase A_2 is necessary for the
1219 biogenesis of lipid droplets. *J Biol Chem* 283: 27369–27382
1220 Guillaume C, Payré C, Jemel I, Jeammet L, Bezzine S, Naika GS, Bollinger J, Grellier P, Gelb
1221 MH, Schrével J, *et al* (2015) In vitro anti-*Plasmodium falciparum* properties of the full set
1222 of human secreted phospholipases A_2. *Infect Immun* 83: 2453–2465
1223 Guijas C, Rodríguez JP, Rubio JM, Balboa MA & Balsinde J (2014) Phospholipase A_2
1224 regulation of lipid droplet formation. *Biochim Biophys Acta* 1841: 1661–1671
1225 Haemmerle G, Moustafa T, Woelkart G, Büttner S, Schmidt A, Weijer T van de, Hesselink M,
1226 Jaeger D, Kienesberger PC, Zierler K, *et al* (2011) ATGL-mediated fat catabolism
1227 regulates cardiac mitochondrial function via PPAR-α and PGC-1. *Nat Med* 17: 1076–1085
1228 Hanasaki K, Ono T, Saiga A, Morioka Y, Ikeda M, Kawamoto K, Higashino K, Nakano K,
1229 Yamada K, Ishizaki J & Arita H (1999) Purified group X secretory phospholipase A_2 induced
1230 prominent release of arachidonic acid from human myeloid leukemia cells. *J Biol Chem*
1231 274: 34203–34211
1232 Hayashi D, Mouchlis VD & Dennis EA (2021) Omega-3 *versus* omega-6 fatty acid availability
1233 is controlled by hydrophobic site geometries of phospholipase A_2s. *J Lipid Res* 62: 100113
1234 doi: 10.1016/j.jlr.2021.100113 [paper in press]
1235 Henne WM, Reese ML & Goodman JM (2018) The assembly of lipid droplets and their roles
1236 in challenged cells. *EMBO J* 37: e98947
1237 Jarc E, Kump A, Malavašič P, Eichmann TO, Zimmermann R & Petan T (2018) Lipid droplets
1238 induced by secreted phospholipase A_2 and unsaturated fatty acids protect breast cancer
1239 cells from nutrient and lipotoxic stress. *Biochim Biophys Acta - Mol Cell Biol Lipids* 1863:
1240 247–265
1241 Jarc E & Petan T (2020) A twist of FATe: lipid droplets and inflammatory lipid mediators.
1242 *Biochimie* 169: 69–87
1243 Koizume S & Miyagi Y (2016) Lipid droplets: a key cellular organelle associated with cancer
1244 cell survival under normoxia and hypoxia. *Int J Mol Sci* 17: 1430
1245 Koliwad SK, Streeper RS, Monetti M, Cornelissen I, Chan L, Terayama K, Naylor S, Rao M,
1246 Hubbard B & Farese RV (2010) DGAT1-dependent triacylglycerol storage by
1247 macrophages protects mice from diet-induced insulin resistance and inflammation. *J Clin*
1248 *Invest* 120: 756–767
1249 Koundouros N, Karali E, Tripp A, Valle A, Inglese P, Perry NJS, Magee DJ, Virmouni SA, Elder
1250 GA, Tyson AL, *et al* (2020) Metabolic fingerprinting links oncogenic PIK3CA with enhanced
1251 arachidonic-acid-derived eicosanoids. *Cell* 181: 1596–1611.e27
1252 Krahmer N, Farese RV & Walther TC (2013) Balancing the fat: lipid droplets and human
1253 disease. *EMBO Mol Med* 5: 905–915

1254 Lambeau G & Gelb MH (2008) Biochemistry and physiology of mammalian secreted
1255 phospholipases A_2. *Annu Rev Biochem* 77: 495–520
1256 Leslie CC (2015) Cytosolic phospholipase A_2: physiological function and role in disease. *J Lipid*
1257 *Res* 56: 1386–1402
1258 Li X, Shridas P, Forrest K, Bailey W & Webb NR (2010) Group X secretory phospholipase A_2
1259 negatively regulates adipogenesis in murine models. *FASEB J* 24: 4313–4324
1260 Liesenfeld DB, Grapov D, Fahrmann JF, Salou M, Scherer D, Toth R, Habermann N, Bohm J,
1261 Schrotz-King P, Gigic B, *et al* (2015) Metabolomics and transcriptomics identify pathway
1262 differences between visceral and subcutaneous adipose tissue in colorectal cancer
1263 patients: the ColoCare study. *Am J Clin Nutrition* 102: 433–443
1264 Listenberger LL, Han X, Lewis SE, Cases S, Farese RV, Ory DS & Schaffer JE (2003)
1265 Triglyceride accumulation protects against fatty acid-induced lipotoxicity. *Proc Natl Acad*
1266 *Sci U S A* 100: 3077–3082
1267 Molenaar MR, Jeucken A, Wassenaar TA, van de Lest CHA, Brouwers JF & Helms JB (2019)
1268 LION/web: a web-based ontology enrichment tool for lipidomic data analysis. *Gigascience*
1269 8: giz061
1270 Moreira LS, Piva B, Gentile LB, Mesquita-Santos FP, D'Avila H, Maya-Monteiro CM, Bozza
1271 PT, Bandeira-Melo C & Diaz BL (2009) Cytosolic phospholipase A_2-driven PGE2 synthesis
1272 within unsaturated fatty acids-induced lipid bodies of epithelial cells. *Biochim Biophys Acta*
1273 *- Mol Cell Biology Lipids* 1791: 156–165
1274 Mounier CM, Ghomashchi F, Lindsay MR, James S, Singer AG, Parton RG & Gelb MH (2004)
1275 Arachidonic acid release from mammalian cells transfected with human groups IIA and X
1276 secreted phospholipase A_2 occurs predominantly during the secretory process and with
1277 the involvement of cytosolic phospholipase A_2-α. *J Biol Chem* 279: 25024–25038
1278 Murakami M (2017) Lipoquality control by phospholipase A_2 enzymes. *Proc Jpn Acad Ser B*
1279 93: 677–702
1280 Murakami M, Sato H & Taketomi Y (2020) Updating phospholipase A_2 biology. *Biomolecules*
1281 10: 1457
1282 Murakami M, Taketomi Y, Miki Y, Sato H, Hirabayashi T & Yamamoto K (2011) Recent
1283 progress in phospholipase A_2 research: from cells to animals to humans. *Prog Lipid Res*
1284 50: 152–192
1285 Murase R, Sato H, Yamamoto K, Ushida A, Nishito Y, Ikeda K, Kobayashi T, Yamamoto T,
1286 Taketomi Y & Murakami M (2016) Group X secreted phospholipase A_2 releases ω3
1287 polyunsaturated fatty acids, suppresses colitis, and promotes sperm fertility. *J Biol Chem*
1288 291: 6895–6911

1289 Nguyen TB, Louie SM, Daniele JR, Tran Q, Dillin A, Zoncu R, Nomura DK & Olzmann JA
1290 (2017) DGAT1-dependent lipid droplet biogenesis protects mitochondrial function during
1291 starvation-induced autophagy. *Dev Cell* 42: 9–21.e5
1292 Nieman KM, Kenny HA, Penicka CV, Ladanyi A, Buell-Gutbrod R, Zillhardt MR, Romero IL,
1293 Carey MS, Mills GB, Hotamisligil GS, *et al* (2010) Adipocytes promote ovarian cancer
1294 metastasis and provide energy for rapid tumor growth. *Nat Med* 17: 1498–1503
1295 Nomura DK, Lombardi DP, Chang JW, Niessen S, Ward AM, Long JZ, Hoover HH & Cravatt
1296 BF (2011) Monoacylglycerol lipase exerts dual control over endocannabinoid and fatty acid
1297 pathways to support prostate cancer. *Chem Biol* 18: 846–856
1298 Nomura DK, Long JZ, Niessen S, Hoover HS, Ng S-W & Cravatt BF (2010) Monoacylglycerol
1299 lipase regulates a fatty-acid network that promotes cancer pathogenesis. *Cell* 140: 49–61
1300 Ogden HL, Lai Y, Nolin JD, An D, Frevert CW, Gelb MH, Altemeier WA & Hallstrand TS (2020)
1301 Secreted phospholipase A_2 group X acts as an adjuvant for type 2 inflammation, leading
1302 to an allergen-specific immune response in the lung. *J Immunol* 204: 3097–3107
1303 Olzmann JA & Carvalho P (2019) Dynamics and functions of lipid droplets. *Nat Rev Mol Cell*
1304 *Biology* 20: 137–155
1305 Paar M, Jungst C, Steiner NA, Magnes C, Sinner F, Kolb D, Lass A, Zimmermann R,
1306 Zumbusch A, Kohlwein SD, *et al* (2012) Remodeling of lipid droplets during lipolysis and
1307 growth in adipocytes. *J Biol Chem* 287: 11164–11173
1308 Pavlova NN & Thompson CB (2016) The emerging hallmarks of cancer metabolism. *Cell*
1309 *Metab* 23: 27–47
1310 Pereira-Dutra FS, Teixeira L, Costa MFS & Bozza PT (2019) Fat, fight, and beyond: the
1311 multiple roles of lipid droplets in infections and inflammation. *J Leukocyte Biol* 106: 563–
1312 580
1313 Pérez-Chacón G, Astudillo AM, Balgoma D, Balboa MA & Balsinde J (2009) Control of free
1314 arachidonic acid levels by phospholipases A_2 and lysophospholipid acyltransferases.
1315 *Biochim Biophys Acta - Mol Cell Biology Lipids* 1791: 1103–1113
1316 Petan T (2020) Lipid droplets in cancer. *Rev Physiol Biochem Pharmacol.* Springer, Berlin,
1317 Heidelberg. https://doi.org/10.1007/112_2020_51 [paper in press]
1318 Pucer A, Brglez V, Payré C, Pungerčar J, Lambeau G & Petan T (2013) Group X secreted
1319 phospholipase A_2 induces lipid droplet formation and prolongs breast cancer cell survival.
1320 *Mol Cancer* 12: 111
1321 Rambold AS, Cohen S & Lippincott-Schwartz J (2015) Fatty-acid trafficking in starved cells:
1322 regulation by lipid droplet lipolysis, autophagy, and mitochondrial fusion dynamics. *Dev*
1323 *Cell* 32: 678–692

1324 Riederer M, Lechleitner M, Köfeler H & Frank S (2017) Reduced expression of adipose
1325 triglyceride lipase decreases arachidonic acid release and prostacyclin secretion in human
1326 aortic endothelial cells. *Arch Physiol Biochem* 123: 249–253
1327 Röhrig F & Schulze A (2016) The multifaceted roles of fatty acid synthesis in cancer. *Nat Rev*
1328 *Cancer* 16: 732–749
1329 Saiga A, Uozumi N, Ono T, Seno K, Ishimoto Y, Arita H, Shimizu T & Hanasaki K (2005) Group
1330 X secretory phospholipase A2 can induce arachidonic acid release and eicosanoid
1331 production without activation of cytosolic phospholipase A2 alpha. *Prostaglandins Other*
1332 *Lipid Mediat* 75: 79–89
1333 Sato H, Isogai Y, Masuda S, Taketomi Y, Miki Y, Kamei D, Hara S, Kobayashi T, Ishikawa Y,
1334 Ishii T, *et al* (2011) Physiological roles of group X-secreted phospholipase A_2 in
1335 reproduction, gastrointestinal phospholipid digestion, and neuronal function. *J Biol Chem*
1336 286: 11632–11648
1337 Sato H, Taketomi Y, Miki Y, Murase R, Yamamoto K & Murakami M (2020) Secreted
1338 phospholipase PLA2G2D contributes to metabolic health by mobilizing ω3
1339 polyunsaturated fatty acids in WAT. *Cell Reports* 31: 107579
1340 Schewe M, Franken PF, Sacchetti A, Schmitt M, Joosten R, Böttcher R, Royen ME van,
1341 Jeammet L, Payré C, Scott PM, *et al* (2016) Secreted phospholipases A_2 are intestinal
1342 stem cell niche factors with distinct roles in homeostasis, inflammation, and cancer. *Cell*
1343 *Stem Cell* 19: 38–51
1344 Schlager S, Goeritzer M, Jandl K, Frei R, Vujic N, Kolb D, Strohmaier H, Dorow J, Eichmann
1345 TO, Rosenberger A, *et al* (2015) Adipose triglyceride lipase acts on neutrophil lipid droplets
1346 to regulate substrate availability for lipid mediator synthesis. *J Leukocyte Biol* 98: 837–850
1347 Schlager S, Vujic N, Korbelius M, Duta-Mare M, Dorow J, Leopold C, Rainer S, Wegscheider
1348 M, Reicher H, Ceglarek U, *et al* (2017) Lysosomal lipid hydrolysis provides substrates for
1349 lipid mediator synthesis in murine macrophages. *Oncotarget* 8: 40037–40051
1350 Schott MB, Weller SG, Schulze RJ, Krueger EW, Drizyte-Miller K, Casey CA & McNiven MA
1351 (2019) Lipid droplet size directs lipolysis and lipophagy catabolism in hepatocytes. *J Cell*
1352 *Biol* 218: 3320–3335
1353 Schuldiner M & Bohnert M (2017) A different kind of love - lipid droplet contact sites. *Biochim*
1354 *Biophys Acta* 1862: 1188–1196
1355 Schweiger M, Romauch M, Schreiber R, Grabner GF, Hütter S, Kotzbeck P, Benedikt P,
1356 Eichmann TO, Yamada S, Knittelfelder O, *et al* (2017) Pharmacological inhibition of
1357 adipose triglyceride lipase corrects high-fat diet-induced insulin resistance and
1358 hepatosteatosis in mice. *Nat Commun* 8: 14859
1359 Serhan CN (2014) Pro-resolving lipid mediators are leads for resolution physiology. *Nature*
1360 510: 92–101

1361 Shimizu T (2009) Lipid mediators in health and disease: enzymes and receptors as therapeutic
1362 targets for the regulation of immunity and inflammation. *Annu Rev Pharmacol* 49: 123–150
1363 Shridas P, Bailey WM, Boyanovsky BB, Oslund RC, Gelb MH & Webb NR (2010) Group X
1364 secretory phospholipase A_2 regulates the expression of steroidogenic acute regulatory
1365 protein (StAR) in mouse adrenal glands. *J Biol Chem* 285: 20031–20039
1366 Slatter DA, Aldrovandi M, O'Connor A, Allen SM, Brasher CJ, Murphy RC, Mecklemann S,
1367 Ravi S, Darley-Usmar V & O'Donnell VB (2016) Mapping the human platelet lipidome
1368 reveals cytosolic phospholipase A_2 as a regulator of mitochondrial bioenergetics during
1369 activation. *Cell Metab* 23: 930–944
1370 Smirnova E, Goldberg EB, Makarova KS, Lin L, Brown WJ & Jackson CL (2005) ATGL has a
1371 key role in lipid droplet/adiposome degradation in mammalian cells. *EMBO Rep* 7: 106–
1372 113
1373 Sohn JH, Lee YK, Han JS, Jeon YG, Kim JI, Choe SS, Kim SJ, Yoo HJ & Kim JB (2018)
1374 Perilipin 1 (Plin1) deficiency promotes inflammatory responses in lean adipose tissue
1375 through lipid dysregulation. *J Biol Chem* 293: 13974–13988
1376 Sulciner ML, Serhan CN, Gilligan MM, Mudge DK, Chang J, Gartung A, Lehner KA, Bielenberg
1377 DR, Schmidt B, Dalli J, *et al* (2018) Resolvins suppress tumor growth and enhance cancer
1378 therapy. *J Exp Med* 215: 115–140
1379 Surrel F, Jemel I, Boilard E, Bollinger JG, Payré C, Mounier CM, Talvinen KA, Laine VJO,
1380 Nevalainen TJ, Gelb MH, *et al* (2009) Group X phospholipase A_2 stimulates the
1381 proliferation of colon cancer cells by producing various lipid mediators. *Mol Pharmacol* 76:
1382 778–790
1383 Thiam AR & Ikonen E (2020) Lipid droplet nucleation. *Trends Cell Biol* 31: 108–118
1384 Triggiani M, Oriente A & Marone G (1994) Differential roles for triglyceride and phospholipid
1385 pools of arachidonic acid in human lung macrophages. *J Immunol* 152: 1394–1403
1386 Walther TC, Chung J & Farese RV (2017) Lipid droplet biogenesis. *Annu Rev Cell Dev Biol*
1387 33: 491–510
1388 Wang D & DuBois RN (2010) Eicosanoids and cancer. *Nat Rev Cancer* 10: 181–193
1389 Wang YY, Attané C, Milhas D, Dirat B, Dauvillier S, Guerard A, Gilhodes J, Lazar I, Alet N,
1390 Laurent V, *et al* (2017) Mammary adipocytes stimulate breast cancer invasion through
1391 metabolic remodeling of tumor cells. *JCI Insight* 2: e87489
1392 Ward KE, Ropa JP, Adu-Gyamfi E & Stahelin RV (2012) C2 domain membrane penetration by
1393 group IVA cytosolic phospholipase A_2 induces membrane curvature changes. *J Lipid Res*
1394 53: 2656–2666
1395 Ward KE, Sengupta R, Ropa JP, Amiar S & Stahelin ARV (2020) The cytosolic phospholipase
1396 $A_2\alpha$ N-terminal C2 domain binds and oligomerizes on membranes with positive curvature.
1397 *Biomolecules* 10: 647

1398 Welte MA & Gould AP (2017) Lipid droplet functions beyond energy storage. *Biochim Biophys*
1399 *Acta* 1862: 1260–1272
1400 Werner M, Jordan PM, Romp E, Czapka A, Rao Z, Kretzer C, Koeberle A, Garscha U, Pace
1401 S, Claesson H, *et al* (2019) Targeting biosynthetic networks of the proinflammatory and
1402 proresolving lipid metabolome. *FASEB J* 33: 6140–6153
1403 Werz O, Gerstmeier J, Libreros S, Rosa XD la, Werner M, Norris PC, Chiang N & Serhan CN
1404 (2018) Human macrophages differentially produce specific resolvin or leukotriene signals
1405 that depend on bacterial pathogenicity. *Nat Commun* 9: 59
1406 Wilcock DJ, Badrock AP, Owen R, Guerin M, Southam AD, Johnston H, Ogden S, Fullwood
1407 P, Watson J, Ferguson H, *et al* (2020) DGAT1 is a lipid metabolism oncoprotein that
1408 enables cancer cells to accumulate fatty acid while avoiding lipotoxicity. bioRxiv
1409 2020.06.23.166603; doi: https://doi.org/10.1101/2020.06.23.166603 [PREPRINT]
1410 Wooten RE, Willingham MC, Daniel LW, Leslie CC, Rogers LC, Sergeant S & O'Flaherty JT
1411 (2008) Novel translocation responses of cytosolic phospholipase $A_2\alpha$ fluorescent proteins.
1412 *Biochim Biophys Acta* 1783: 1544–1550
1413 Yin H, Li W, Mo L, Deng S, Lin W, Ma C, Luo Z, Luo C & Hong H (2021) Adipose triglyceride
1414 lipase promotes the proliferation of colorectal cancer cells via enhancing the lipolytic
1415 pathway. *J Cell Mol Med* 25: 3963–3975
1416 Zagani R, El-Assaad W, Gamache I & Teodoro JG (2015) Inhibition of adipose triglyceride
1417 lipase (ATGL) by the putative tumor suppressor G0S2 or a small molecule inhibitor
1418 attenuates the growth of cancer cells. *Oncotarget* 6: 28282–28295
1419 Zechner R, Madeo F & Kratky D (2017) Cytosolic lipolysis and lipophagy: two sides of the
1420 same coin. *Nat Rev Mol Cell Biol* 18: 671–684
1421 Zechner R, Zimmermann R, Eichmann TO, Kohlwein SD, Haemmerle G, Lass A & Madeo F
1422 (2012) FAT SIGNALS - Lipases and lipolysis in lipid metabolism and signaling. *Cell Metab*
1423 15: 279–291
1424 Zimmermann R, Strauss JG, Haemmerle G, Schoiswohl G, Birner-Gruenberger R, Riederer
1425 M, Lass A, Neuberger G, Eisenhaber F, Hermetter A, *et al* (2004) Fat mobilization in
1426 adipose tissue is promoted by adipose triglyceride lipase. *Science* 306: 1383–1386
1427 Zoni V, Khaddaj R, Campomanes P, Thiam AR, Schneiter R & Vanni S (2021) Pre-existing
1428 bilayer stresses modulate triglyceride accumulation in the ER *versus* lipid droplets. *Elife*
1429 10: e62886
1430
1431
1432

1433 # Figure legends

1434

1435 **Figure 1. $sPLA_2$ promotes enrichment of lipid droplets with long-chain PUFA-containing**
1436 **triglycerides.** (**A, B**) Lipid droplet levels in control cells and cells treated with 10 nM
1437 recombinant hGX $sPLA_2$ for 48 h in serum-rich medium. (**A**) Neutral lipid content was quantified
1438 by Nile Red staining and flow cytometry (n = 3 independent experiments; 20000 cells per
1439 treatment). (**B**) Representative live-cell confocal microscopy imaging of lipid droplets stained
1440 with BODIPY 493/503 (green) and nuclei with Hoechst 33342 (blue). (**C**) Diagram illustrating
1441 the hypothesis that unsaturated fatty acids released through $sPLA_2$ membrane hydrolysis are
1442 incorporated into triacylglycerols (TAGs) and lead to lasting changes in lipid droplet TAG acyl-
1443 chain composition. (**D**) hGX-$sPLA_2$-induced changes in the incorporation of radiolabelled
1444 oleate into cellular TAGs in MDA-MB-231 cells grown in complete medium for 24 h (Fed), in
1445 complete medium for 24 h followed by 96 h of serum starvation (Fed + Starved), and in serum-
1446 free medium for 96 h (Starved) (n = 4 independent experiments). (**E**) Diagram illustrating the
1447 experimental treatments used for lipidomic analysis in (F)–(K). (**F–K**) TAG lipidomic analyses
1448 of MDA-MB-231 cells treated with recombinant hGX $sPLA_2$ in complete medium for 48 h (Fed;
1449 F–H, J, K) or in the absence of serum for 96 h (Starved; F, I). Cell lysates were collected and
1450 analysed by UPLC/qTOF-MS (n = 4 independent experiments). (**G–I**) $sPLA_2$-induced changes
1451 in the levels of individual TAG species presented as a representative z-score heat-map (**G**)
1452 and volcano plots (**H, I**) prepared by log_2 data transformation and multiple t-test analyses (n =
1453 4 independent experiments). Statistically significant changes ($-log_{10}$(P value) > 1.30) in TAGs
1454 containing mostly saturated and mono-unsaturated FAs (SFA/MUFA-TAGs with 0–2 double
1455 bonds; blue) and those containing polyunsaturated FAs (PUFA-TAGs with 3–12 double bonds;
1456 red) are shown. (**J, K**) $sPLA_2$-induced changes in relative levels of TAG species grouped by
1457 number of acyl-chain C-atoms (chain length) and double bonds (chain unsaturation). (**A–K**)
1458 Data are means ±SEM of at least three independent experiments. *, P <0.05; **, P <0.01; ***,
1459 P <0.001 (unpaired t-tests).

1460

1461 **Figure 2. ATGL-mediated lipid droplet breakdown is required for PGE_2 production in**
1462 **serum-starved cancer cells.** (**A**) Diagram illustrating the experimental set-up used to load
1463 cells with lipid droplets (Feeding) and then to induce their breakdown (Starvation). (**B**) PGE_2
1464 levels in cell supernatants of control and hGX-$sPLA_2$-treated cells quantified by ELISA at the
1465 end of the starvation period. (**C**) Diagram illustrating the experimental conditions used in (D)–
1466 (F) and Fig. EV1(E)–(O). (**D, E**) Lipid droplet levels and PGE_2 production in ATGL-silenced
1467 control and $sPLA_2$-treated cells grown as shown in (C) and analysed at the beginning (Fed)
1468 and at the end of the serum starvation period (Fed + Starved). Neutral lipids were quantified

1469 by Nile Red staining and flow cytometry, PGE_2 was quantified by ELISA. (**F**) Representative
1470 confocal microscopy images showing effects of ATGL depletion on cellular lipid droplet content
1471 in control and hGX-$sPLA_2$-treated cells, under serum-rich (Fed) and serum-free (Fed +
1472 Starved) conditions. Lipid droplets and nuclei were stained using BODIPY 493/503 and
1473 Hoechst 33342, respectively. (**G**) Diagram illustrating the experimental set-up used in (H), (I)
1474 and Figure EV1P, R. (**H, I**) Glycerol release and PGE_2 production in ATGL-overexpressing
1475 serum-starved cells (both untreated and hGX $sPLA_2$ pretreated), in comparison with cells co-
1476 transfected with ATGL-specific siRNAs ($ATGL^{KD+OE}$), non-targeting siRNA (scrambled) and
1477 control plasmid (empty), grown as illustrated in (G). (**J**) Diagram illustrating the proposed model
1478 of lipid droplet-mediated eicosanoid production in cancer cells. Data are means ±SEM of two
1479 (H) or three (B–E, I) independent experiments. *, P <0.05; **, P <0.01; ***, P <0.001 (two-way
1480 ANOVA with Tukey (I) or Bonferroni (D, E, H) adjustment; unpaired t-tests (B)).
1481
1482 **Figure 3. ATGL-mediated lipolysis drives production of a wide spectrum of bioactive**
1483 **lipid mediators.** (**A–D**) Comparative analysis of the profiles of lipid mediators released from
1484 serum-starved MDA-MB-231 cells pre-treated with hGX $sPLA_2$, and from ATGL-depleted cells
1485 without and with hGX $sPLA_2$ pre-treatment, presented as volcano plots (A) a heat map (B),
1486 and individual graphs (C, D). Cells were treated as shown in Fig. 2C. Volcano plots were
1487 prepared using log_2-transformed fold-change values and multiple t-test analysis, and the heat
1488 map by –logP data transformation and two-way ANOVA with Sidak adjustment (n = 3
1489 independent experiments). (**E**) Diagram illustrating the involvement of hGX $sPLA_2$ and ATGL
1490 in the production of a wide range of PUFA-derived cyclooxygenase (COX) and lipoxygenase
1491 (LOX) signalling molecules. Data are means ±SEM of three independent experiments. *, P
1492 <0.05; **, P <0.01; ***, P <0.001 (two-way ANOVA with Sidak adjustment).
1493
1494 **Figure 4. Lipid droplets are required for PGE_2 production in serum-starved cancer cells.**
1495 (**A**) Diagram illustrating the experimental conditions used (top) and cellular neutral lipid content
1496 before (Fed) and after (Fed + Starved) serum starvation in cells treated with DGAT1 (T863)
1497 and DGAT2 (PF-06427878) inhibitors (DGATi), without and with stimulation of lipid droplet
1498 biogenesis by hGX $sPLA_2$ during serum starvation. (**B**) Representative confocal microscopy
1499 images of live cells under nutrient-replete conditions and treated with DGAT inhibitors in the
1500 absence and presence of hGX $sPLA_2$. Lipid droplets and nuclei were visualised using BODIPY
1501 493/503 and Hoechst 33342 staining, respectively, and confocal microscopy. (**C**) DGATi-
1502 induced changes in PGE_2 production in serum-starved cancer cells (Fed + Starved), without
1503 and with additional stimulation of lipid droplet biogenesis by hGX $sPLA_2$ pre-treatment. Cells
1504 were treated according to (A). (**D, E**) DGATi-induced changes in neutral lipids (D) and PGE_2
1505 production (E) in serum-starved MDA-MB-231 cancer cells (Fed + Starved), without and with

1506 additional stimulation of lipid droplet biogenesis by arachidonic acid (AA) pre-treatment. Cells
1507 were treated according to (A). (**F, G**) Diagrams illustrating the experimental conditions used
1508 (top), and changes in neutral lipid accumulation and PGE_2 production induced by DGATi
1509 treatments during serum starvation in control (SCR) and ATGL-depleted ($ATGL^{KD}$) MDA-MB-
1510 231 (F) and A549 (G) cancer cells, without and with hGX $sPLA_2$ pre-treatment. (**A, D, F, G**)
1511 Neutral lipid content was quantified by Nile Red staining and flow cytometry. (**C, E, F, G**) PGE_2
1512 levels were determined in cell supernatants as described in Methods. Data are means ±SEM
1513 of at least three independent experiments. *, P <0.05; **, P <0.01; ***, P <0.001 (two-way
1514 ANOVA with Tukey (**A, F, G**) or Bonferroni (**C, D, E**) adjustment).
1515
1516 **Figure 5. $cPLA_2\alpha$ depends on lipid droplet turnover to drive lipid mediator production.**
1517 (**A**) Scheme illustrating three hypothetical models of interplay between $cPLA_2\alpha$ and ATGL in
1518 providing arachidonic acid (AA) for lipid mediator production. (**B**) Changes in neutral lipid
1519 content and PGE_2 production induced by ATGL ($ATGL^{KD}$) and $cPLA_2\alpha$ ($cPLA_2\alpha^{KD}$) single and
1520 double ($Double^{KD}$) knockdowns, in comparison with control siRNA-treated cells (SCR), without
1521 and with stimulation of lipid droplet biogenesis by hGX $sPLA_2$ pre-treatment. (**C**) PGE_2
1522 production in cells with reciprocal knockdown/overexpression of $cPLA_2\alpha$ and ATGL. Cells were
1523 reverse transfected with siRNAs specific for ATGL ($ATGL^{KD}$) and/or $cPLA_2\alpha$ ($cPLA_2\alpha^{KD}$), then
1524 forward transfected with ATGL-encoding ($ATGL^{OE}$) and/or $cPLA_2\alpha$-encoding ($cPLA_2\alpha^{OE}$)
1525 plasmids, without and with pre-treated with hGX $sPLA_2$, as illustrated in the scheme (top). In
1526 controls (control), non-targeting siRNA reverse transfections were combined with backbone
1527 ('empty') vector forward transfections. (**D**) DGAT inhibition (DGATi)-induced changes in PGE_2
1528 production in serum-starved control cells (empty) and in cells overexpressing ATGL ($ATGL^{OE}$)
1529 or $cPLA_2\alpha$ ($cPLA_2\alpha^{OE}$), without and with additional stimulation of lipid droplet biogenesis by
1530 hGX $sPLA_2$ pre-treatment. Neutral lipid content was quantified by Nile Red staining and flow
1531 cytometry (B), PGE_2 levels were determined in cell supernatants using ELISA (C, D). Data are
1532 means ±SEM of two (B, A549 cells) or at least three independent experiments *, P <0.05; **,
1533 P <0.01; ***, P <0.001 (two-way ANOVA with Tukey (B, D) or Dunnet (C) adjustment).
1534
1535 **Figure 6. $cPLA_2\alpha$ affects lipid droplet turnover.** (**A**) Diagram illustrating the experimental
1536 conditions used (top) and representative live-cell confocal microscopy imaging of lipid droplets
1537 in ATGL ($ATGL^{KD}$) and $cPLA_2\alpha$ ($cPLA_2\alpha^{KD}$) single and double ($Double^{KD}$) knockdown MDA-
1538 MB-231 cells, in comparison with control siRNA-treated cells (SCR), without and with
1539 stimulation of lipid droplet biogenesis by hGX $sPLA_2$ pre-treatment. The corresponding
1540 microscopy images for HeLa and A549 cells are shown in Figure EV4A, C. Lipid droplets were
1541 stained with BODIPY 493/503 (green) and nuclei with Hoechst 33342 (blue) and images
1542 analysed using ImageJ and the Lipid Droplet Counter Plugin. (**B**) Box plots and curves showing

1543 changes in lipid droplet diameters in cells treated as in (A) (n >40 cells/sample). (**C–E**) Lipid
1544 droplet numbers per cell in serum-fed (Fed) and serum-starved (Starved) cells (n >40
1545 cells/sample) grown and treated as in (A). Data are geometric means (B) or means (C–E)
1546 ±SEM (n >40 cells/sample) of two independent experiments. *, P <0.05; **, P <0.01; ***, P
1547 <0.001 (two-way ANOVA with Tukey adjustment; nested one-way ANOVA with Sidak
1548 adjustment (B)).
1549
1550 **Figure 7. ATGL and cPLA$_2$α cooperatively modulate PUFA trafficking between**
1551 **triglycerides and membrane phospholipids.** (**A–C**) Untargeted lipidomic analysis of
1552 phospholipids and triglycerides (TAGs) in serum-starved MDA-MB-231 cells depleted of ATGL
1553 (ATGL^{KD}), cPLA$_2$α (cPLA$_2$α^{KD}), or both (Double^{KD}), without and with hGX sPLA$_2$ pre-treatment
1554 under serum-rich conditions, and grown as shown in Figure EV5B. Volcano plots show
1555 significant changes (–log$_{10}$(P value) >1.30) in individual lipids between each treatment
1556 condition *versus* control cells (unless otherwise indicated), and were prepared by log$_2$ fold-
1557 change (FC) data transformation and multiple t-test analysis (n=3 independent experiments).
1558 TAGs and phospholipids (PLs) containing saturated and mono-unsaturated acyl chains
1559 (SFA/MUFA-TAGs, SFA/MUFA-PLs, with 0–3 and 0–2 double bonds, respectively) and those
1560 containing polyunsaturated FAs (PUFA-TAGs, PUFA-PLs, with at least 4 and 3 double bonds,
1561 respectively) are colour-coded as indicated. TG, triglyceride; PC, phosphatidylcholine; PE,
1562 phosphatidylethanolamine; PI, phosphatidylinositol, PS, phosphatidylserine. (**D**) Schematic
1563 illustration of the predominant pathways involved in lipid droplet-mediated PUFA trafficking
1564 between the membrane phospholipid and TAG pools in serum-starved cancer cells.
1565
1566 **Figure 8. Lipid droplet-mediated lipid mediator production promotes cancer-cell**
1567 **proliferation.** (**A**) Proliferation of MDA-MB-231 cells treated with T863 (DGAT1i) and PF-
1568 06427878 (DGAT2i), or an equimolar mix of both DGAT inhibitors (DGATi), grown under
1569 nutrient-rich conditions in the absence and presence of hGX sPLA$_2$. (**B, C**) Proliferation of
1570 MDA-MB-231 cells overexpressing ATGL (ATGL^{OE}), treated with indomethacin (B) or
1571 nordihydroguaiaretic acid (NDGA) (C), in the absence and presence of hGX sPLA$_2$. (**D**)
1572 Proliferation of MDA-MB-231 cells treated with exogenous PGE$_2$ in the absence and presence
1573 of T863 (DGAT1i) and PF-06427878 (DGAT2i), or an equimolar mix of both DGAT inhibitors
1574 (DGATi). (**E**) Proliferation of A549 cells overexpressing cPLA$_2$α (cPLA$_2$α^{OE}) and grown in the
1575 absence and presence of DGATi, indomethacin and recombinant hGX sPLA$_2$. (**F**) Proliferation
1576 of MDA-MB-231 cells overexpressing cPLA$_2$α (cPLA$_2$α^{OE}) and grown in the absence and
1577 presence of DGATi and recombinant hGX sPLA$_2$. Data are means ±SEM of three independent
1578 experiments. *, P <0.05; **, P <0.01; ***, P <0.001 (two-way ANOVA with Bonferroni (A–D) or
1579 Sidak (E, F) adjustments).

1580 # Expanded View Figure legends

1581

1582 **Figure EV1. ATGL-mediated lipid droplet breakdown drives PGE_2 production in starving**
1583 **MDA-MB-231 and HeLa cells, but not in A549 cells.** (**A, B**) Neutral lipid contents in control
1584 and hGX-$sPLA_2$-treated cells at the beginning of and after serum starvation, quantified by Nile
1585 Red staining and flow cytometry. (**C**) Glycerol released from fed and starving control and hGX-
1586 $sPLA_2$-treated cells. (**D**) PGE_2 levels in cell supernatants of control and AA-treated cells
1587 quantified by ELISA at the end of the starvation period. (**E**) Representative western blot
1588 showing siRNA-induced ATGL knock down ($ATGL^{KD}$) in comparison with control cells
1589 (untransfected [untr.] and non-targeting siRNA-transfected [SCR] cells), treated with hGX
1590 $sPLA_2$ (or left untreated) and grown as shown in (Fig. 2C). (**F, G, I, J**) Lipid droplet levels and
1591 PGE_2 production in ATGL-silenced control and $sPLA_2$-treated cells grown as shown in Fig. 2C
1592 and analysed at the beginning (Fed) and at the end of the serum starvation period (Fed +
1593 Starved). Neutral lipids were quantified by Nile Red staining and flow cytometry, PGE_2 was
1594 quantified by ELISA. (**H, K**) Representative confocal microscopy images showing effects of
1595 ATGL depletion on cellular lipid droplet content in control and hGX-$sPLA_2$-treated cells, under
1596 serum-rich (Fed) and serum-free (Fed + Starved) conditions. Lipid droplets and nuclei were
1597 stained using BODIPY 493/503 and Hoechst 33342, respectively. (**L, M**) Changes in lipid
1598 droplet levels and PGE_2 production induced by ATGL silencing in control and arachidonic acid
1599 (AA)-treated cells at the beginning (Fed) and end of the serum starvation (Fed + Starved). (**N,**
1600 **O**) Glycerol release as a measure of lipolytic activity in control and ATGL-depleted serum-fed
1601 and serum-starved cells, either untreated or treated with hGX $sPLA_2$. (**P**) Representative
1602 Western blot showing ATGL protein overexpression in cells transfected with ATGL-encoding
1603 plasmid ($ATGL^{OE}$) in comparison with those transfected with control (Empty) vector or ATGL-
1604 specific siRNA ($ATGL^{KD}$), grown as illustrated in Fig. 3J. (**R**) Neutral lipid levels in ATGL-
1605 overexpressing in untreated and hGX-$sPLA_2$-pretreated serum-starved cells, in comparison
1606 with those co-transfected with ATGL-specific siRNA ($ATGL^{KD+OE}$), non-targeting siRNA
1607 (scrambled) and control plasmid (empty), grown as shown in Fig. 2G. Neutral lipids were
1608 quantified by Nile Red staining and flow cytometry. Data are means ±SEM of two (D) or three
1609 (A–C, F, G, I, J, L–O) independent experiments. *, $P < 0.05$; **, $P < 0.01$; ***, $P < 0.001$ (two-
1610 way ANOVA with Bonferroni (F, G, I, J, L–O) or Tukey (A, C, R) adjustment; unpaired t-test
1611 (D)).

1612

1613 **Figure EV2. Inhibition of DGAT-mediated lipid droplet biogenesis supresses PGE_2**
1614 **production.** (**A, B**) Diagrams illustrating the experimental conditions used (top) and
1615 representative live-cell confocal microscopy images of control (SCR) and ATGL-depleted

1616 (ATGL^{KD}) MDA-MB-231 and HeLa cells treated with DGAT inhibitors during serum feeding (A)
1617 and during serum starvation (B), without and with hGX sPLA$_2$ pre-treatment. Lipid droplets and
1618 nuclei were visualised using BODIPY 493/503 and Hoechst 33342 staining and confocal
1619 microscopy. (**C**) Diagram illustrating the experimental conditions (top) and graph showing
1620 DGAT inhibition (DGATi)-induced changes in PGE$_2$ production in serum-starved control (SCR)
1621 and ATGL-depleted (ATGL^{KD}) A549 cells, without and with stimulation of lipid droplet
1622 biogenesis by hGX sPLA$_2$ pre-treatment. PGE$_2$ levels were determined in cell supernatants as
1623 described in Methods. Data are means ±SEM of three independent experiments. *, P <0.05;
1624 **, P <0.01; ***, P <0.001 (two-way ANOVA with Bonferroni adjustment).
1625
1626 **Figure EV3. cPLA$_2$α cooperates with ATGL in mediation of lipid droplet-driven lipid**
1627 **mediator production.** (**A**) Quantitative PCR analysis of cPLA$_2$α gene expression in control
1628 (SCR) and cPLA$_2$-knockdown (cPLA$_2$α^{KD}) cells grown for 48 h in complete medium and serum
1629 starved for 24 h. (**B**) Representative Western blots showing cPLA$_2$α and ATGL protein
1630 expression in single and double knockdown A549 cells, without and with hGX sPLA$_2$ pre-
1631 treatment, plus basal levels of cPLA$_2$α protein expression in the four cancer cell lines. (**C**)
1632 Diagram illustrating the experimental conditions used (top), and changes in neutral lipid
1633 content in serum-fed cells induced by ATGL (ATGL^{KD}) and cPLA$_2$α (cPLA$_2$α^{KD}) single and
1634 double (Double^{KD}) knockdowns, in comparison with control siRNA-treated cells (SCR), without
1635 and with stimulation of lipid droplet biogenesis by hGX sPLA$_2$ treatment. (**D**) Quantitative PCR
1636 analysis of cPLA$_2$α gene expression in control (empty) and cPLA$_2$α-overexpressing (cPLA$_2$α^{OE})
1637 cells grown for 48 h in complete medium and serum starved for 24 h. (**E**) Diagram illustrating
1638 the experimental conditions used (top), and neutral lipid levels in cells with reciprocal
1639 knockdown/ overexpression of cPLA$_2$α and ATGL. Cells were reverse transfected with ATGL-
1640 targeting (ATGL^{KD}) and/or cPLA$_2$α-targeting (cPLA$_2$α^{KD}) siRNAs, then forward transfected with
1641 ATGL-encoding (ATGL^{OE}) and/or cPLA$_2$α-encoding (cPLA$_2$α^{OE}) plasmids, and/or pre-treated
1642 with hGX sPLA$_2$. In controls (control), non-targeting siRNA reverse transfections were
1643 combined with backbone ('empty') vector forward transfections. (**F**) Diagram illustrating the
1644 experimental conditions used (top), and DGAT inhibition (DGATi)-induced changes in PGE$_2$
1645 production in serum-starved control cells (empty) and in cells overexpressing ATGL (ATGL^{OE})
1646 or cPLA$_2$α (cPLA$_2$α^{OE}), without and with additional stimulation of lipid droplet biogenesis by
1647 hGX sPLA$_2$ pre-treatment. Neutral lipid content was quantified by Nile Red staining and flow
1648 cytometry. Data are means ±SEM of two (**A**, **D**; **C**, A549 cells) or at least three independent
1649 experiments. *, P <0.05; **, P <0.01; ***, P <0.001 (unpaired t-tests (**A, D**); two-way ANOVA
1650 with Tukey (**C, E**) or Dunnet (**F**) adjustments).
1651

1652 **Figure EV4. $cPLA_2\alpha$ affects lipid droplet turnover in Hela and A549 cells.** (**A, C**)
1653 Representative live-cell confocal microscopy imaging of lipid droplets in ATGL ($ATGL^{KD}$) and
1654 $cPLA_2\alpha$ ($cPLA_2\alpha^{KD}$) single and double ($Double^{KD}$) knockdown HeLa (**A**) and A549 (**C**) cells in
1655 comparison with control siRNA-treated cells (SCR), without and with stimulation of lipid droplet
1656 biogenesis by hGX $sPLA_2$, treated as shown in Figure 7A. Lipid droplets were stained with
1657 BODIPY 493/503 (green) and nuclei with Hoechst 33342 (blue) and images analysed using
1658 ImageJ and the Lipid Droplet Counter Plugin. (**B, D**) Box plots and curves showing changes in
1659 lipid droplet diameters in cells shown in (A, C), respectively (n >40 cells/sample). Data are
1660 geometric means ±SEM (n >40 cells/sample) of two independent experiments. *, P <0.05; **,
1661 P <0.01; ***, P <0.001 (nested one-way ANOVA with Sidak adjustment (B, D)).
1662
1663 **Figure EV5. Membrane phospholipid PUFA content is modulated by $sPLA_2$, $cPLA_2\alpha$ and**
1664 **ATGL.** (**A**) Illustration of hypothetical pathways of ATGL-mediated and $cPLA_2\alpha$-mediated
1665 modulation of PUFA trafficking between membrane phospholipids and triglycerides (TAGs)
1666 stored in lipid droplets. (**B**) Diagram illustrating experimental scheme for the untargeted
1667 lipidomic analysis in Figure 7 and (C) and (D). (**C, D**) Untargeted lipidomic analysis of
1668 phospholipids in MDA-MB-231 cells depleted of ATGL ($ATGL^{KD}$), $cPLA_2\alpha$ ($cPLA_2\alpha^{KD}$) or both
1669 ($Double^{KD}$), without and with hGX $sPLA_2$ pre-treatment, and grown as shown in (B). Volcano
1670 plots show significant changes ($-\log_{10}$(P value) >1.30) in individual lipids between each
1671 treatment condition *versus* control cells (unless otherwise indicated), and were prepared by
1672 $\log_2$ fold-change (FC) data transformation and multiple t-test analysis (n=3 independent
1673 experiments). Phospholipids (PLs) containing saturated and mono-unsaturated acyl chains
1674 (SFA/MUFA-PLs with 0–2 double bonds) and those containing polyunsaturated FAs (PUFA-
1675 PLs with at least 3 double bonds) are colour-coded as indicated. PC, phosphatidylcholine; PE,
1676 phosphatidylethanolamine; PI, phosphatidylinositol, PS, phosphatidyserine.
1677
1678
1679

1680 # Appendix Figure Legends

1681

1682 **Appendix Figure S1. sPLA$_2$-induced changes in lipid droplet metabolism and**
1683 **composition.** (**A**) Total cellular triglycerides (TAGs) in control and hGX-sPLA$_2$-treated MDA-
1684 MB-231 and HeLa cells quantified using a biochemical assay. (**B, C**) Diagram illustrating the
1685 experimental set-up for oleate incorporation analyses using thin layer chromatography (TLC)
1686 shown in (**C**) and in Figure 1D. (**C**) Representative TLC plate showing that in hGX-sPLA$_2$-
1687 treated cells, oleate is preferentially incorporated into TAGs, but not into phosphatidylcholine
1688 (PC) or cholesterol esters (CE). (**D, E**) Lipidomic analysis of hGX-sPLA$_2$-induced PUFA-TAG
1689 enrichment in MDA-MB-231 cells grown under serum-rich conditions. (**D**) Representative XY
1690 z-score plot showing colour-coded changes in the levels of TAG acyl-chain unsaturation. Data
1691 are means ±SEM of two (**A**) and four (**E**) independent experiments. *, P <0.05; **, P <0.01; ***,
1692 P <0.001 (two-way ANOVA with Bonferroni adjustment (**A**); unpaired t-tests (**E**)).

1693

1694 **Appendix Figure S2. Depletion of ATGL suppresses both basal and hGX-sPLA$_2$-**
1695 **stimulated lipid mediator production in breast cancer cells.** hGX-sPLA$_2$-induced and
1696 ATGL knockdown (ATGL^{KD})-induced changes in selected lipid mediators (as indicated)
1697 released from serum-starved MDA-MB-231 cells. Cells were treated as shown in Figure 3A.
1698 Data are means ±SEM of three independent experiments. *, P <0.05; **, P <0.01; ***, P <0.001
1699 (two-way ANOVA with Sidak adjustment). EPA, eicosapentaenoic acid; HEPE,
1700 hydroxyeicosapentaenoic acid; AA, arachidonic acid; TXB$_2$, thromboxane B$_2$; PD1, protectin
1701 D1; AT-PD1, aspirin-triggered protectin D1; MaR1, maresin 1; RvD2, resolvin D2; RvD3,
1702 resolvin D3; RvD4, resolvin D4.

1703

1704 **Appendix Figure S3. LION-term enrichment analysis for significant changes in**
1705 **membrane properties induced by sPLA$_2$, cPLA$_2$α and ATGL.** (**A**) Heat map of z-score
1706 scaled lipid levels of phospholipids and triglycerides in serum-starved MDA-MB-231 cells
1707 depleted of ATGL (ATGL^{KD}), cPLA$_2$α (cPLA$_2$α^{KD}) or both (Double^{KD}), without and with hGX
1708 sPLA$_2$ pre-treatment under serum-rich conditions, and grown as shown in Figure EV5B. (**B, C**)
1709 LION-term enrichment analysis of the full data set (B) and pairwise comparisons of
1710 phospholipid data from cPLA$_2$α-depleted and control (SCR) cells (C) in ranking mode. The cut-
1711 off value of significant enrichments is indicated by the grey line (q <0.05). Data were analysed
1712 using three principal components, and lipids were clustered into five groups by hierarchical
1713 clustering (A, B). Bar colours are scaled according to the enrichment (−log q-values). FDR,
1714 false-discovery rate.

1715

Figure 1

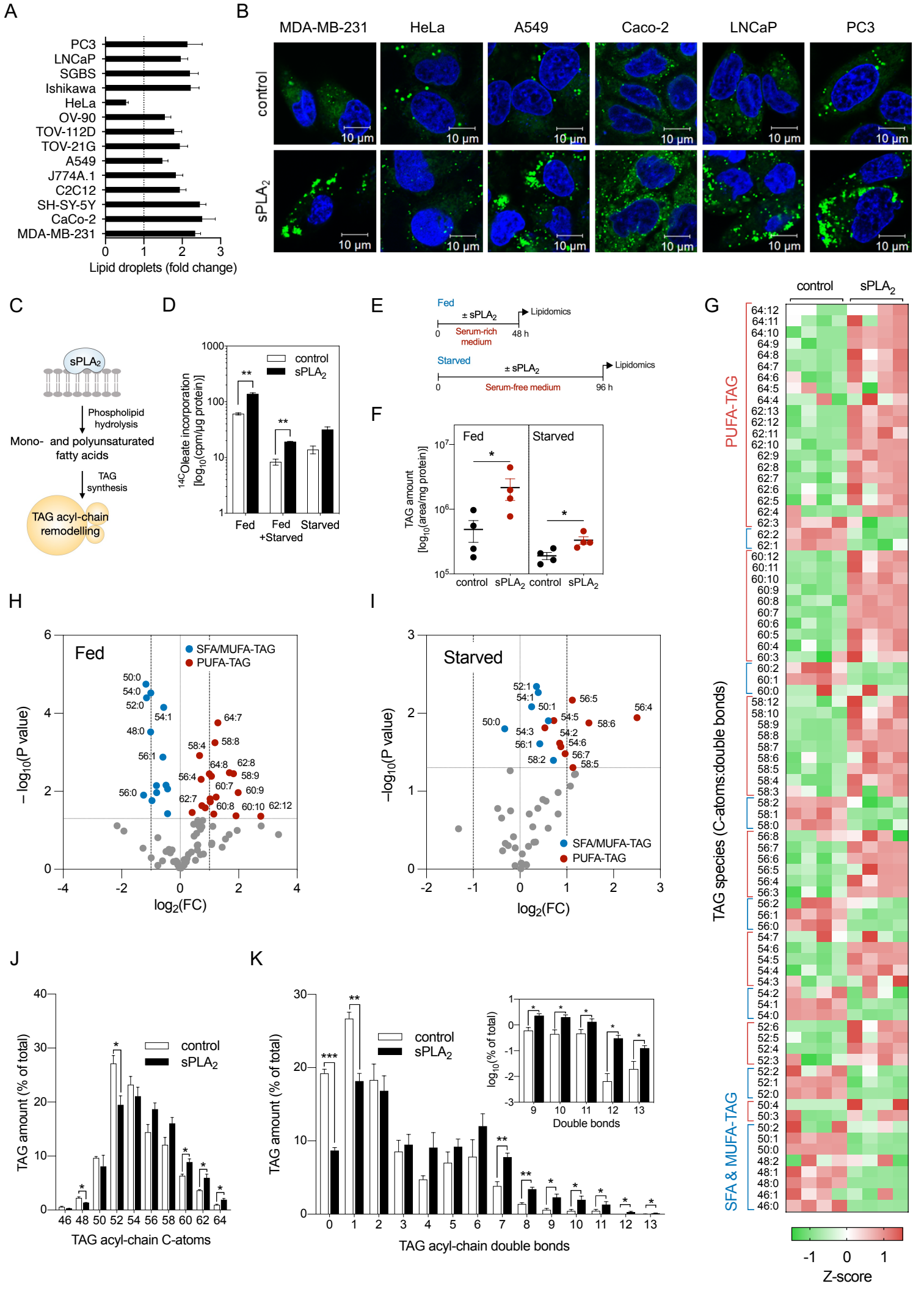
A
PC3
LNCaP
SGBS
Ishikawa
HeLa
OV-90
TOV-112D
TOV-21G
A549
J774A.1
C2C12
SH-SY-5Y
CaCo-2
MDA-MB-231
Lipid droplets (fold change)
B
MDA-MB-231
HeLa
A549
Caco-2
LNCaP
PC3
control
sPLA2
10 µm
C
sPLA2
Phospholipid hydrolysis
Mono- and polyunsaturated fatty acids
TAG synthesis
TAG acyl-chain remodelling
D
control
sPLA2
14C Oleate incorporation [log10(cpm/µg protein)]
Fed
Fed +Starved
Starved
E
Fed
± sPLA2
Lipidomics
Serum-rich medium
48 h
Starved
Serum-free medium
96 h
F
Fed
Starved
TAG amount [log10(area/mg protein)]
control
sPLA2
G
control
sPLA2
PUFA-TAG
SFA & MUFA-TAG
TAG species (C-atoms:double bonds)
Z-score
H
Fed
SFA/MUFA-TAG
PUFA-TAG
– log10(P value)
log2(FC)
I
Starved
SFA/MUFA-TAG
PUFA-TAG
–log10(P value)
log2(FC)
J
control
sPLA2
TAG amount (% of total)
TAG acyl-chain C-atoms
K
control
sPLA2
TAG amount (% of total)
log10(% of total)
Double bonds
TAG acyl-chain double bonds

Figure 2

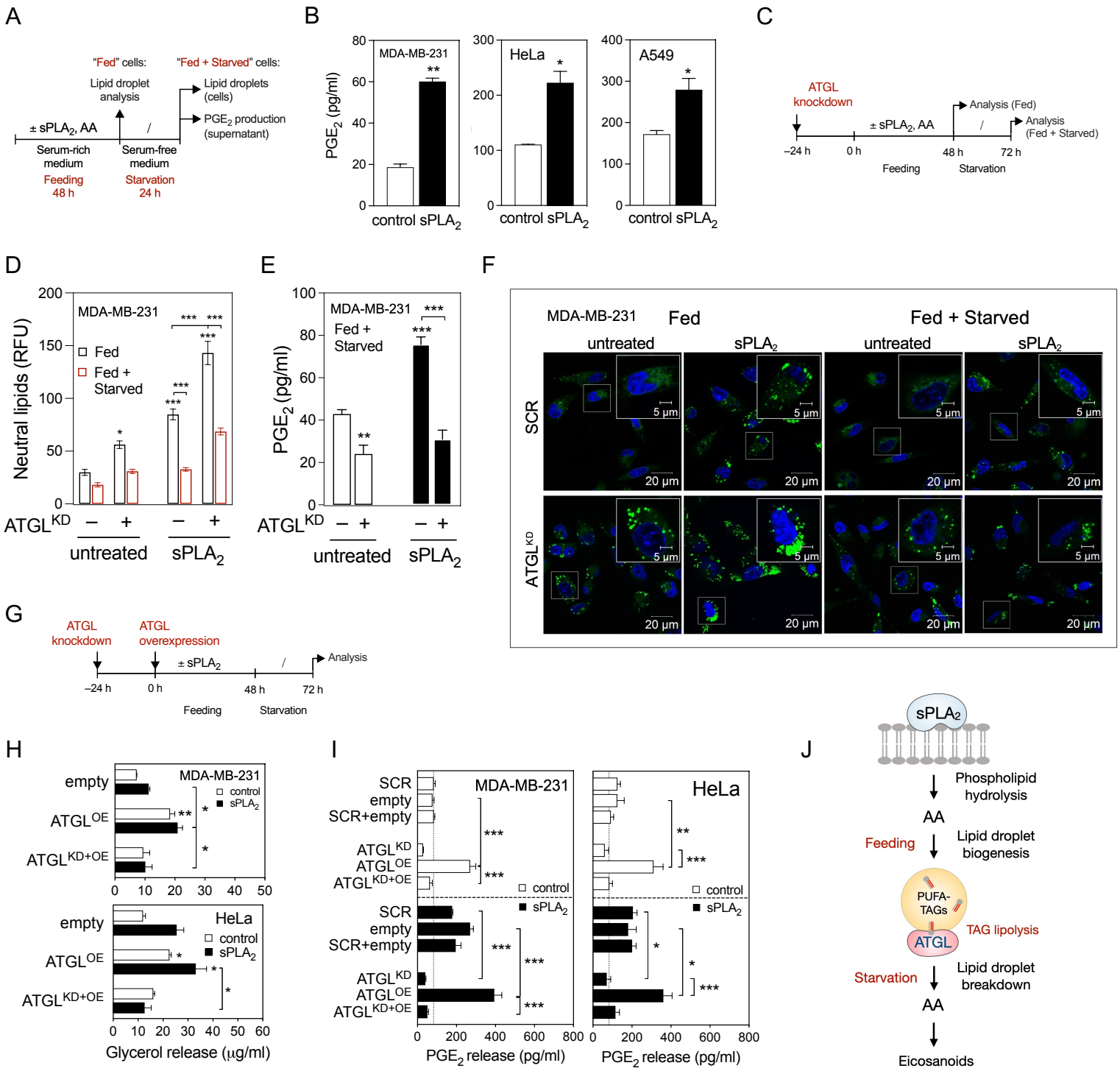
A
"Fed" cells:
Lipid droplet analysis
"Fed + Starved" cells:
Lipid droplets (cells)
PGE2 production (supernatant)
± sPLA2, AA
Serum-rich medium
Serum-free medium
Feeding 48 h
Starvation 24 h
B
MDA-MB-231
HeLa
A549
PGE2 (pg/ml)
control sPLA2
C
ATGL knockdown
± sPLA2, AA
Analysis (Fed)
Analysis (Fed + Starved)
–24 h
0 h
48 h
72 h
Feeding
Starvation
D
MDA-MB-231
Fed
Fed + Starved
Neutral lipids (RFU)
ATGLKD
untreated
sPLA2
E
MDA-MB-231
Fed + Starved
PGE2 (pg/ml)
ATGLKD
untreated
sPLA2
F
MDA-MB-231
Fed
Fed + Starved
untreated
sPLA2
SCR
ATGLKD
5 µm
20 µm
G
ATGL knockdown
ATGL overexpression
± sPLA2
Analysis
–24 h
0 h
48 h
72 h
Feeding
Starvation
H
MDA-MB-231
HeLa
empty
ATGLOE
ATGLKD+OE
control
sPLA2
Glycerol release (µg/ml)
I
MDA-MB-231
HeLa
SCR
empty
SCR+empty
ATGLKD
ATGLOE
ATGLKD+OE
control
sPLA2
PGE2 release (pg/ml)
J
sPLA2
Phospholipid hydrolysis
AA
Feeding
Lipid droplet biogenesis
PUFA-TAGs
ATGL
TAG lipolysis
Starvation
Lipid droplet breakdown
AA
Eicosanoids

Figure 3

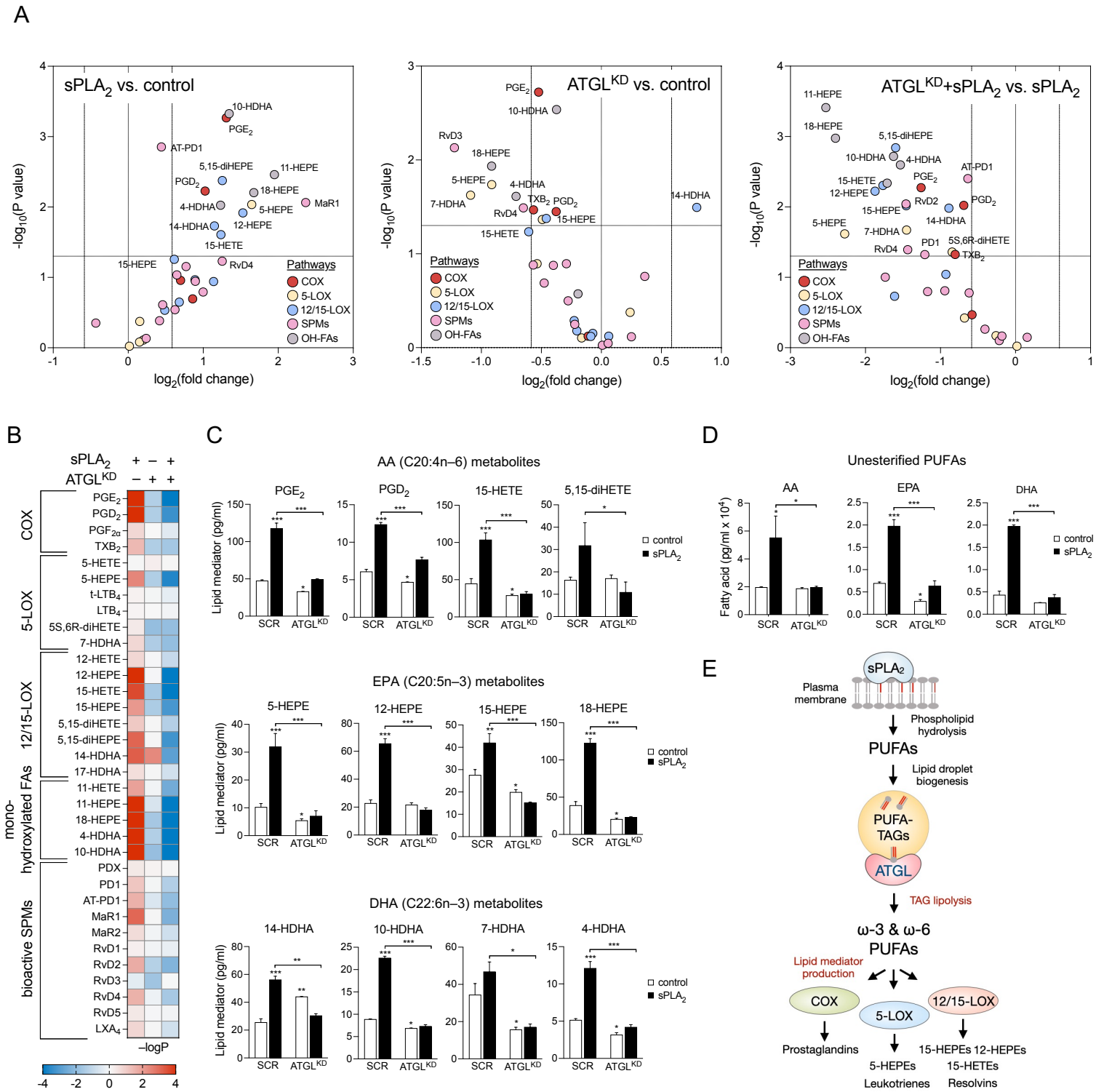
A
sPLA2 vs. control
ATGLKD vs. control
ATGLKD+sPLA2 vs. sPLA2
-log10(P value)
log2(fold change)
Pathways
COX
5-LOX
12/15-LOX
SPMs
OH-FAs
B
sPLA2
ATGLKD
COX
5-LOX
12/15-LOX
mono-hydroxylated FAs
bioactive SPMs
–logP
C
AA (C20:4n–6) metabolites
EPA (C20:5n–3) metabolites
DHA (C22:6n–3) metabolites
Lipid mediator (pg/ml)
SCR
ATGLKD
control
sPLA2
D
Unesterified PUFAs
AA
EPA
DHA
Fatty acid (pg/ml x 10^4)
E
sPLA2
Plasma membrane
Phospholipid hydrolysis
PUFAs
Lipid droplet biogenesis
PUFA-TAGs
ATGL
TAG lipolysis
ω-3 & ω-6 PUFAs
Lipid mediator production
COX
5-LOX
12/15-LOX
Prostaglandins
5-HEPEs
Leukotrienes
15-HEPEs 12-HEPEs
15-HETEs
Resolvins

Figure 4

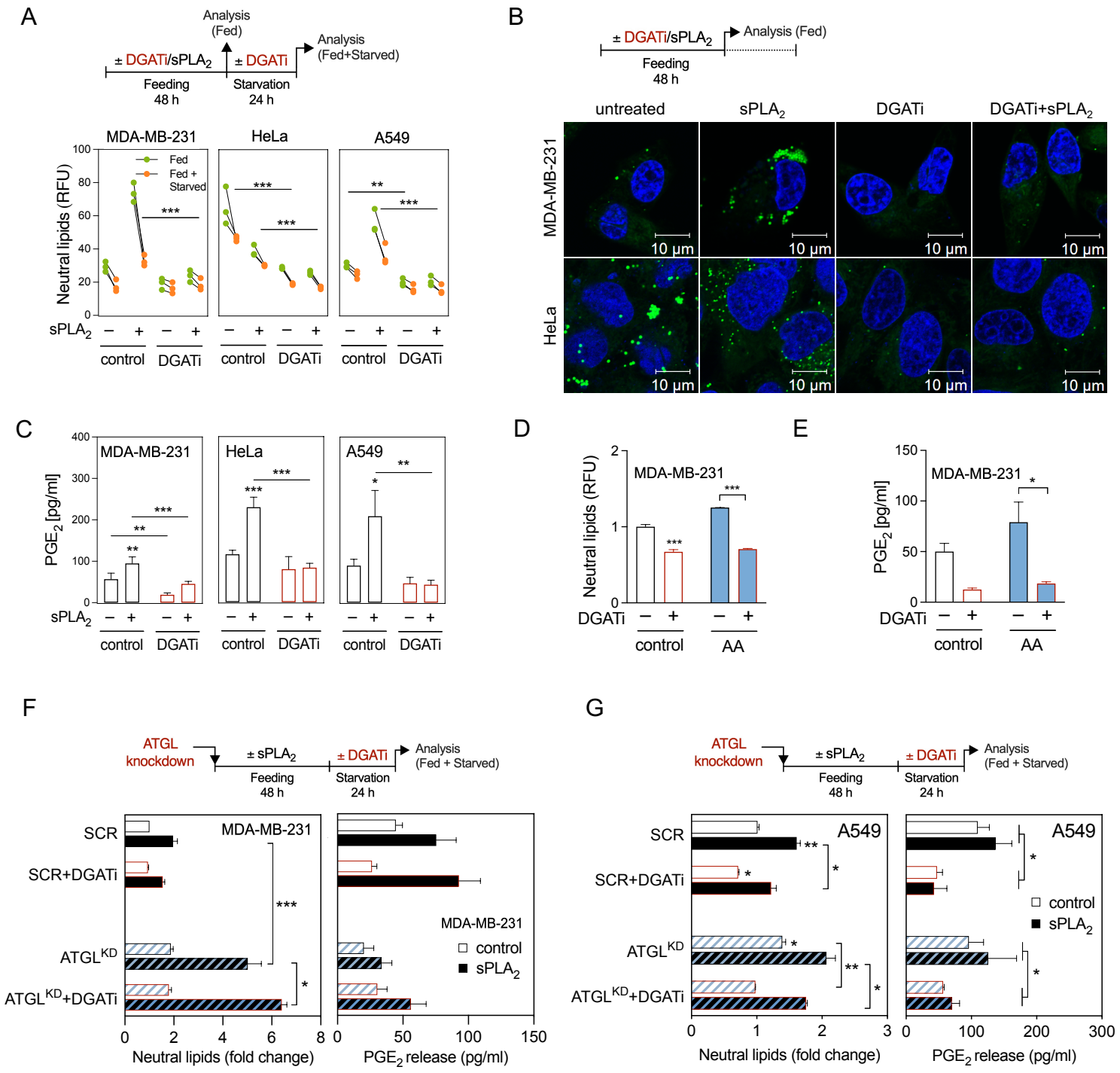
A
Analysis (Fed)
± DGATi/sPLA2
± DGATi
Analysis (Fed+Starved)
Feeding 48 h
Starvation 24 h
MDA-MB-231
HeLa
A549
Neutral lipids (RFU)
Fed
Fed + Starved
sPLA2
control
DGATi
B
± DGATi/sPLA2
Analysis (Fed)
Feeding 48 h
untreated
sPLA2
DGATi
DGATi+sPLA2
MDA-MB-231
HeLa
10 µm
C
PGE2 [pg/ml]
MDA-MB-231
HeLa
A549
sPLA2
control
DGATi
D
Neutral lipids (RFU)
MDA-MB-231
DGATi
control
AA
E
PGE2 [pg/ml]
MDA-MB-231
DGATi
control
AA
F
ATGL knockdown
± sPLA2
± DGATi
Analysis (Fed + Starved)
Feeding 48 h
Starvation 24 h
SCR
SCR+DGATi
ATGLKD
ATGLKD+DGATi
MDA-MB-231
control
sPLA2
Neutral lipids (fold change)
PGE2 release (pg/ml)
G
ATGL knockdown
± sPLA2
± DGATi
Analysis (Fed + Starved)
Feeding 48 h
Starvation 24 h
SCR
SCR+DGATi
ATGLKD
ATGLKD+DGATi
A549
control
sPLA2
Neutral lipids (fold change)
PGE2 release (pg/ml)

Figure 5

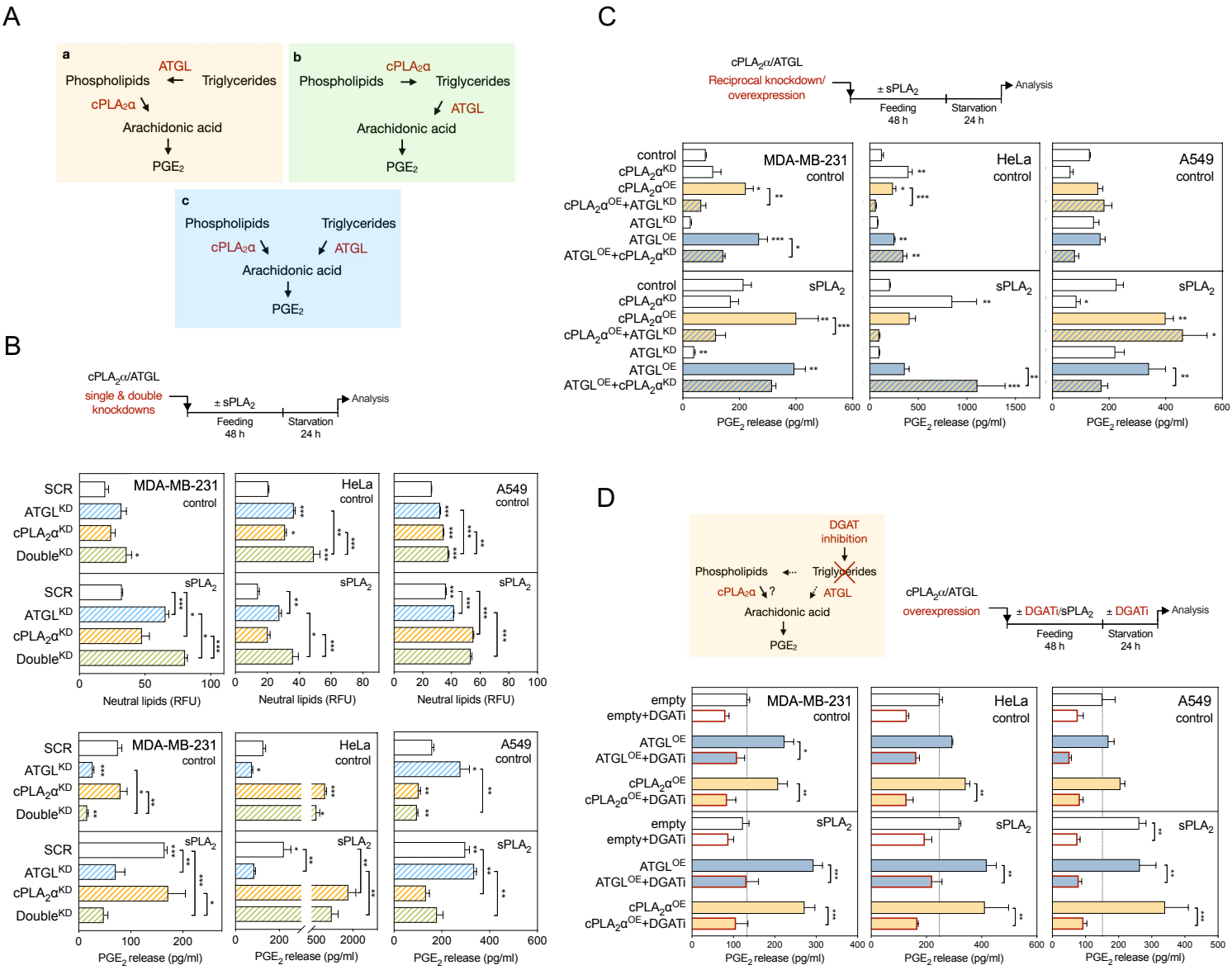
A
a
ATGL
Phospholipids
Triglycerides
cPLA2α
Arachidonic acid
PGE2
b
cPLA2α
Phospholipids
Triglycerides
ATGL
Arachidonic acid
PGE2
c
Phospholipids
Triglycerides
cPLA2α
ATGL
Arachidonic acid
PGE2
B
cPLA2α/ATGL
single & double knockdowns
± sPLA2
Analysis
Feeding 48 h
Starvation 24 h
SCR
ATGLKD
cPLA2αKD
DoubleKD
MDA-MB-231 control
HeLa control
A549 control
sPLA2
Neutral lipids (RFU)
PGE2 release (pg/ml)
C
cPLA2α/ATGL
Reciprocal knockdown/ overexpression
control
cPLA2αKD
cPLA2αOE
cPLA2αOE+ATGLKD
ATGLKD
ATGLOE
ATGLOE+cPLA2αKD
D
DGAT inhibition
Phospholipids
Triglycerides
cPLA2α
ATGL
Arachidonic acid
PGE2
cPLA2α/ATGL
overexpression
± DGATi/sPLA2
± DGATi
empty
empty+DGATi
ATGLOE
ATGLOE+DGATi
cPLA2αOE
cPLA2αOE+DGATi

Figure 6

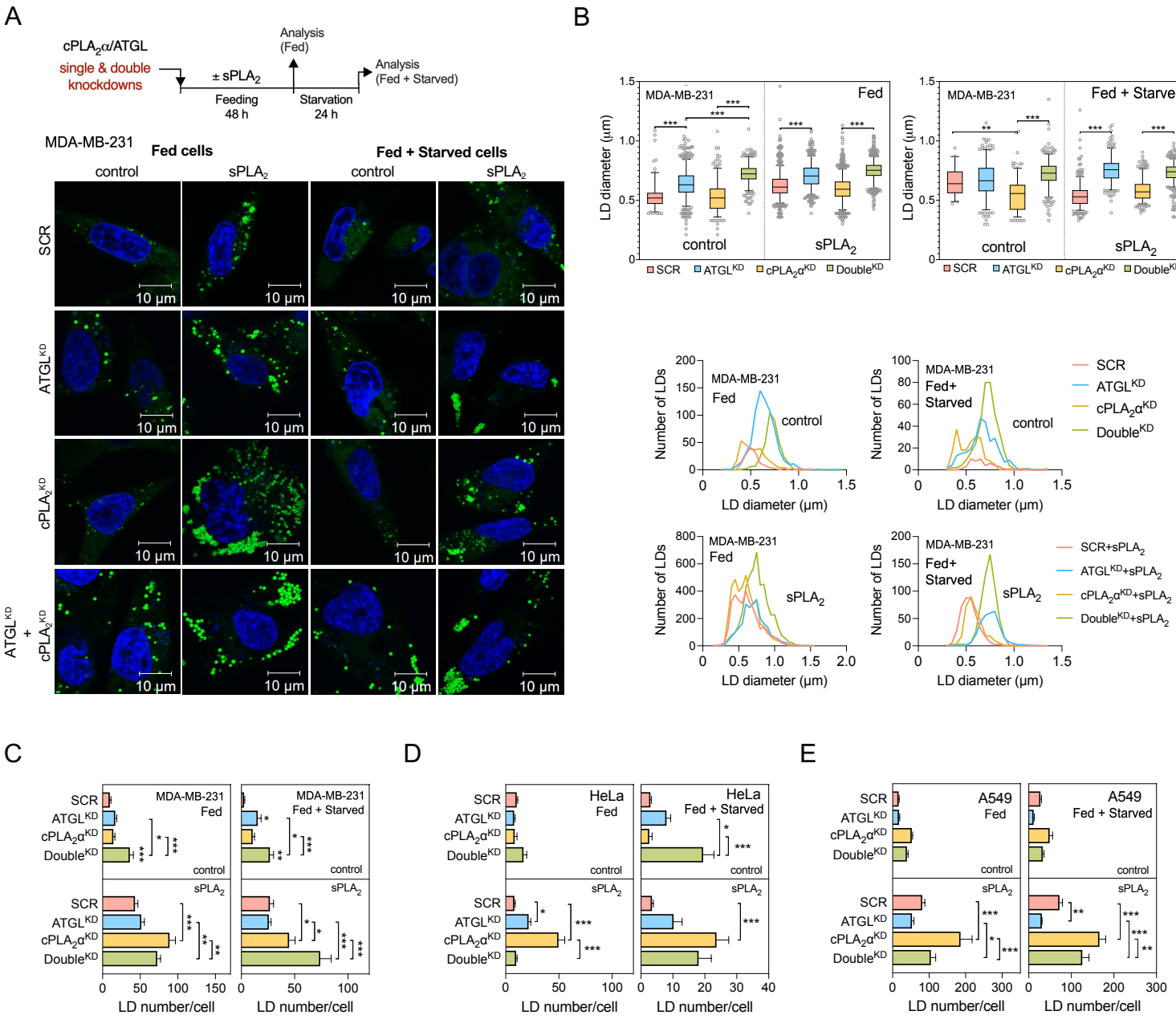
A
cPLA2α/ATGL
single & double
knockdowns
± sPLA2
Analysis
(Fed)
Analysis
(Fed + Starved)
Feeding
48 h
Starvation
24 h
MDA-MB-231
Fed cells
Fed + Starved cells
control
sPLA2
SCR
ATGLKD
cPLA2αKD
ATGLKD
+
cPLA2αKD
10 µm
B
MDA-MB-231
Fed
Fed + Starved
LD diameter (µm)
control
sPLA2
SCR
ATGLKD
cPLA2αKD
DoubleKD
Number of LDs
Fed+
Starved
SCR+sPLA2
ATGLKD+sPLA2
cPLA2αKD+sPLA2
DoubleKD+sPLA2
C
MDA-MB-231
Fed
Fed + Starved
LD number/cell
D
HeLa
E
A549

Figure 7

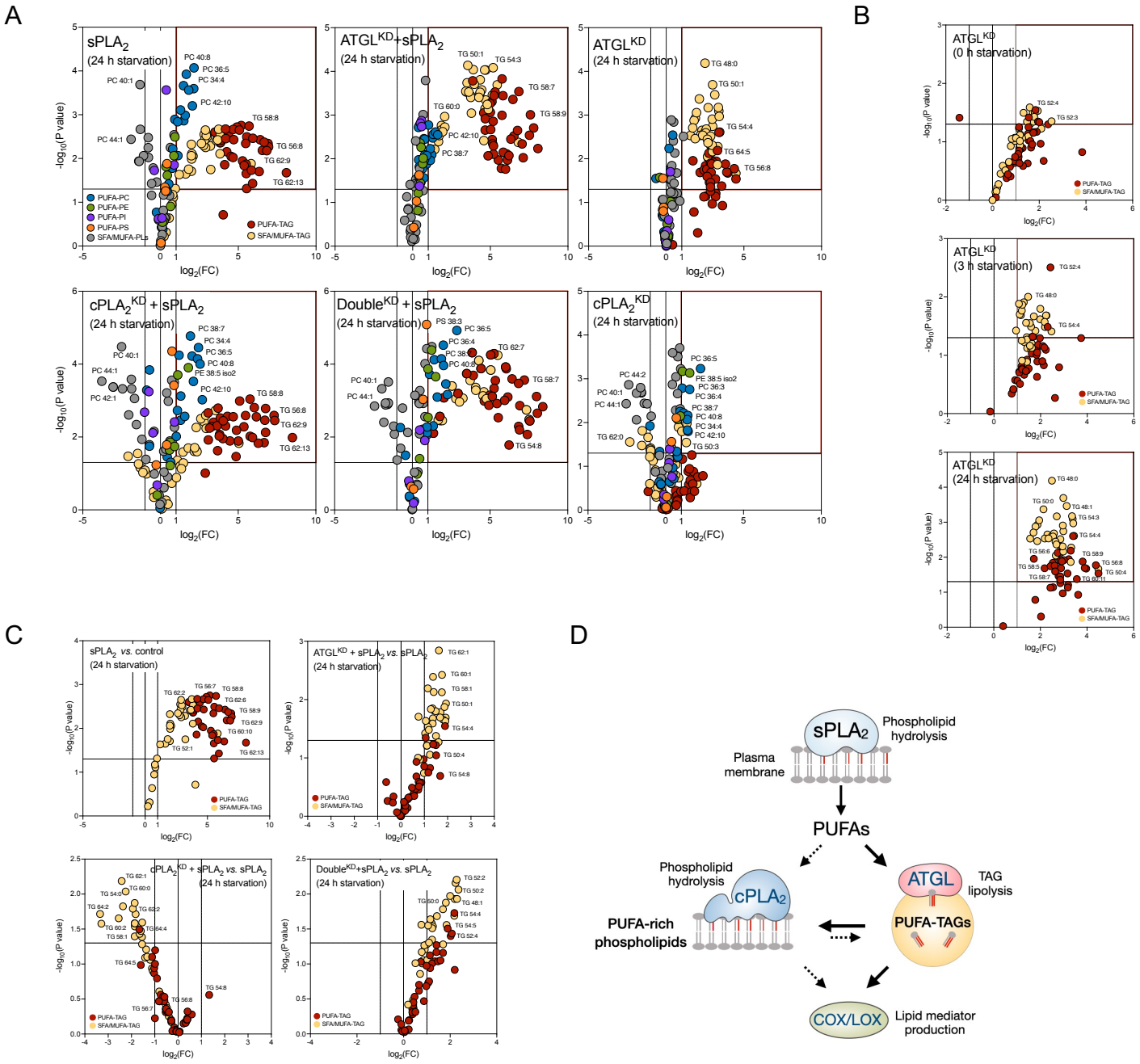
A
sPLA2 (24 h starvation)
ATGLKD+sPLA2 (24 h starvation)
ATGLKD (24 h starvation)
cPLA2KD + sPLA2 (24 h starvation)
DoubleKD + sPLA2 (24 h starvation)
cPLA2KD (24 h starvation)
-log10(P value)
log2(FC)
PUFA-PC
PUFA-PE
PUFA-PI
PUFA-PS
SFA/MUFA-PLs
PUFA-TAG
SFA/MUFA-TAG
B
ATGLKD (0 h starvation)
ATGLKD (3 h starvation)
ATGLKD (24 h starvation)
C
sPLA2 vs. control (24 h starvation)
ATGLKD + sPLA2 vs. sPLA2 (24 h starvation)
cPLA2KD + sPLA2 vs. sPLA2 (24 h starvation)
DoubleKD+sPLA2 vs. sPLA2 (24 h starvation)
D
sPLA2
Phospholipid hydrolysis
Plasma membrane
PUFAs
Phospholipid hydrolysis
cPLA2
PUFA-rich phospholipids
ATGL
TAG lipolysis
PUFA-TAGs
COX/LOX
Lipid mediator production

Figure 8

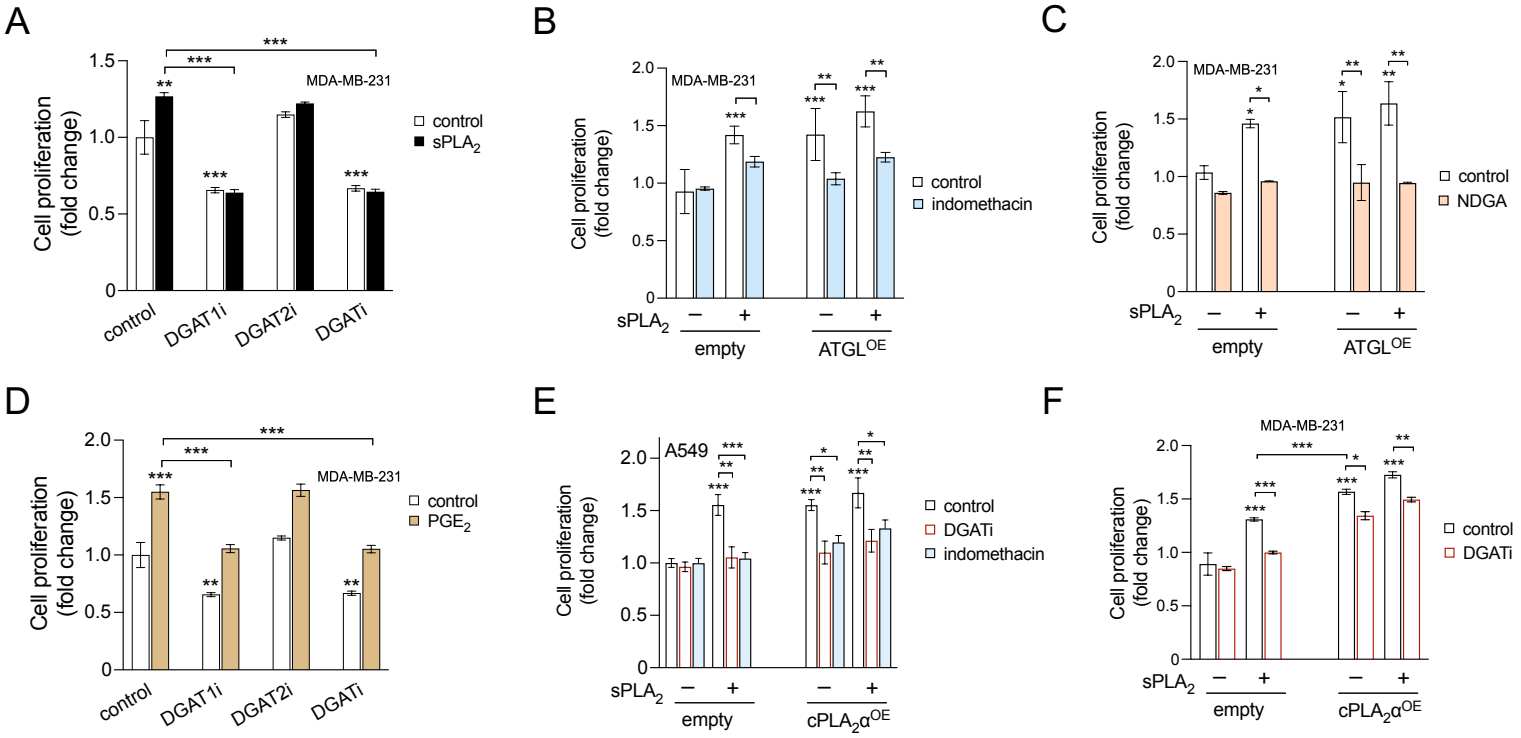
A
Cell proliferation (fold change)
MDA-MB-231
control
sPLA2
control
DGAT1i
DGAT2i
DGATi
B
MDA-MB-231
control
indomethacin
sPLA2
empty
ATGLOE
C
MDA-MB-231
control
NDGA
sPLA2
empty
ATGLOE
D
MDA-MB-231
control
PGE2
control
DGAT1i
DGAT2i
DGATi
E
A549
control
DGATi
indomethacin
sPLA2
empty
cPLA2αOE
F
MDA-MB-231
control
DGATi
sPLA2
empty
cPLA2αOE

Figure EV1

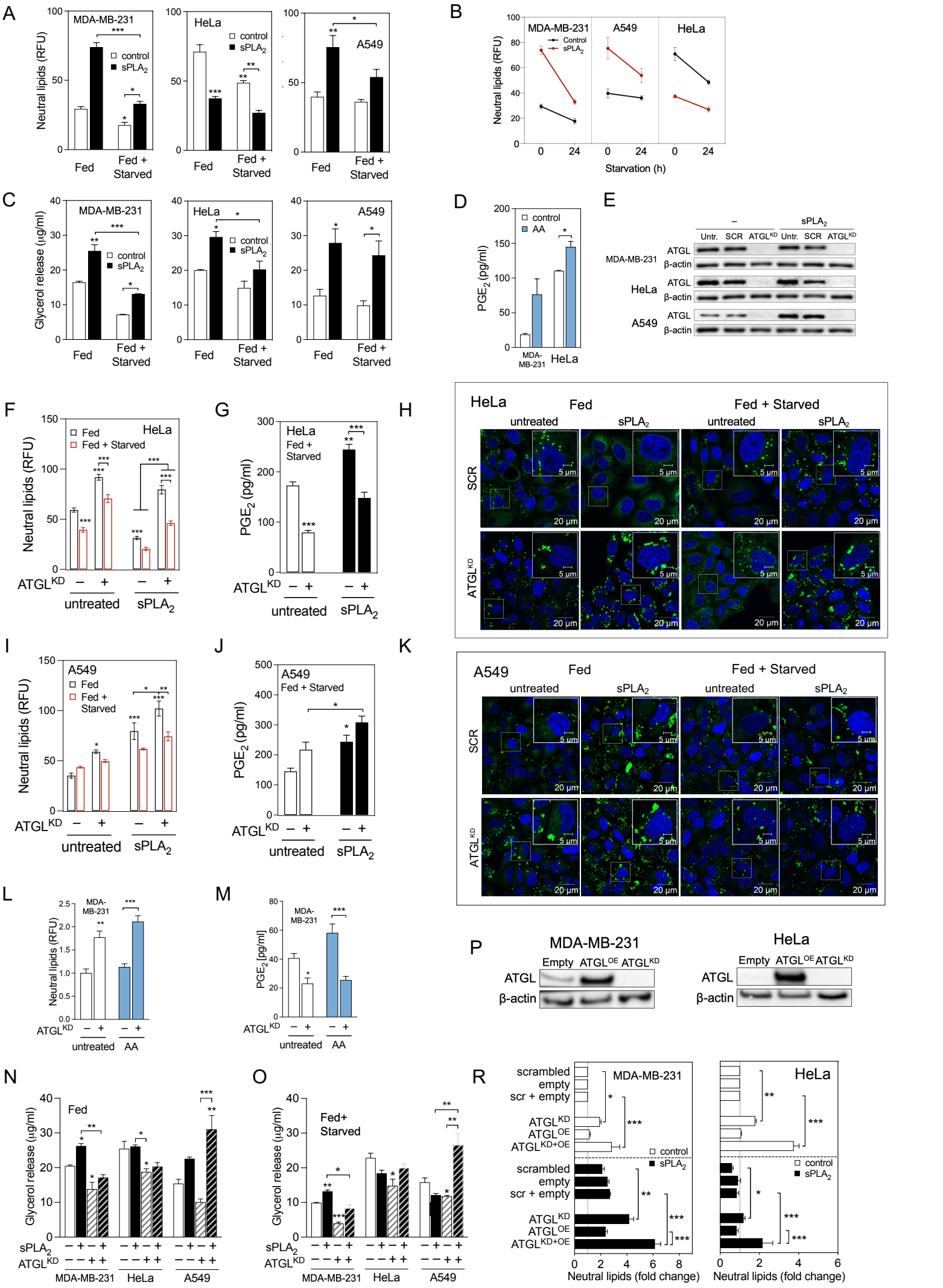

A
MDA-MB-231
HeLa
A549
control
sPLA2
Neutral lipids (RFU)
Fed
Fed + Starved
B
MDA-MB-231
A549
HeLa
Control
sPLA2
Neutral lipids (RFU)
Starvation (h)
C
MDA-MB-231
HeLa
A549
Glycerol release (µg/ml)
D
control
AA
PGE2 (pg/ml)
MDA-MB-231
HeLa
E
sPLA2
Untr.
SCR
ATGLKD
ATGL
β-actin
F
HeLa
Fed
Fed + Starved
Neutral lipids (RFU)
ATGLKD
untreated
sPLA2
G
HeLa
Fed + Starved
PGE2 (pg/ml)
H
HeLa
Fed
Fed + Starved
untreated
sPLA2
SCR
ATGLKD
5 µm
20 µm
I
A549
Fed
Fed + Starved
Neutral lipids (RFU)
J
A549
Fed + Starved
PGE2 (pg/ml)
K
A549
Fed
Fed + Starved
untreated
sPLA2
SCR
ATGLKD
L
MDA-MB-231
Neutral lipids (RFU)
untreated
AA
M
MDA-MB-231
PGE2 [pg/ml]
untreated
AA
P
MDA-MB-231
HeLa
Empty
ATGLOE
ATGLKD
ATGL
β-actin
N
Fed
Glycerol release (µg/ml)
sPLA2
ATGLKD
MDA-MB-231
HeLa
A549
O
Fed+ Starved
Glycerol release (µg/ml)
sPLA2
ATGLKD
MDA-MB-231
HeLa
A549
R
scrambled
empty
scr + empty
ATGLKD
ATGLOE
ATGLKD+OE
control
sPLA2
Neutral lipids (fold change)

Figure EV2

A

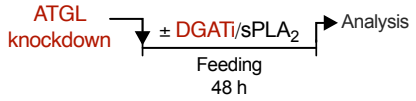

MDA-MB-231

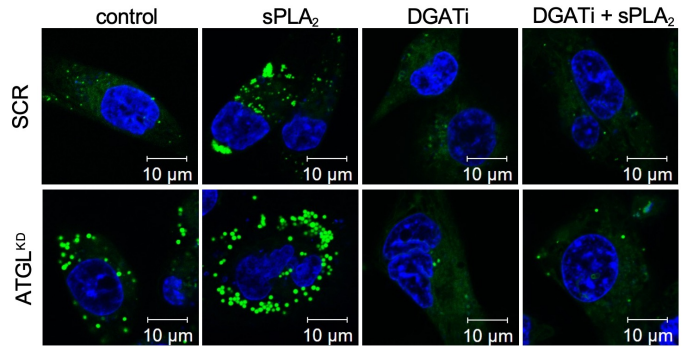

HeLa

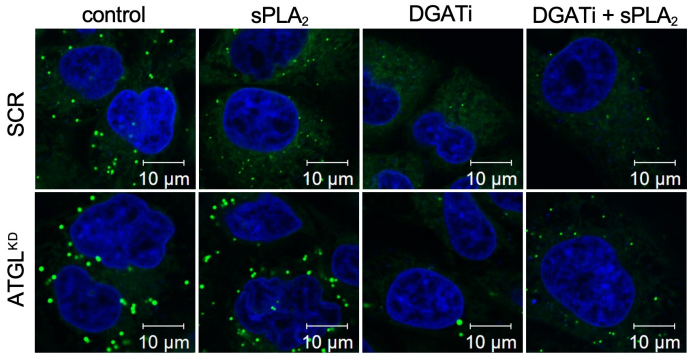

B

MDA-MB-231

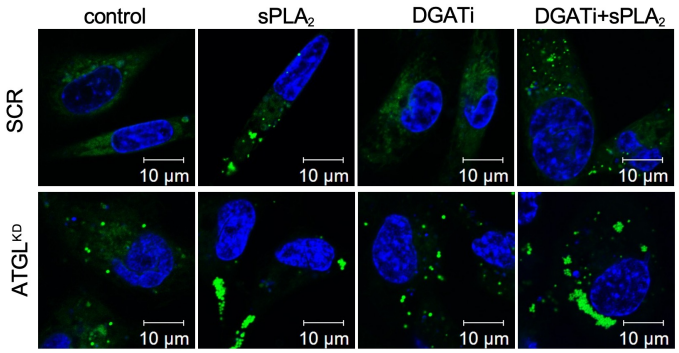

HeLa

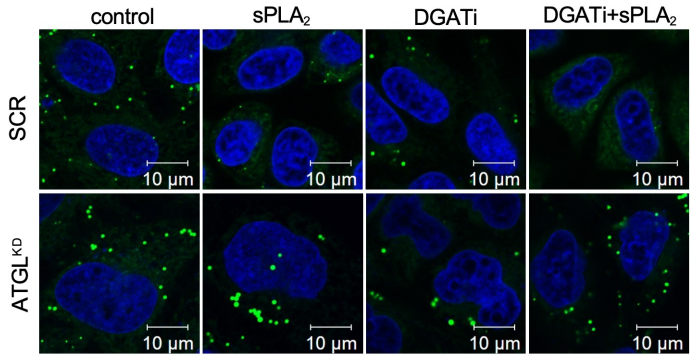

C

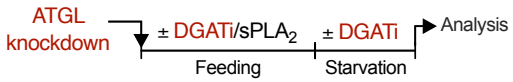

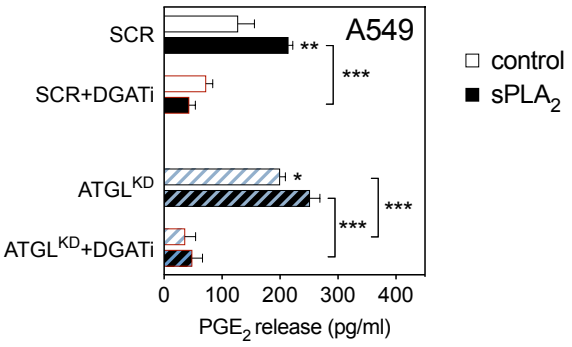

Figure EV3

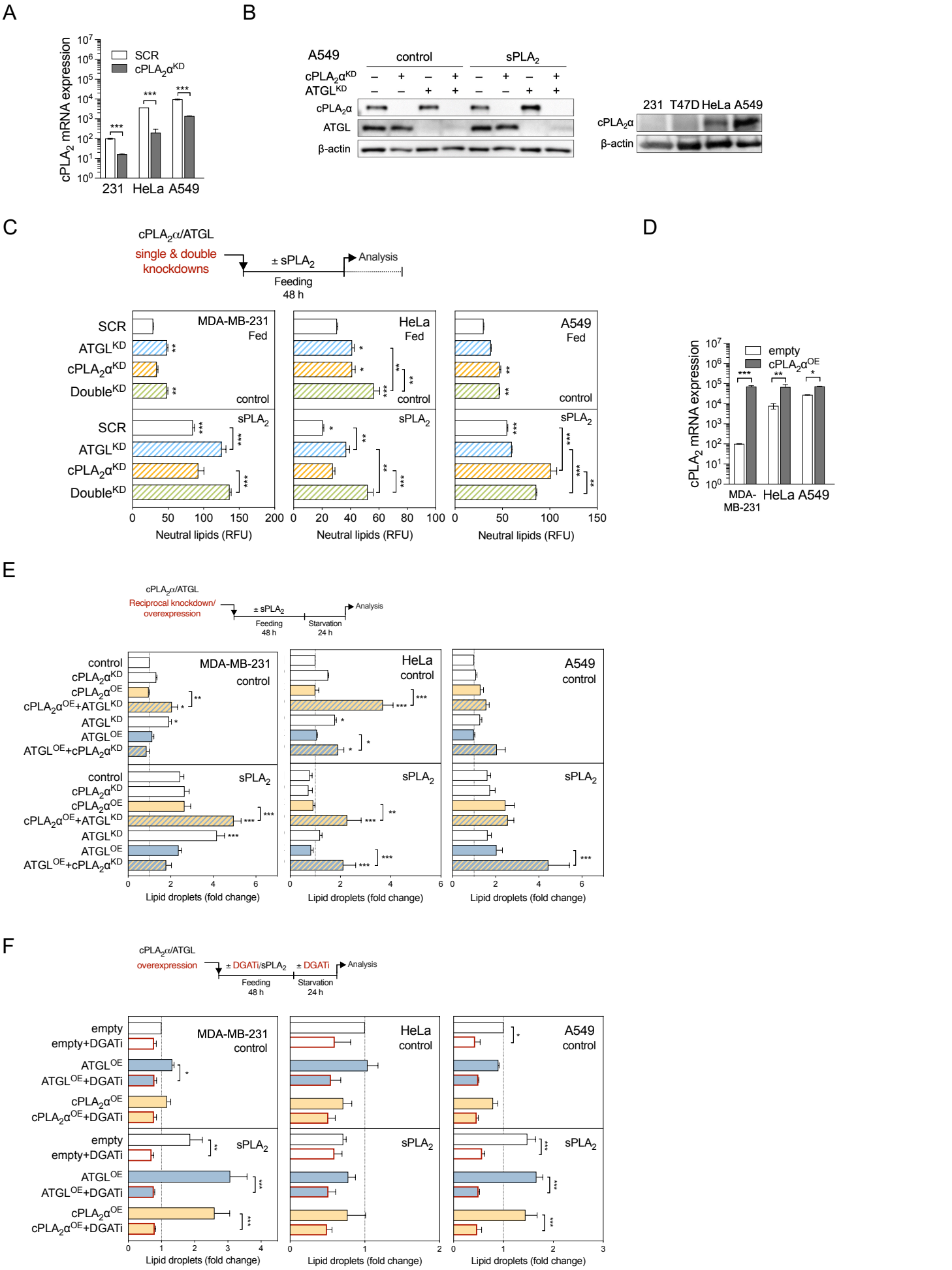
A
cPLA2 mRNA expression
SCR
cPLA2αKD
231 HeLa A549
B
A549
control
sPLA2
cPLA2αKD
ATGLKD
cPLA2α
ATGL
β-actin
231 T47D HeLa A549
C
cPLA2α/ATGL
single & double knockdowns
± sPLA2
Analysis
Feeding 48 h
MDA-MB-231
HeLa
A549
Fed
control
sPLA2
SCR
ATGLKD
cPLA2αKD
DoubleKD
Neutral lipids (RFU)
D
empty
cPLA2αOE
MDA-MB-231
HeLa
A549
E
cPLA2α/ATGL
Reciprocal knockdown/ overexpression
Feeding 48 h
Starvation 24 h
control
cPLA2αKD
cPLA2αOE
cPLA2αOE+ATGLKD
ATGLKD
ATGLOE
ATGLOE+cPLA2αKD
Lipid droplets (fold change)
F
cPLA2α/ATGL
overexpression
± DGATi/sPLA2
± DGATi
empty
empty+DGATi
ATGLOE
ATGLOE+DGATi
cPLA2αOE
cPLA2αOE+DGATi

Figure EV4

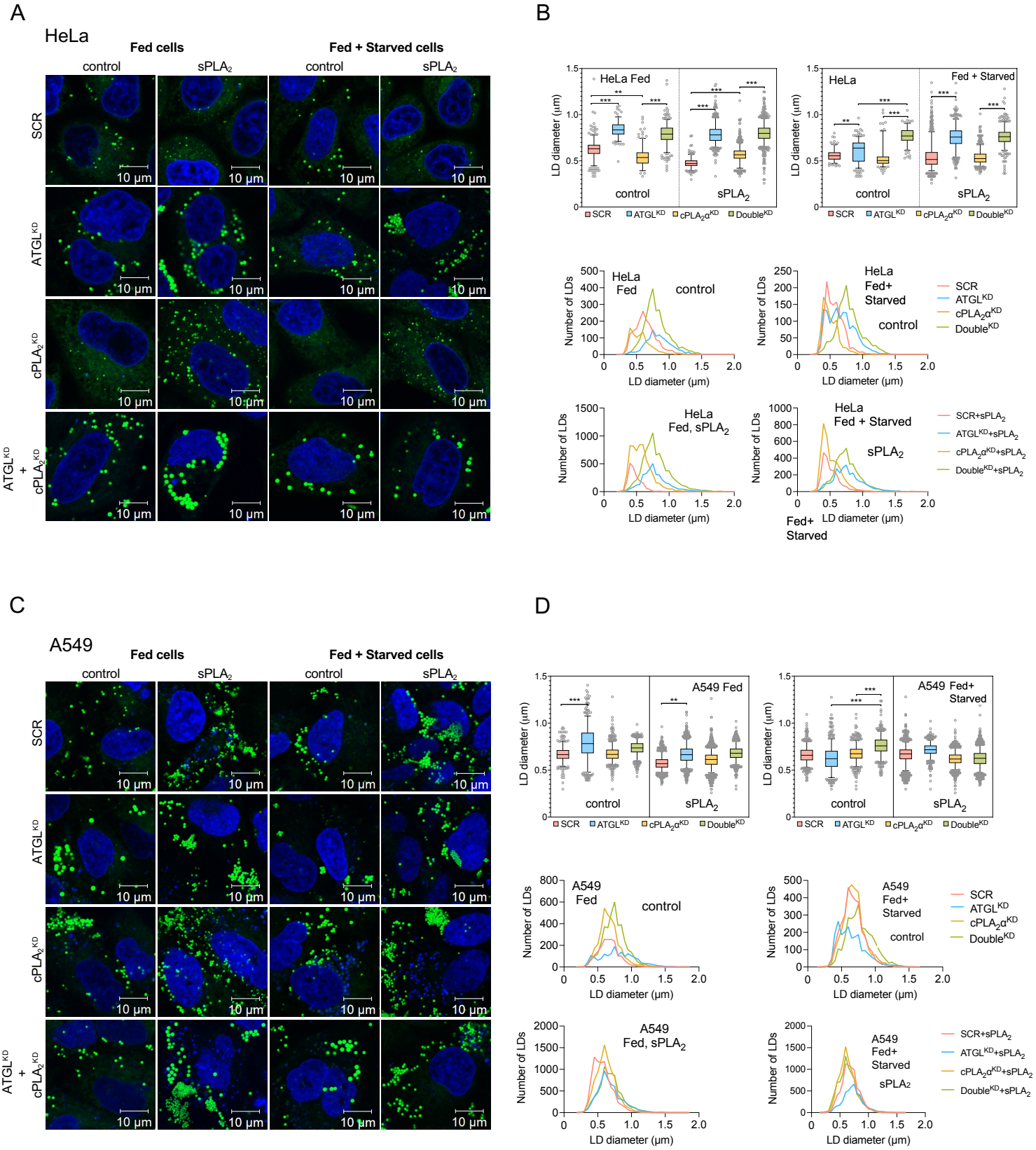
A
HeLa
Fed cells
Fed + Starved cells
control
sPLA2
SCR
ATGLKD
cPLA2KD
ATGLKD + cPLA2KD
10 µm
B
HeLa Fed
HeLa
Fed + Starved
LD diameter (µm)
control
sPLA2
SCR
ATGLKD
cPLA2αKD
DoubleKD
Number of LDs
HeLa Fed
HeLa Fed+ Starved
HeLa Fed, sPLA2
HeLa Fed + Starved
SCR+sPLA2
ATGLKD+sPLA2
cPLA2αKD+sPLA2
DoubleKD+sPLA2
Fed+ Starved
C
A549
D
A549 Fed
A549 Fed+ Starved
A549 Fed, sPLA2

Figure EV5

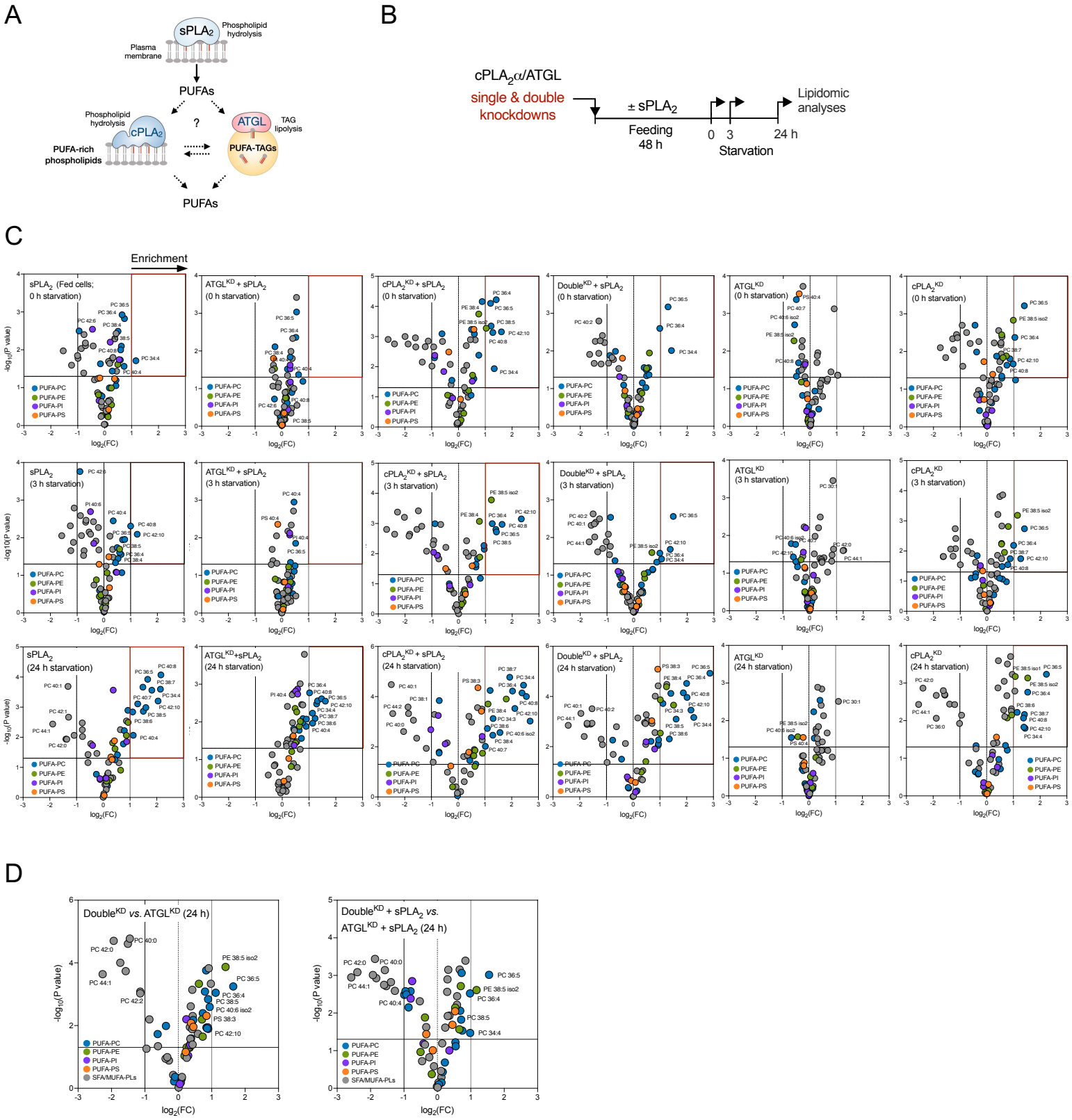
A
sPLA2
Phospholipid hydrolysis
Plasma membrane
PUFAs
Phospholipid hydrolysis
cPLA2
?
ATGL
TAG lipolysis
PUFA-rich phospholipids
PUFA-TAGs
PUFAs
B
cPLA2α/ATGL
single & double knockdowns
± sPLA2
Feeding 48 h
0 3 24 h
Starvation
Lipidomic analyses
C
Enrichment
sPLA2 (Fed cells; 0 h starvation)
ATGLKD + sPLA2 (0 h starvation)
cPLA2KD + sPLA2 (0 h starvation)
DoubleKD + sPLA2 (0 h starvation)
ATGLKD (0 h starvation)
cPLA2KD (0 h starvation)
sPLA2 (3 h starvation)
ATGLKD + sPLA2 (3 h starvation)
cPLA2KD + sPLA2 (3 h starvation)
DoubleKD + sPLA2 (3 h starvation)
ATGLKD (3 h starvation)
cPLA2KD (3 h starvation)
sPLA2 (24 h starvation)
ATGLKD+sPLA2 (24 h starvation)
cPLA2KD + sPLA2 (24 h starvation)
DoubleKD + sPLA2 (24 h starvation)
ATGLKD (24 h starvation)
cPLA2KD (24 h starvation)
PUFA-PC
PUFA-PE
PUFA-PI
PUFA-PS
-log10(P value)
log2(FC)
D
DoubleKD vs. ATGLKD (24 h)
DoubleKD + sPLA2 vs. ATGLKD + sPLA2 (24 h)
SFA/MUFA-PLs

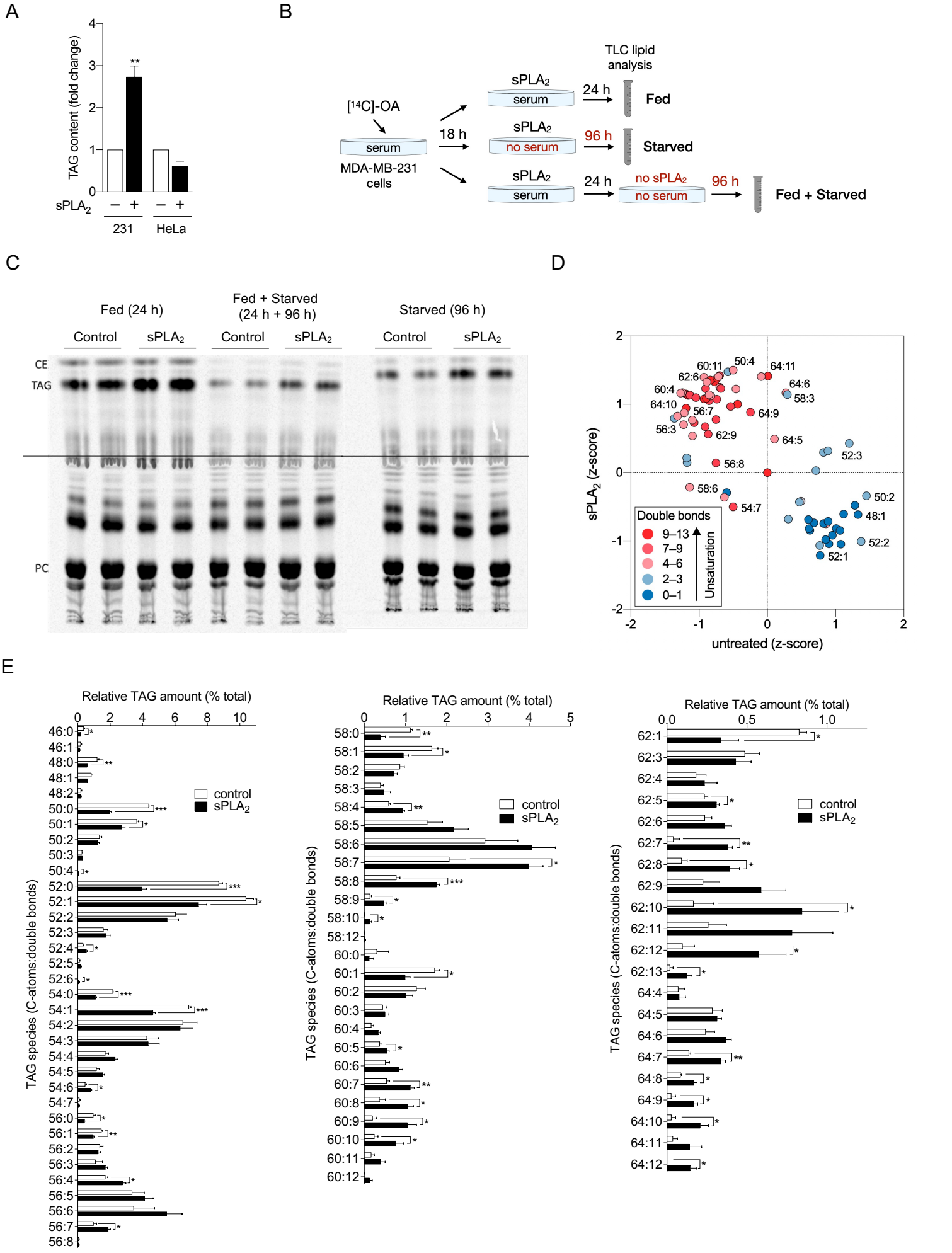
A
TAG content (fold change)
sPLA2
231
HeLa
B
[14C]-OA
serum
MDA-MB-231 cells
18 h
sPLA2
serum
no serum
24 h
96 h
no sPLA2
TLC lipid analysis
Fed
Starved
Fed + Starved
C
Fed (24 h)
Fed + Starved (24 h + 96 h)
Starved (96 h)
Control
sPLA2
CE
TAG
PC
D
sPLA2 (z-score)
untreated (z-score)
Double bonds
9–13
7–9
4–6
2–3
0–1
Unsaturation
E
Relative TAG amount (% total)
TAG species (C-atoms:double bonds)
control
sPLA2

EPA metabolites

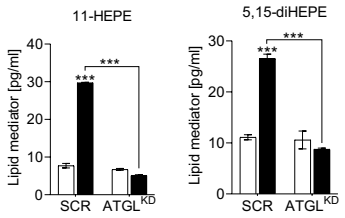

AA metabolites

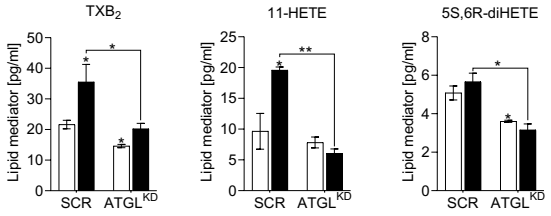

DHA metabolites

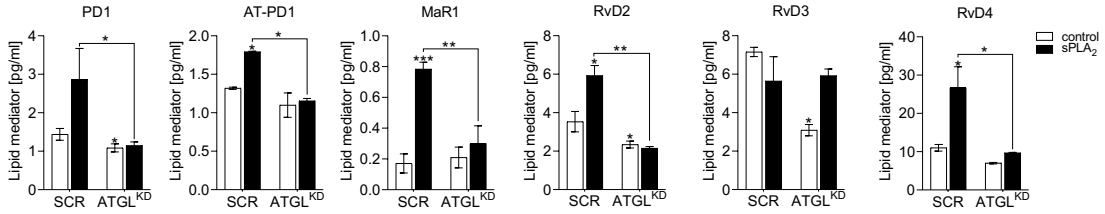

Appendix Fig. S3

A

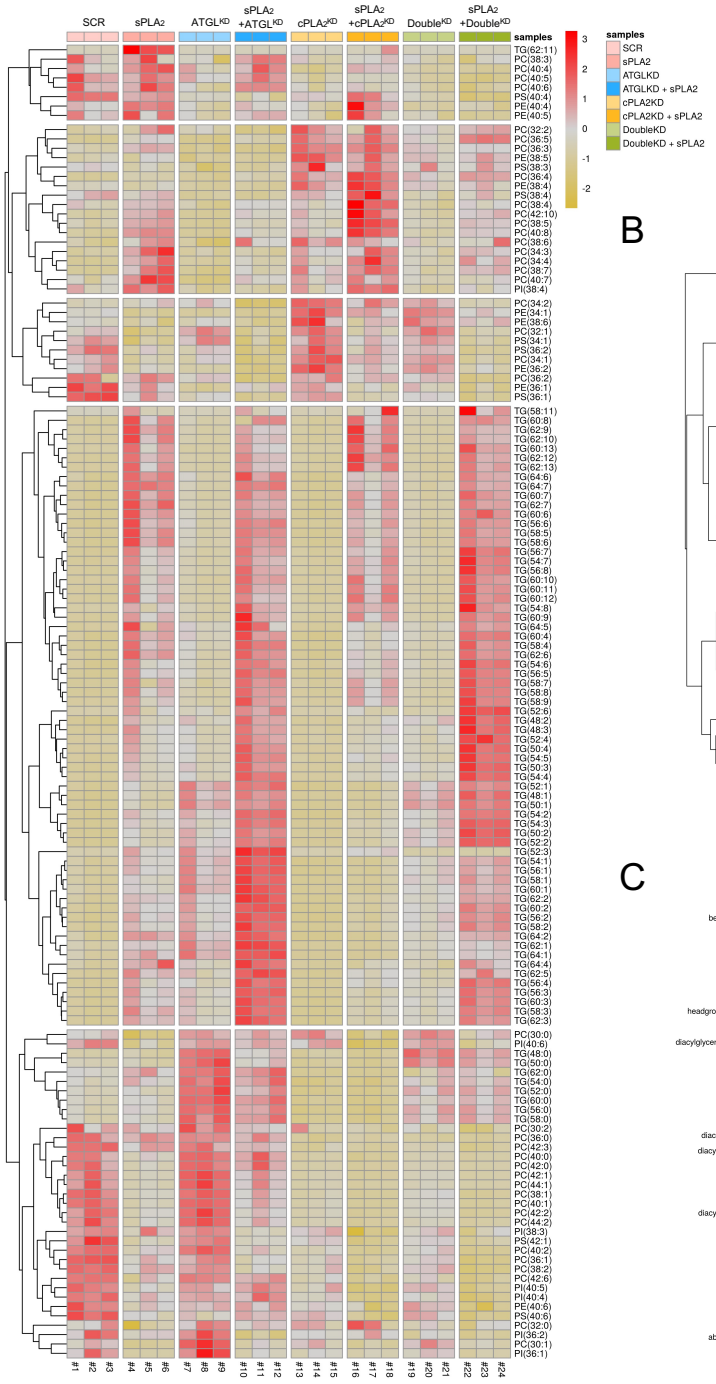

B

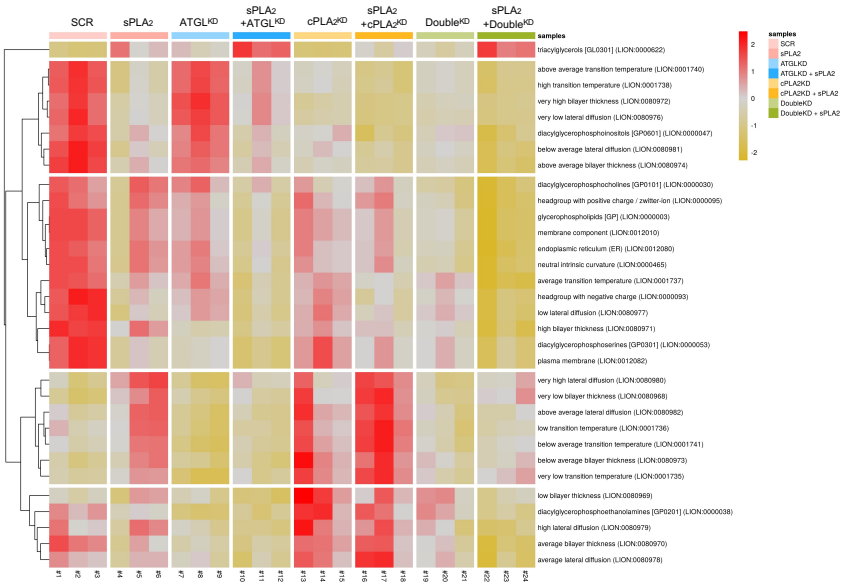
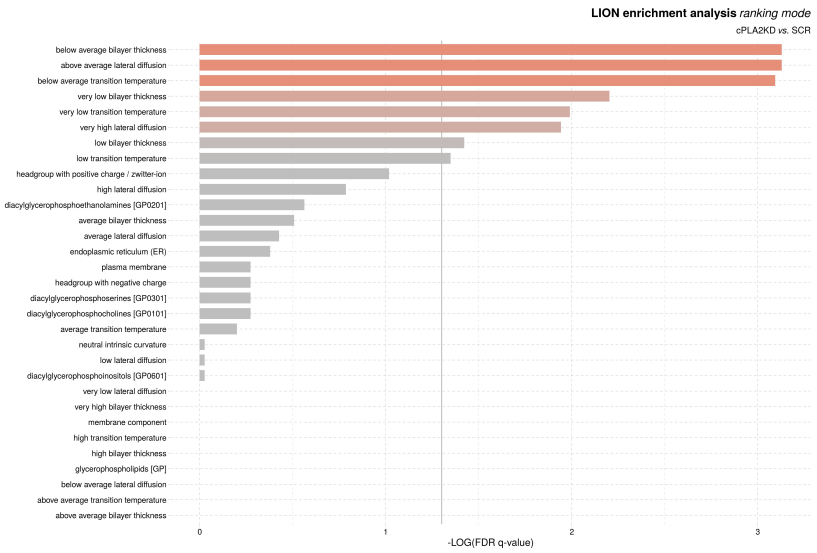
C